國科會研究計畫成果報告

計畫名稱: 黑潮於台灣東南、西南海域的時空變化

Temporal and spatial variations of Kuroshio off Southeast and southwest of Taiwan (II)

主持人: 唐存勇

台灣大學海洋研究所

計畫編號： NSC 90-2611-M-002-018-OP2

1. Introduction

We promised to perform four works in the proposal. The topics of works are

I. To study the Kuroshio intrusion and its behavior on the southwest of Taiwan;

II. To deploy 2 sets ADCP moorings in between the Lanyu and Taiwan monitoring the upper ocean Kuroshio

III. To study the temporal and spatial structures of current and hydrograph east of Taiwan.

IV. To update the Sb-ADCP current velocity measurement.

The promised works might not be well done, but they were properly done. All of the works are worthy having more sophisticated study. For work (a), one manuscript has been submitted to the JPO and one manuscript is in preparation. The title of submitted manuscript is "Kuroshio Intrusion in Luzon Strait". This manuscript is listed in section 2. We did great effect on this manuscript, but there remain a number of mysteries. For example, we don't have a proper explanation on the intra-seasonal variation of current velocity in Luzon Strait. A study of "Intraseasonal variation in the northern SCS" is doing. The preliminary results are also

briefly stating in Section 2. Section 3 presents the data collected from the 2 moorings deployed in between Lanyu and Taiwan. We have not have a chance to investigate the data. However, the fieldwork is relatively successful. Section 4 states the preliminary results for the study of the temporal and spatial structures of current and hydrograph east of Taiwan. Attention is specially drawn to the eddy on the northwest Pacific. A manuscript, entitled as "Upper Ocean Current around Taiwan", is listed in Section 5. Personally, I don't think the manuscript had a lot of scientific result, but I truly hope that this result would replace the result of Nitani (1972). Taiwan needs her own updated current velocity distribution.

2. Topic I

We used the 3 mooring current velocity measurement and a northwest Pacific Ocean numerical model to study the Kuroshio Intrusion in the Luzon Strait. The major findings are:

a. The Kuroshio consistently and persistently intrudes into the South China Sea through the central Luzon Strait.

b. The current velocity in the Luzon Strait had large intra-seasonal fluctuations. The local wind is not the only factor causing such fluctuations.

c. The zonal transport across the Luzon Strait had large seasonal variation, which could primarily relate with the meridional pressure gradient across the Luzon Strait.

d. The variation of meridional pressure gradient could be mainly caused by the thermal variation west of Luzon, which could be related with the wind stress curl in the South China Sea.

The manuscript has been submitted to the Journal of Physical Oceanography. A copy of this manuscript is listed in Appendix I.

Another study on the intra-seasonal variation west of Luzon Strait is on-going. We plan to submit the manuscript to the special issue of ASIAEX of Journal of Ocean Engineering, IEEE on coming March. The preliminary results state briefly below.

a. The current velocity measurements obtained from 3 mooring west of Luzon Strait indicates the current velocity variation west of Luzon Strait had large intra-seasonal but small seasonal variation.

b. The seasonal variation west of central Luzon Strait had relatively clear feature. The westward current was weak but had large fluctuation during the Southwest Monsoon. It became larger (over 30cm/s) but was relatively stable when the Northeast Monsoon was intensified.

c. An anti-cyclonic and cyclonic flow alternatively presented at the southern opening of Taiwan Strait, but the former one is more often observed.

d. The local wind had impact on the intra-seasonal variation, but these two's overall coherence was low for all three mooring locations. The local wind obviously is not the only role causing the intra-seasonal variation.

e. A numerical model outputs provided by Dr. Dong-Shan Ko at Naval Research Lab (NRL) to investigate the intra-seasonal fluctuation in more complete feature. The observation/model output comparison indicates the validation of the model output. The comparison is shown in Figure 2-1.

f. The model output properly represents the current velocity in the deep basin of northern SCS, but poorly represents the current velocity near the shelf break where the water depth varies vigorously. However, both model output and observation represented a similar feature; the current velocity in the northern SCS had large intra-seasonal but small seasonal variation.

g. The model outputs show that the intra-seasonal variation is the result of

interaction between the intruded Kuroshio and circulation in the SCS. When the SCS cyclonic flow became a basin-wide feature during the northeast monsoon season, it dominates the flow in the deep basin of northern SCS. The westward current velocity at A became more stable. In the southwest monsoon season, the cyclonic flow became fragmental and confined in the northern SCS. The completion between the intruded Kuroshio and cyclonic flow caused large intra-seasonal fluctuation at A.

h. The current velocity at southern opening of Taiwan Strait is primarily related with the intruded Kuroshio. In general, the intruded Kuroshio consistently spilled its water clockwisely passing across the southern opening of Taiwan Strait on the way the intruded Kuroshio penetrated westward into the SCS. An anti-cyclonic flow presented in the southern opening of Taiwan Strait, but it was not a unity. The flow at eastern portion (for example C) leaded it at western portion (for example B).

i. As the Kuroshio speed increased, it either leaps over the Luzon Strait or directly impinges the southern opening of Taiwan Strait. A cyclonic flow is shown in the southern opening of Taiwan Strait. This cyclonic flow could be originated from the Kuroshio in the case of Kuroshio

directly impinges on the southern opening of Taiwan Strait. It also could be originated from the SCS cyclonic flow, when the Kuroshio intrusion was significantly reduced.

j. In the measurement, the TS diagram analysis shows that the water at southern opening of Taiwan Strait is more favor with the SCS water when the cyclonic flow. This result indicates that the later postulation in (i) is more reliable. However, there only had 5 months measurement. The model result indicates the case of Kuroshio directly impinged onto the southern opening of Taiwan Strait is not often.

3. Topic II

Two subsurface ADCP moorings were deployed in between LanYu and Taiwan, and one subsurface ADCP mooring was deployed east of Lanyu. The moorings were retrieved safely. The data need more time than usual to process because some of instruments have problem. For example, one of SEACAT was out of function. The observed current velocity has difficulty to do depth correction. A specific method is developing to solve this problem. Another example is that one of ADCP has calibration problem. We plan to re-calibrate this instrument to obtain correct current velocity.

However, most of data are correct. A part of data is shown to illustrate the work we performed.

Figure 3-1 show near 6-month current velocity time series at A, which is close to the Taiwan. The east and north components of current velocity are u and v, respectively. The u was much larger than the v. The current velocity was primarily northward. Both u and V fluctuated largely. The low-frequency current velocity was generally less than 90cm/s. The v was negative when the northeast monsoon was large. The countercurrent could be extended from the coast to more offshore. Near the end of record, the v increased greatly. This increase could be related with that the northeast monsoon was relaxed and the countercurrent was retreated to the coastal area. The correlation between the current and wind velocity at the near further.

Figure 3-2 show the 6-month current velocity time series at B, where close to the western Lanyu. Both u and v at B was significantly larger them at A. This location could be close to the main stream of Kuroshio. The current primarily directed to the NNE. It was more eastward than it at A. The low-frequency current speed was generally larger than 90cm/sec. The maximum speed could reach 135cm/s. The current was accelerated since

the mid-December. Obviously, the northeast monsoon did not reduce the speed of Kuroshio. The acceleration could be related with the development of countercurrent. The extension of countercurrent made the pathway of Kuroshio narrow in between the Taiwan and Lanyu. Therefore, the current speed increased. However, this hypothesis cannot hold for the period when the northeast monsoon was relaxed at March/April. Further investigate is required.

Figure 3-3 show the 6-month current velocity time series at C, where locates east of Lanyu. Again, the v was generally larger than the u. The current velocity primarily directed NNE. This location was still in the pathway of Kuroshio. However, the speed of current was smaller than it at B. The current had larger fluctuations at C than B. The impact of northeast monsoon was unclearly. The most notable variation was at Mid-November to Mid-December. The v decreased/increased went through around on-month oscillation. This variation could not relate with the local wind variation because the wind had no large fluctuation at that time. The westward propagating eddy could be responsible for this change. We would examine the seal level height variation to examination the postulation in the near future.

4. Topic III

Two large-scale hydrographic surveys have been done. Figure 4-1 show the Sb-ADCP measured current velocity at 16m along the cruise track. The sea surface height anomalies estimated from the TOPEX/ERS-2 is also shown. The current velocity distribution was complicated west of Kuroshio. The sea surface height suggested that the current velocity variation in space could be related with the westward propagating warm/cold eddy. On the other hand, the measured current velocity provided the ground truth of the existence of eddy. To examine the relation between eddy and measured current velocity, the result indicates that some of eddies were illusion. An study to verify the existence of eddy has been proposed. I believe that we would get some interesting results. The results should benefit the studies of remote sensing.

Figure 4-2 shows the current velocity along 18oN on 10/1999 and 9/2000. The upper panel is the measured Sb-ADCP meridional current velocity. The lower panel is the absolute geostrophic meridional current velocity, which calculated using the CTD measurement, and using the Sb-ADCP current velocity in between 100-100m as a reference. The Sb-ADCP current velocity had finer structure than the geostrophic current velocity, but they

were alike, in general. The measurement at 1999 indicates that the Kuroshio along 18oN was confined in the upper 300m ocean. A strong countercurrent was seen beneath the Kuroshio. In 2000, the CTD measurement was not performed close to the coast of Philippines primarily due to the typhoon. The influence depth of Kuroshio is unknown. However, they had similar countercurrent, which was beneath the Kuroshio. This feature implicitly pointed out that the Kuroshio along 18oN in 2000 could be also confined in the upper ocean. This finding is different than the old believe. A further study might be need.

Similar to Figure 4-2, Figure 4-3 shows the current velocity along 23.5oN on 10/1999 and 9/2000. The two current velocity distributions were alike. Near the coast of Taiwan, the SB-ADCP measurement showed there had a subsurface countercurrent. In fact, this kind of the countercurrent was observed frequently along the eastern coast of Taiwan. The geostrophic current could not reveal this countercurrent because the grid is small and the calculation geostrophic current is based upon the small Rossby number. The width of Kuroshio was around 150km, and the maximum speed could be over 90 cm/s. The speed and influence depth of Kuroshio greatly increased east of Taiwan. The North Equatorial Current (NEC) could continuously

pour into the Kuroshio east of Taiwan. The difference between two years' measurement of Kuroshio was small. However, the current west of Kuroshio varied from year from year. It could not be an interannual variation because the westward propagating eddy could contribute this difference.

Definitely, the above results are preliminary. We would continuously work on this study.

5. Topic IV

The Sb-ADCP current velocity has been updated. Software has developed and provide to the Data Bank. The updated current velocity has been written as a scientific paper, which would be published soon. The manuscript is listed in Appendix B. The updated current velocity is not only used for the scientific study, it also used for the sea rescue. We provided the flow chart for the emergency center when the tragedy of China Airline clash occurred. The rescuer told us that the trajectory wreckage and bodies drifted quite followed with the flow. The chart we provided help for the searching. We sorry for the tragedy, but we are proud of our effect. Hopefully, the Data Bank of NCOR will continuously update the data. Eventually, the current velocity around Taiwan would be properly understood.

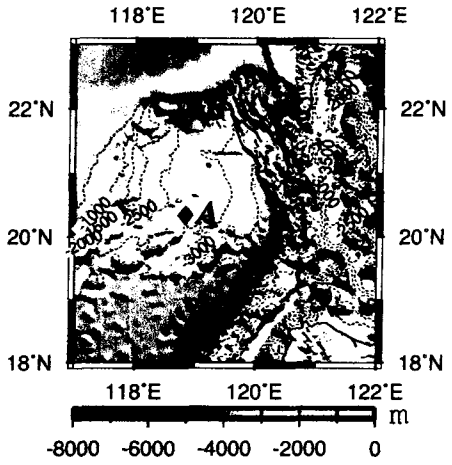

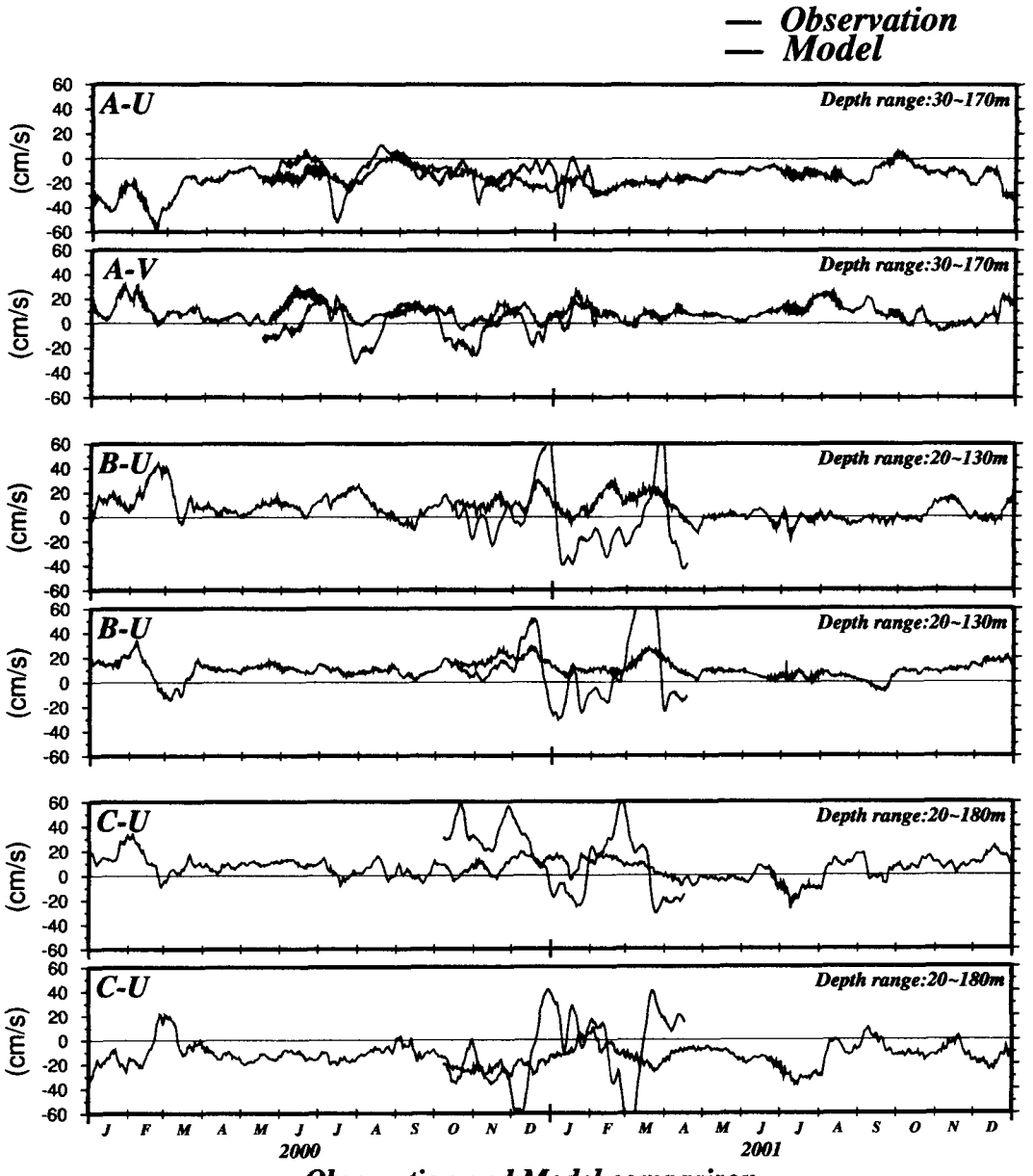

Observation and Model comparison

fig 2-1

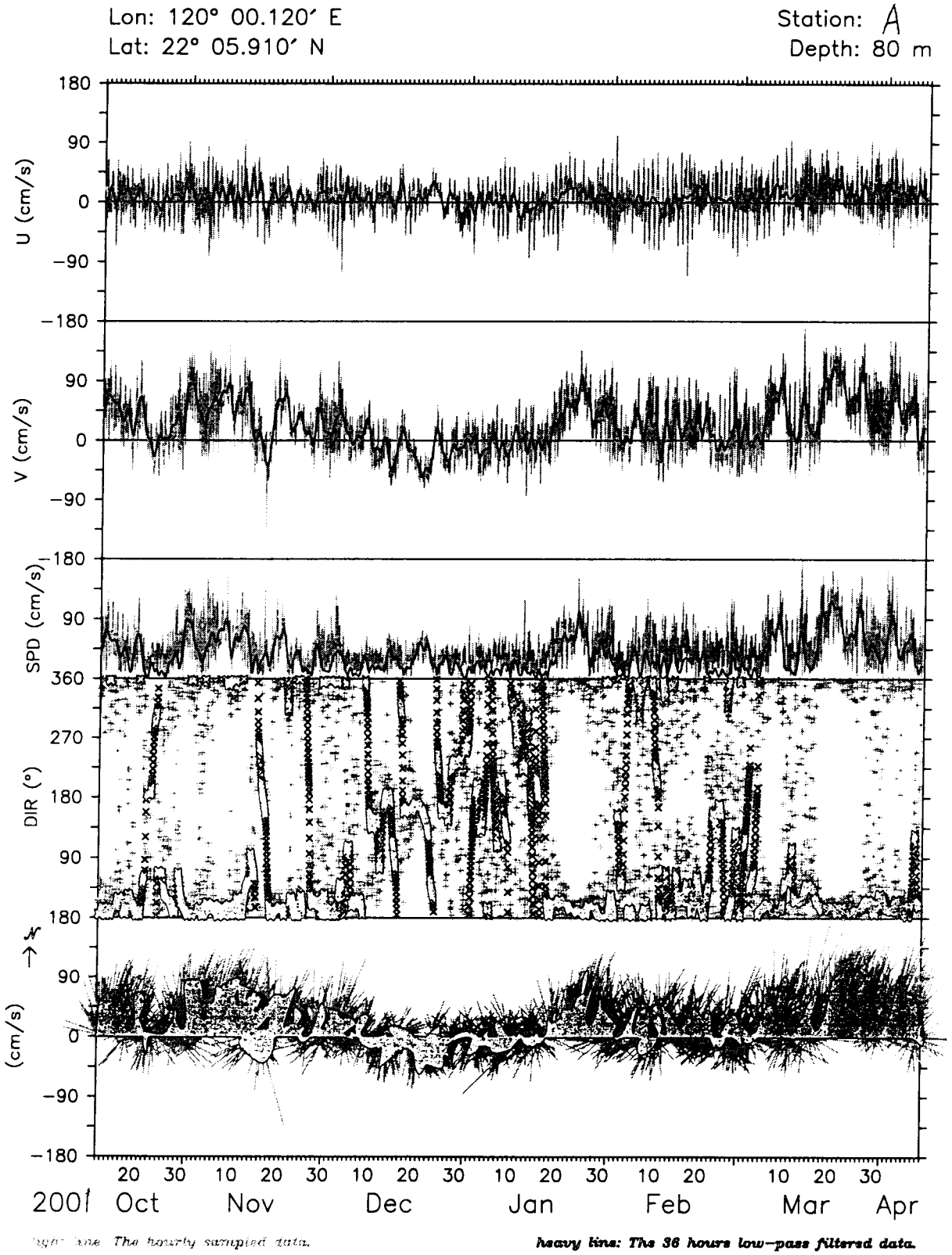
Lon: 120° 00.120′ E
Lat: 22° 05.910′ N
Station: A
Depth: 80 m
U (cm/s)
V (cm/s)
SPD (cm/s)
DIR (°)
(cm/s)
180
90
0
-90
-180
360
270
2001 Oct Nov Dec Jan Feb Mar Apr
20 30 10 20 30 10 20 30 10 20 30 10 20 10 20 30
The hourly sampled data.
heavy line: The 36 hours low-pass filtered data.

Figure 3-1

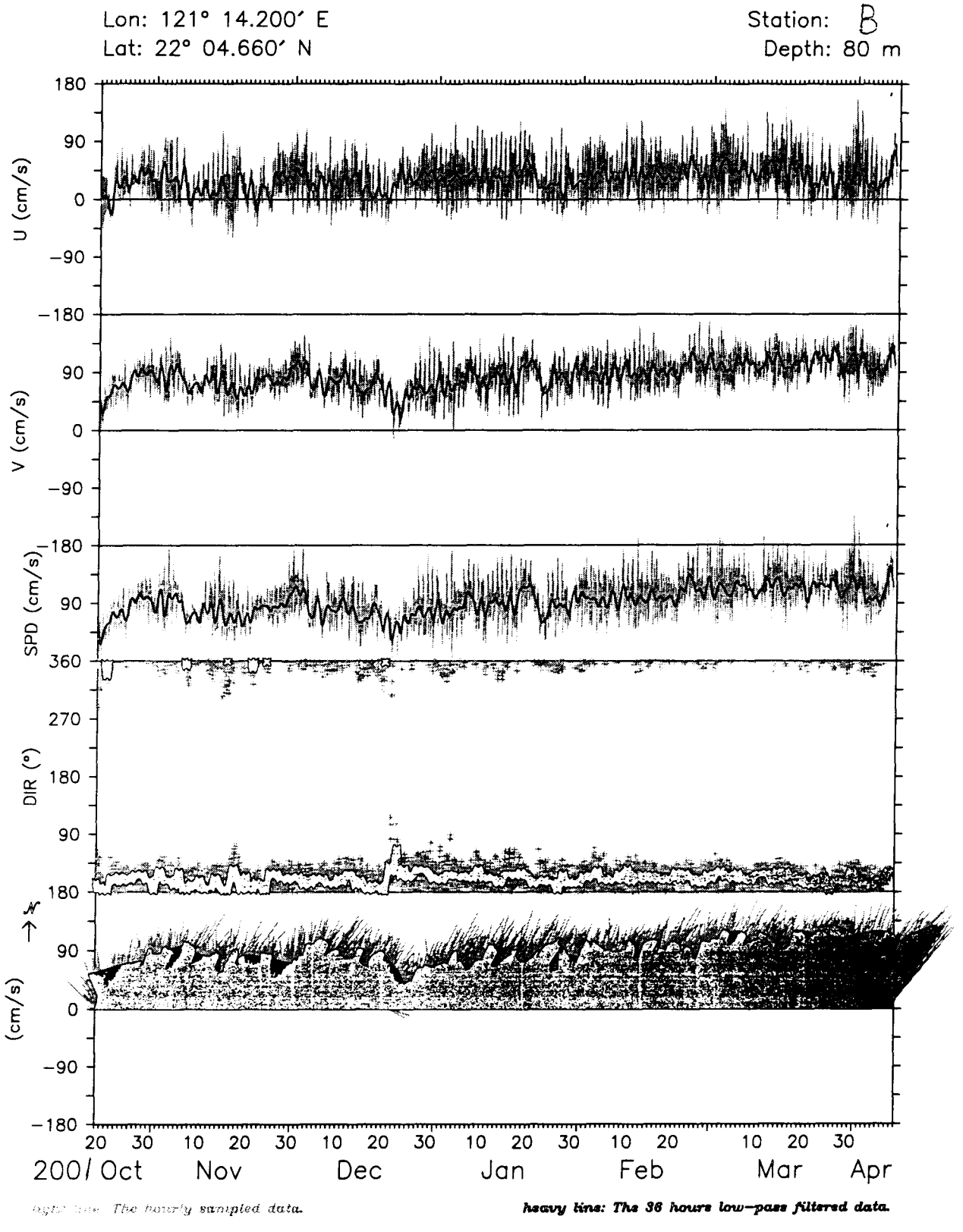
Lon: 121° 14.200′ E
Lat: 22° 04.660′ N
Station: B
Depth: 80 m
U (cm/s)
V (cm/s)
SPD (cm/s)
DIR (°)
(cm/s)
180
90
0
−90
−180
360
270
20 30 10 20 30 10 20 30 10 20 30 10 20 10 20 30
200/ Oct Nov Dec Jan Feb Mar Apr
The hourly sampled data.
heavy line: The 36 hours low-pass filtered data.

Figure 3-2

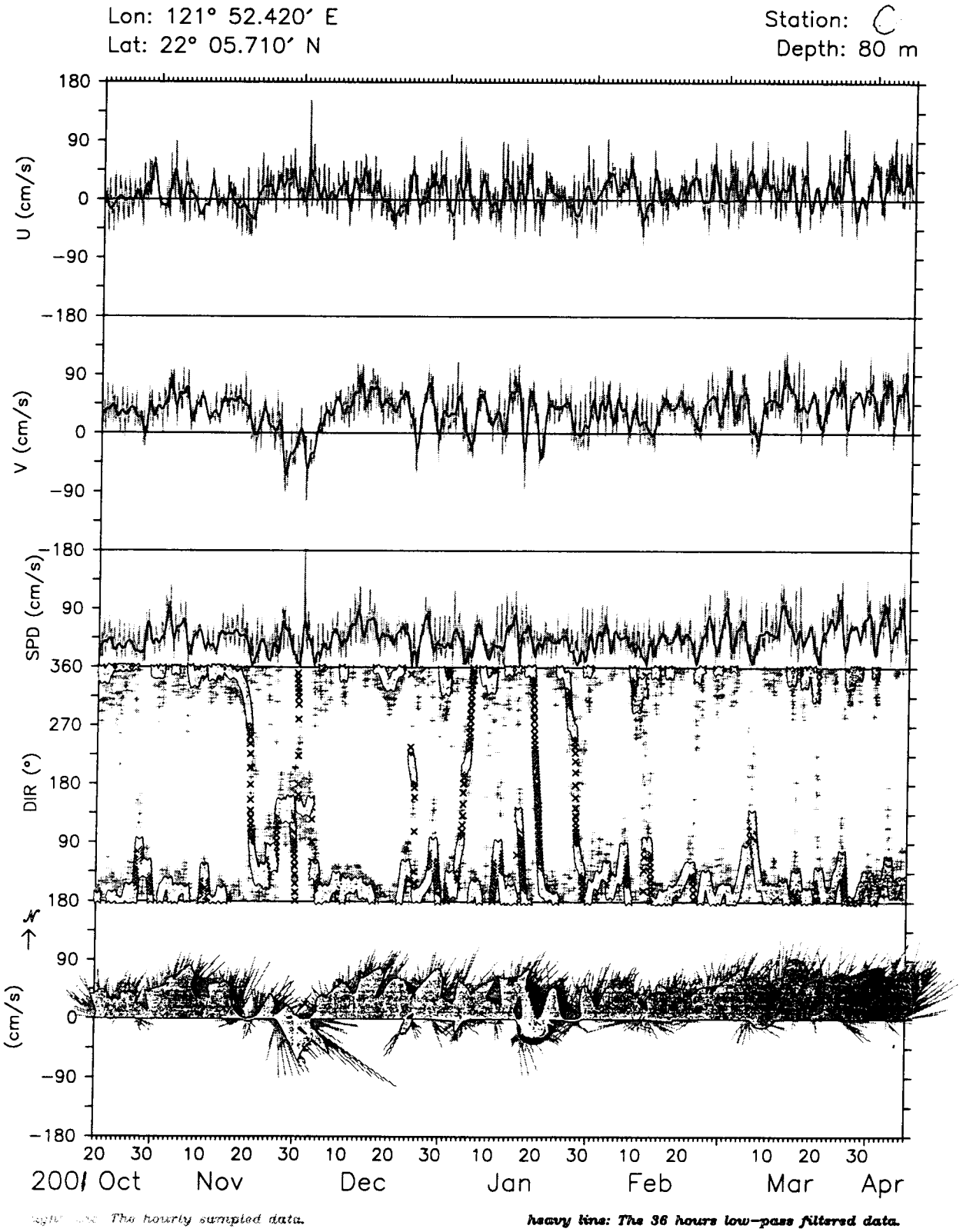
Lon: 121° 52.420′ E
Lat: 22° 05.710′ N
Station: C
Depth: 80 m
U (cm/s)
V (cm/s)
SPD (cm/s)
DIR (°)
(cm/s)
180
90
0
-90
-180
360
270
20 30 10 20 30 10 20 30 10 20 30 10 20 10 20 30
2001 Oct Nov Dec Jan Feb Mar Apr
The hourly sampled data.
heavy line: The 36 hours low-pass filtered data.

Figure 3-3

Current Vectors at 16m During Oct 11~16 1999

TOPEX/ERS-2 Analysis Oct 15 1999

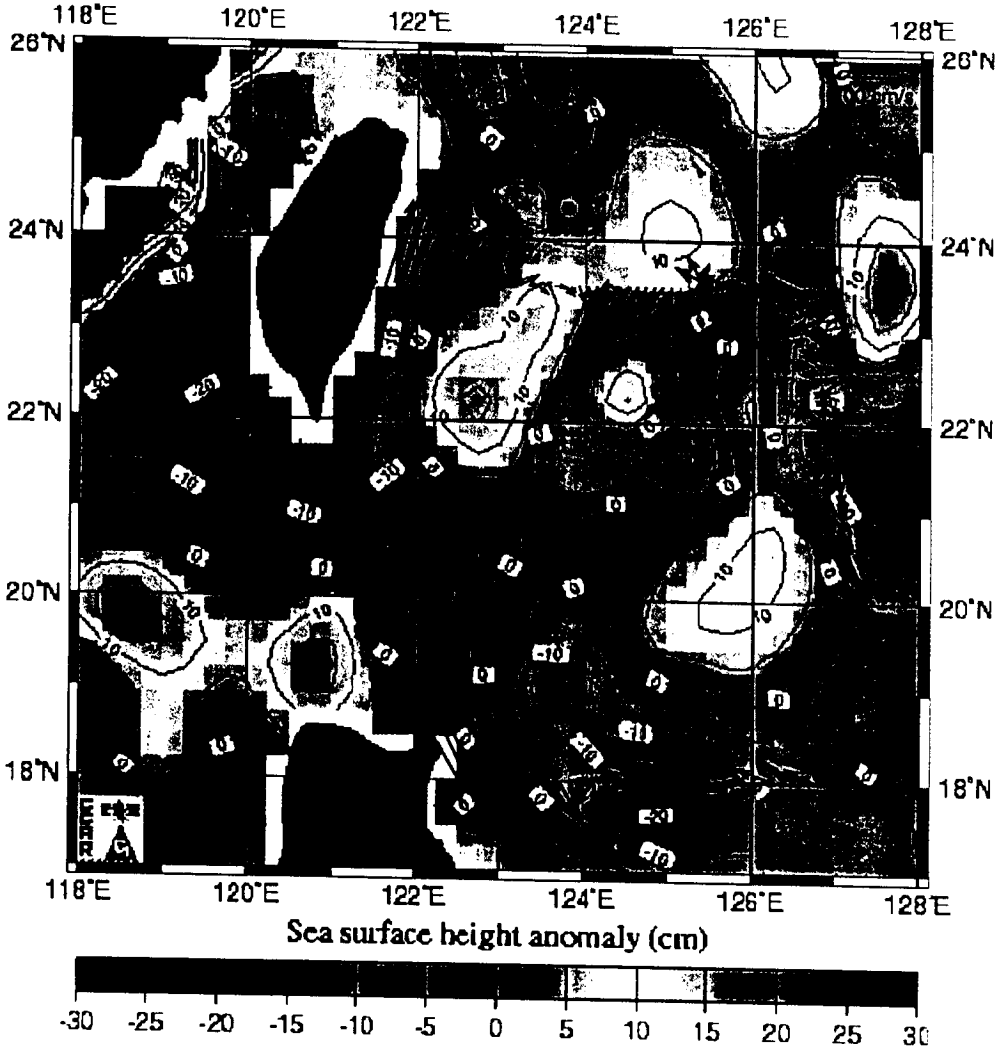

Current Vectors at 16m During Sep 3~9 2000

TOPEX/ERS-2 Analysis Sep 6 2000

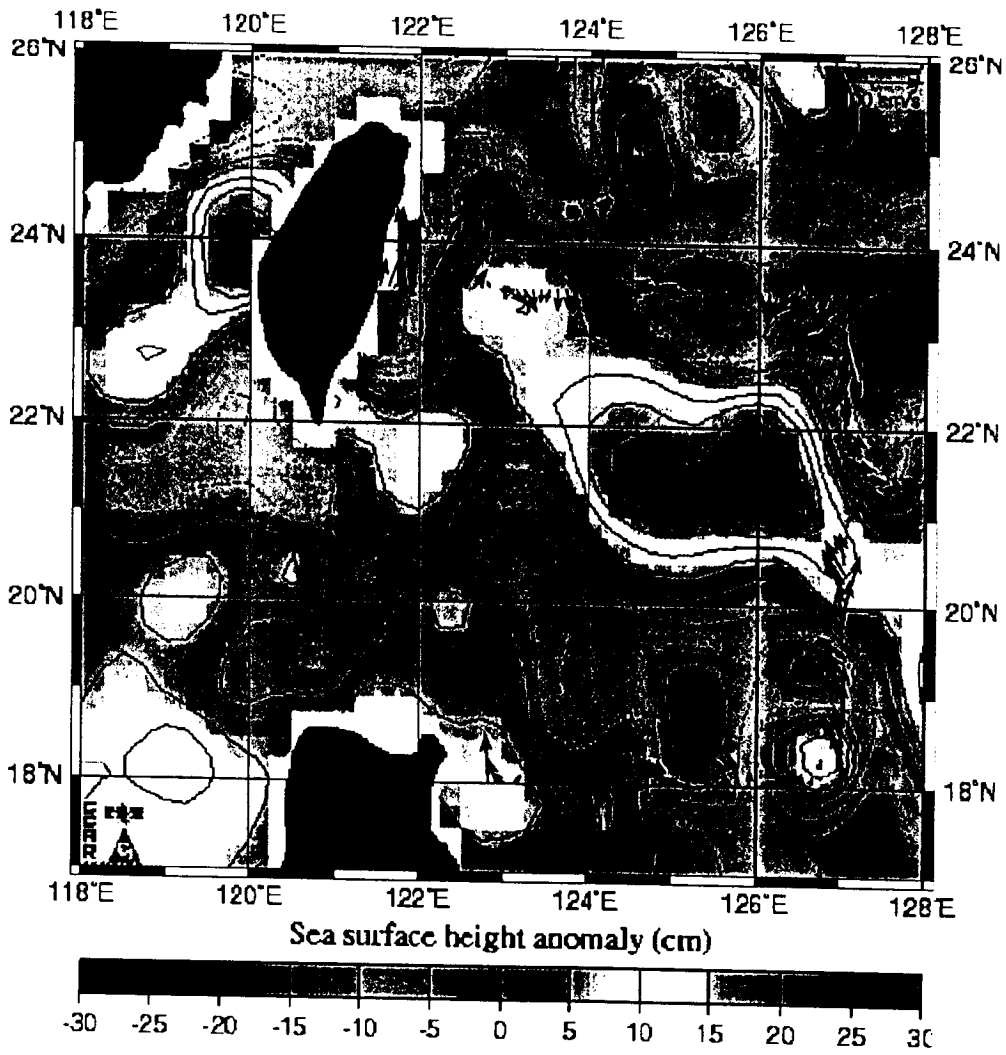

Figure 4-1

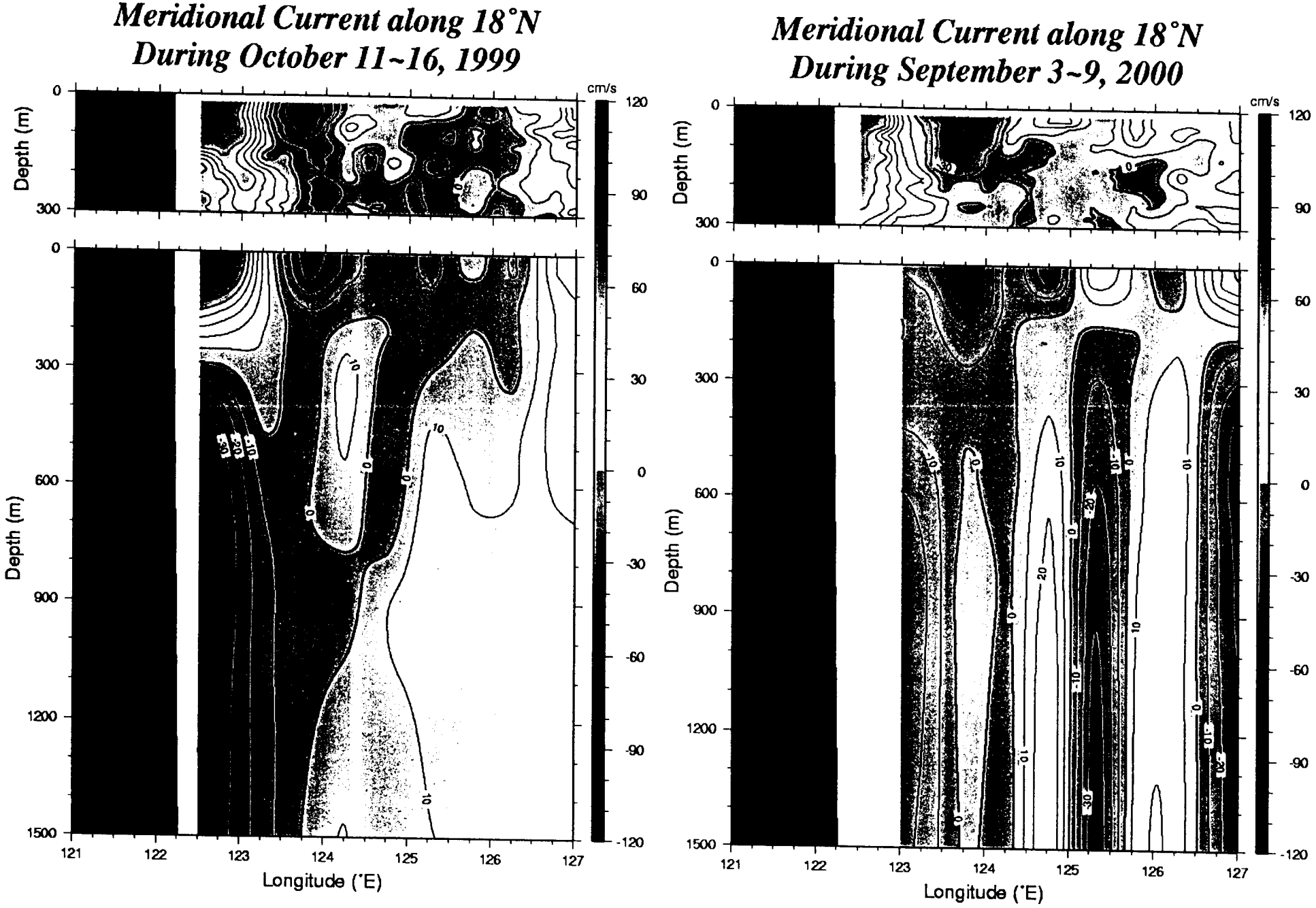
Meridional Current along 18°N
During October 11~16, 1999
Meridional Current along 18°N
During September 3~9, 2000
Depth (m)
Longitude (°E)
cm/s
120
90
60
30
0
-30
-60
-90
-120
0
300
600
900
1200
1500
121
122
123
124
125
126
127

Figure 4-2

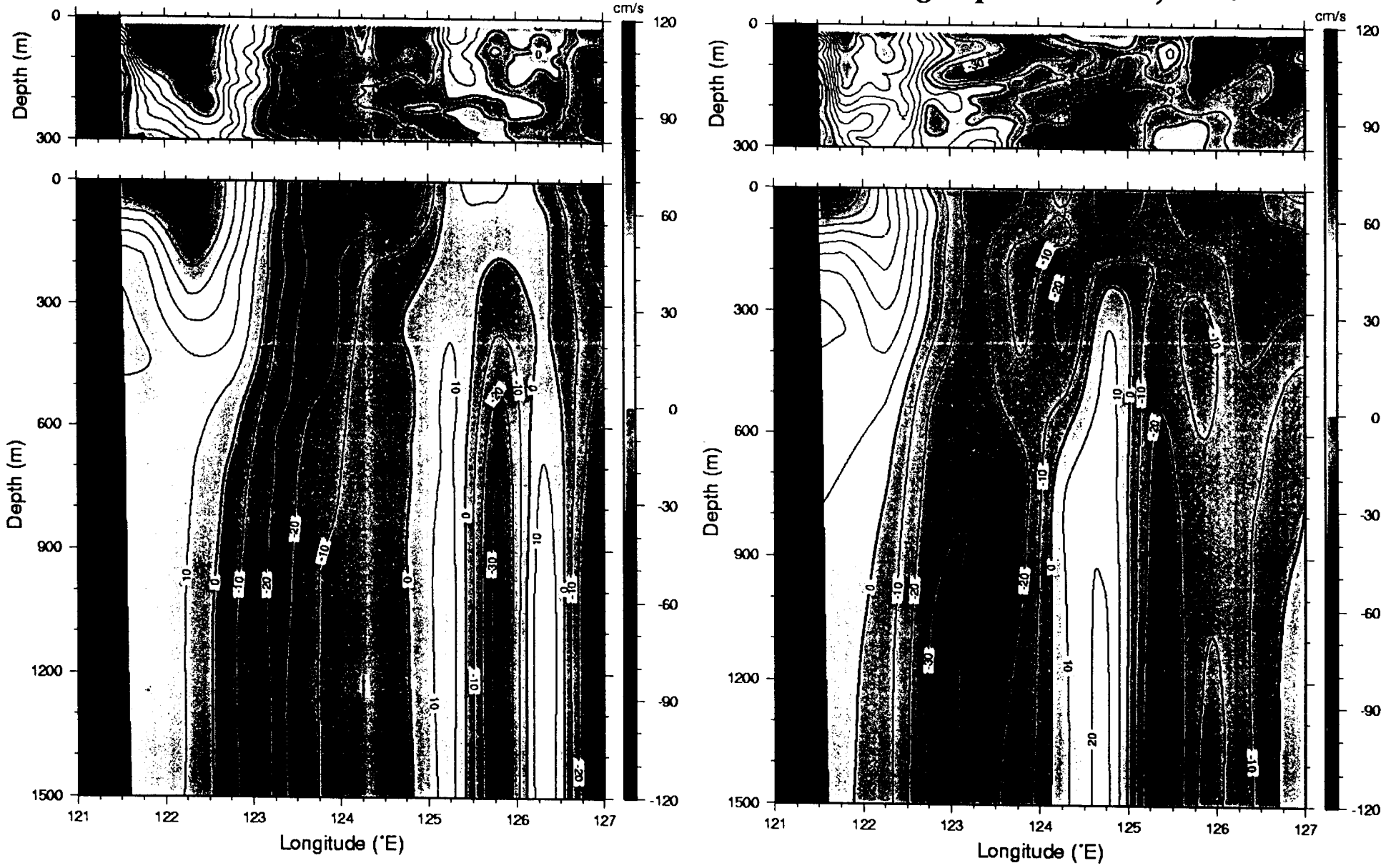
Meridional Current along 23.5°N
During October 11~16, 1999
Meridional Current along 23.5°N
During September 3~9, 2000
Depth (m)
Longitude (°E)
cm/s
0
300
600
900
1200
1500
121
122
123
124
125
126
127
120
90
60
30
0
-30
-60
-90
-120

Figure 4-3

Appendix I

Kuroshio Intrusion in the Luzon Strait

By

T. Y. TANG[1], W.-D LIANG[2], Y. J. YANG[3], and W.-S. CHUANG[1]

[1]*Institute of Oceanography, National Taiwan University, Taipei, Taiwan, ROC*
[2]*National Center for Ocean Research, Taipei, Taiwan, ROC*
[3]*Department of Marine Science, Chinese Naval Academy, Tsoying, Kaohsiung, Taiwan, ROC*

Submitted to Journal of Physical Oceanography

October 2002

ABSTRACT

Three Acoustic Doppler Current Profilers (ADCP) were deployed in the central Luzon Strait to monitor current velocity. The duration of deployment varied with location and spanned from 1997 to 1999. The observed current velocity indicated that the Kuroshio consistently intruded into the South China Sea. The current velocity demonstrated small annual variation, but large intraseasonal variation. The change of monsoons, from northeast to southwest, did not cause noticeable variation in current velocity.

The Miami Isopycnic Coordinate Ocean Model (MICOM) forced by the wind data provided by the European Centre for Medium-Range Weather Forecasts (ECMWF) was used to interpret the observed current velocity. Comparison between the model output and observation validates the use of the model result in interpreting annual and interannual current velocity variation in the Luzon Strait. The numerical model result also shows that the Kuroshio consistently intruded into the South China Sea, displaying a noticeable annual variation in the central Luzon Strait. The large interannual variation masked the annual variation so that the annual variation was difficult to observe. The interaction between the Kuroshio and the South China Sea cyclonic flow caused the current velocity variation in the both the Luzon Strait and the northern sector of the South China Sea. In winter, the Kuroshio intrudes deeply into the South China Sea. In summer, the intruded

Kuroshio was primarily confined to the northern South China Sea.

The annual transport variation across the Luzon Strait is primarily westward. The eastward transport was found in summer during certain years when the Kuroshio intrusion was weak. In spite of the fact that the Kuroshio intruded consistently into the South China Sea, transport out of the South China Sea was observed. In summer, the current on the northern South China Sea shelf break contributed to the transport out. The variation in zonal transport was caused by the Sea Surface Height (SSH) variation occurring west of northern Luzon. Wind stress curl is responsible for this SSH variation. Kuroshio variation had little impact on the intrusion.

1. Introduction

The Luzon Strait is located between Taiwan and Luzon. It is the primary channel for exchanging water between the South China Sea and the North Pacific Ocean. The width of the Luzon Strait, from southern Taiwan to northern Luzon, is around 350 km. It is shallow at both the northern and southern ends and is deep in the central portion. The maximum water depth is over 2500 m. The topography is generally complicated in and around the Strait. A number of small islands are located at the southern end of the Luzon Strait. The water depth increases rapidly to the east and west of the Strait, where it meets the basins of the northern Pacific and South China Sea. A shelf break occurs northwest of the Luzon Strait, where the Taiwan Strait joins the South China Sea and the East China Sea. The current in the Luzon Strait might affect the flow in the Taiwan Strait and possibly even the East China Sea.

The Luzon Strait is the first large meridional gap for the principal North Pacific Western Boundary Current (the Kuroshio). Whether the northward Kuroshio leaps across the Luzon Strait or intrudes into the South China Sea through the Luzon Strait is an issue that has often drawn oceanographers' attention. Wyrtki (1961) and Nitani (1972) suggested that the Kuroshio intruded into the South China Sea when the northeast monsoon prevailed, halting when the southwest monsoon was dominant. This seasonal intrusion

feature was re-confirmed by many scientists. Levitus (1982) studied the Volunteer Observing Ship data (VOS); Shaw (1991) analyzed historical hydrographic measurements, and Farris and Wimbush (1996) examined satellite-derived Sea Surface Temperature (SST) images. All reached a similar conclusion; Kuroshio intrusion occurs seasonally. Shaw and Chao (1994) forced a numerical model based on the monthly climatological wind and also re-produced the above findings. Nevertheless, a few studies obtained different results. For example, Chu (2000) used the climatological hydrographic data to estimate intruded Kuroshio transport in the Luzon Strait. The transport varied seasonally, but was consistently westward, with the largest amount 13.7 Sv in February and the smallest amount 1.4 Sv in September. Using the historical temperature profiles, Qu (2000) obtained similar results; the transport was westward consistently, but with different estimated amounts of transport. The largest intruded volume was 5.3 Sv in January through February and the smallest intruded volume was 0.2 Sv in June through July. The numerical model produced by Metzger and Hurlburt (1996) displayed the features stated in the findings of Qu (2000).

The mechanisms causing Kuroshio intrusion have also been a subject of controversy. Stommel and Arons (1960) claimed that the western boundary current always intruded as it encountered a meridional gap since the β advection. Sheremet (2001) indicated that the

western boundary current could leap across the meridional gap when the gap is small or the inertia is large. He inferred that the Kuroshio intruded into the South China Sea in the season of northeast monsoon because the speed of the Kuroshio was weakened by the head wind. Analyzing the hydrographic measurements, Wang and Chern (1987) postulated that the Ekman transport, induced by the monsoon, could be important for Kuroshio intrusion. The current in the South China Sea could also be a factor affecting Kuroshio intrusion (Shaw and Chao, 1994). Qu (2000) and Metzger and Hurlburt (1996) concluded that Kuroshio intrusion in the Luzon Strait was primarily related to the meridional pressure gradient across the Strait. All of these controversies are primarily the result of insufficient data, especially in long-term moored current velocity measurements.

Liang et al. (2002) presented a composite current velocity, which was obtained from 10 years of Ship-board Acoustic Doppler Current Velocity Profilers (Sb-ADCP), positioned around Taiwan. The data revealed that the Kuroshio intruded into the South China Sea through the central Luzon Strait. The volume transport in the upper 300 m water column across the Strait was 3.3 Sv westwardly. The intruded Kuroshio interacted with the current in the South China Sea, forming a complicated spatial distribution west of the Luzon Strait. Liang et al. (2002) produced a few moored current velocity time series around the Luzon Strait, which indicated that the Kuroshio intrusion might be constant.

Similar, but more complete moored current velocity measurements are presented in this paper to study Kuroshio intrusion. The moored current velocities are used to examine the validation of outputs of the Miami Isopycnic Coordinate Ocean Model (MICOM; Bleck and Smith 1990; Bleck et al. 1992; Bleck and Chassignet 1994), which was forced by the European Centre for Medium-Range Weather Forecasts [ECMWF (1995)] wind. Using the model outputs, the factors causing Kuroshio intrusion are investigated. Since only monthly wind data was applied, the studies focus on the annual and interannual variations of Kuroshio intrusion in the Luzon Strait. This paper proceeds as follows. In Section 2, the moored current velocity in the Luzon Strait is presented. The Kuroshio intrusion is described. In Section 3, the scheme of the numerical model is stated and the observation and model output comparison is shown. The validation of model outputs is discussed. Section 4 states the annual and interannual evolutions of Kuroshio intrusion. The mechanisms causing such evolutions are examined. A discussion and summary are provided in Section 5.

2. Observation

Figure 1 shows the locations of 3 moorings (named L1, L2, and L3), their surrounding bathymetry, and the composite Sb-ADCP current velocity vectors at 30 m around Taiwan.

The asterisk indicates Lanyu Island, where the wind record was used. The moorings were located in the central portion of the Luzon Strait. L1 and L3 were 120 km away from the tips of southern Taiwan and northern Luzon, respectively. L2 is located between them. Moorings were located about 50 km from each other. The water depth at L2 was deepest (over 2000 m), with L1 and L3 depths of around 1300 m and 1650 m, respectively. The composite current velocities, adopted from Liang et al. (2002), indicate that L1 and L2 were located on the main path of Kuroshio intrusion, while L3 was positioned near the southern intrusion boundary. The duration of deployments varied with location. A few refurbishments had to be made during deployment. Table 1 lists the start and ending times, the depth of the instrument position, and local water depths for each deployment. The moorings in the Luzon Strait had a large vertical excursion, especially at L2, where the vertical excursion was occasionally greater than 200 m. The large vertical excursion was primarily caused by the high tidal current speed. The tidal current speed (recorded by VACM current meter and not shown) at 1100 m was nearly 100 cm s^{-1} during spring tide. An attempt was made to increase floatation in order to keep the mooring line upright. The mooring line broke and one mooring was lost. Fortunately, all of the moorings had small pitching and rolling angles. As a result, the moored ADCP transducers remained upright. At L2, the ADCP was kept at a much shallower depth than the range (around 300 m) of the

narrow-band ADCP. The design, in combination with the ADCP range being larger than the monitor range, made it possible to record the upper layer current velocities simultaneous with the depth correction. A SEACAT CTD was mounted immediately beneath the ADCP. It provided pressure data, which was used for the depth correction. Short time gaps occasionally occurred at the uppermost depths and were interpolated linearly. Fluctuations of horizontal speed caused by the vertical excursions were estimated. Assuming that the maximum vertical excursion was 300 m, the ADCP moved horizontally about 1054 m over half of the semidiurnal tidal period (6.21 hours) at a location where water depth was 2000 m. The estimated maximum horizontal speed caused by the vertical excursion was less than 10 cm s^{-1}. It would not significantly bias the large subtidal current velocity in the Luzon Strait.

Figure 2 shows the eastward (U) and northward (V) components of current velocity at L1, where water depth is 1300 m. The depth (30-220 m) average of U, V, and their velocity sticks time series are also shown. The time series was low-pass filtered to remove the fluctuations for frequencies higher than 0.0139 cycles per hour (cph). The data covers a period of 1.5 months in 1997 and nearly 12 months beginning April 1998. Westward velocity dominated in U. Eastward current was only apparent for short periods of time. The westward current had high speed (maximum around 70 cm s^{-1}) at the surface and

gradually decreased with depth. The seasonal change was vague. The transition of monsoons usually occurred in April and September (Chuang and Liang 1994) and had no significant impact on the U. Northward current dominated in the V. Southward current was rarely observed. The greatest V (maximum over 110 cm s^{-1}) occurred at the uppermost depth, decreasing with increasing depth. The V at depths below 200 m was generally less than 20 cm s^{-1}. The V was weak from December through February when the northeast monsoon gained full strength. The depth-averaged time series showed that the U and V fluctuated, but their variance spectra (not shown) had no significant peak in the specific frequency band. In general, the U had smaller amplitude than V. In a peak-to-peak comparison, the north and east component velocities frequently varied out of phase. The velocity sticks showed that the current at L1 moved primarily to the north-northwest, but was more westward as velocity stick amplitude decreased. The impact of typhoon on the current velocity was not clear. For example, the super Typhoon, Zeb (minimum surface pressure of 880 mbar), moved almost exactly along the mooring array in the Luzon Strait from south to north on October 14-16 of 1998. It only induced short-term velocity fluctuations in the upper ocean, and can be barely observed in the present figures.

The low-pass filtered U and V at L2 are shown in Fig. 3. L2 is near the center of the Luzon Strait where the water is deep (around 2200 m). The ADCP was mounted at depths

of 130 and 160 m for the two deployments in 1997, respectively. These depths were shallower than the range of the ADCP. The rationale for keeping the ADCP at shallow depth was explained above. Due to a mistake in mooring line length, the ADCP was deployed at deeper depths in 1998. The range of available current velocity was from 130 to 280 m. Nearly 9 months of current velocity data, obtained in 1997, was used to describe the upper ocean current velocity at L2. The current velocity obtained in 1998 was used as a reference. Like the current at L1, U and V at L2 were dominated by the westward and northward component velocities, respectively. Eastward and southward component velocities were rarely observed. The maximum speed was around 100 cm s^{-1} for both westward and northward component velocities. The greatest velocity occurred in the uppermost layer, decreasing with depth. The depth-averaged U and V had similar amplitudes. The current flowed primarily northwest, which was more westward than the current at L1. Peak-to-peak comparison indicated that the variations of V and U were frequently out of phase. Although the recorded velocity time series was shorter than a year, it covered the periods when the northeast and southwest monsoons were strong. No clear seasonal difference was found. For example, the velocity in January through February, when the northeast monsoon was dominant, showed little difference from the velocity in May through July, when the southwest monsoon prevailed. The variance spectra of U and

V showed no distinctive peak at any specific frequency band. The current fluctuated with various time scales. The velocity sticks indicated that the current usually flowed toward the northwest. The deeper current velocity, measured in 1998, was more northward than the shallower current velocity, measured in 1997. This dissimilarity might be caused by the difference in depth.

Figure 4 shows the low-pass filtered U and V at L3. The current velocity at L3 had quite different characteristics than it did at L1 and L2. The U was weak (maximum speed around 50 cm s^{-1}) and changed its sign repeatedly. The V, dominated by northward velocity, was also weaker (maximum speed less than 80 cm s^{-1}) than it was at the previous two stations. No seasonal preference was observed in either U or V. For all of the nearly 9-month record, the mean of U was near zero, while the mean of V was about 11 cm s^{-1} (northward). The depth (30-160 m) averaged current fluctuated with different time scales and different directions. However, the current was northward more often than not.

In combination with the moored current velocity and Sb-ADCP composite current velocity spatial distribution in the Luzon Strait, a conclusion can be drawn. The Kuroshio intruded consistently into the South China Sea through the central Luzon Strait. It had small annual variations. L1 and L2 were located in the main path of the Kuroshio intrusion. L3 appears to be a southern boundary of Kuroshio intrusion where the Kuroshio intrusion

was frequently observed to change to South China Sea outflow. Figure 5 shows the T-S diagrams at L1, L2, L3, the South China Sea and the upstream Kuroshio. An average of 5 CTD measurements (marked by asterisk in Fig. 5) west of Luzon represents the South China Sea water. An average of 3 CTD measurements (marked by cross in Fig. 5) northeast of Luzon represents the upstream Kuroshio. The Kuroshio was saltier and warmer than the South China Sea in the upper water column, but was less salty and colder in the lower water column. Two T-S curves intersected at σ_t = 25.66. The T-S curve at L3 was close to the South China Sea, but gradually moved closer to the curve of Kuroshio water as the location moved north. This finding provides extra evidence that L3 could be the southern boundary of the intruded Kuroshio. However, the T-S curves at 3 stations were notably different than T-S curves from the South China Sea and the Kuroshio. This result implies that the Kuroshio and South China Sea water mix vigorously in the Luzon Strait. The intense current could cause the water mixing.

The northeast-southwest (main) component wind velocity at Lanyu Island in 1997 is shown in Fig. 6. The positive/negative wind velocity flows to the northeast/southwest. The depth-average current velocity of U and V at L2 are also shown. Overall coherences (not shown) between the current and wind velocities were generally low. However, the peak-to-peak comparison shows that the current fluctuation coincided occasionally with

wind fluctuation. For example, the large southwesterly wind oscillation in early June corresponded to the variations in both U and V. Similar features were also found at L1 and L3, indicating that the local wind played a role, but not the only one.

3. Numerical model

a. Model description

The MICOM model was applied in the numerical simulation. It is a primitive equation numerical model that describes the evolution of momentum, mass, heat, and salt in the ocean, configured with realistic topography and stratification. In contrast to the traditional vertical coordinate of water depth in the level model, MICOM uses equations that have a coordinate of density in the vertical direction. The advantage of a layer model using density coordinate is that the system suppresses the diapycnal component of numerically caused dispersion of material and thermodynamic properties. This characteristic allows isopycnal models to avoid the artificial warming of deep-water masses, as has been shown to occur in level model applications (Chassignet et al. 1996).

The model domain includes the western Pacific and the South China Sea with boundaries at 20.8°S, 45.1°N and 95°E, 160°E (Fig. 7). The horizontal grid is defined on a Mercator projection with resolution given by 1/4° × 1/4°cosϕ (meridional × zonal), where

ϕ is the latitude. The vertical density structure has 15 isopycnic layers, topped by a Kraus-Turner mixed layer (Kraus and Turner 1967). The topography was interpolated from the ETOPO5 dataset (NOAA 1988). The model is spun up for 10 years from rest; with an initial thermohaline condition interpolated from the 1994 World Ocean Atlas (WOA94) (Levitus and Boyer 1994; Levitus et al. 1994) January temperature and salinity data. The model was forced by the climatological monthly atmospheric momentum, heat and freshwater flux. The momentum flux was calculated from 1985-1999 wind data provided by the ECMWF with the drag coefficient described in Trenberth et al. (1989). The heat flux, evaporation and precipitation were taken from the Comprehensive Ocean-Atmosphere Data Set (COADS) (da Silva et al. 1994). The layer thickness, temperature and salinity were relaxed to the climatology of the WOA94 monthly data in a 4° buffer zone at the borders of model domain. This 10-year spin up model was continuously forced using 1996-2001 ECMWF monthly wind data, while the heat and freshwater flux were still forced by the climatology.

b. Observation and model comparison

Figure 8 shows the comparison between the observation and model output of monthly average current velocity vectors at various depths and locations. The agreement between

model output and observation was good at L1, fair at L2, and poor at L3. The two velocities at L1 were almost identical in direction, but the observed current velocity had slightly larger amplitude than the model. At L2, good agreement was also found in the upper 100 m water columns in 1997. The model output velocity was only slightly more westward than the observed velocity. In the lower water column (130-240 m) in 1998, the two current velocities had noticeable differences in direction. The model output velocity was more westward. At L3, the direction difference between the two velocities became more pronounced. The observed current was primarily northward while the model output velocity was principally northwestward. Although the difference between the two velocities at L3 was noteworthy, for both, the speed was smaller than it was at L1 and L2. L3 is close to the margin of Kuroshio intrusion.

The comparison between model output and observed depth-averaged velocity time series at L1, L2, and L3 is shown in Fig. 9. A 5-day convolution average was applied to both observation and model output. In general, the model output and observation agree well in the low frequency variations at L1 and L2. Fluctuations with time scales of several days to months, were large in the observed velocity, but were not found in the model output. This could be related to the fact that the coarse grid and monthly wind were applied to the model. The mean velocities, calculated from model and observation, are nearly the same.

Only slight differences were found in V at L1 and U at L2. The annual variation was small for both model and observed velocities. Even with the assistance of model output, such small annual variation was not easily discernible. At L3, the model and observation had good agreement in the low frequency variation of V, but not U. The mean of observed U was nearly zero, while the mean of modeled U was -27 cm s^{-1}. In the model output, the Kuroshio consistently intruded into the South China Sea through L3. This disagreement could be due to the fact that islands in the southern Luzon Strait were not adequately represented in the model.

The above comparison both validates and limits the use of model output. Good agreement in low frequency variation allows us to use the model output to study annual and interannual variations. Conversely, the fact that model output lacks high frequency variations prohibits its use for study of the intraseasonal variation, observed in the Luzon Strait.

c. Model output

The current velocity distributions at 50 m depth in June and December obtained from the 10th year spin up model outputs in the region of 105°-130°E, 5°-25°N are shown in Fig. 10. The Sea Surface Height (SSH) of the model output is also shown. In June, the

westward North Equatorial Current (NEC) in the western Pacific was located primarily in the region of 10°-17°N. It separated into the northward Kuroshio and southward Mindanao Current around 13°N as it approached Mindanao. The Kuroshio flowed primarily northward along the eastern coast of the Philippines, bending into the Luzon Strait, after leaving Luzon, but not immediately after. The inertia effect might keep the swift Kuroshio flowing in its original direction when it first leaves its western continental boundary. Meanwhile, the eastward current in the southern Luzon Strait might prevent the Kuroshio from immediately intruding into the South China Sea. The eastward current originates from the central or southwestern South China Sea. A cyclonic flow, with double or tripe low-pressure (low SSH) centers, was observed west of the Luzon Strait. This cyclonic flow varied seasonally. It was weak and primarily confined to the northern South China Sea during the southwest monsoon season, while it was strong and became a basin-wide feature during the season of northeast monsoon. This cyclonic flow is referred to, hereafter, as South China Sea cyclonic flow. In the Luzon Strait, the Kuroshio separates into two branches. One branch curves slightly clockwise and then flows primarily northward and leaps across the Luzon Strait. The other branch intrudes into the South China Sea and gradually merges and then cycles with the South China Sea cyclonic flow. Only a small portion of the Kuroshio spilled over the shelf and entered the Taiwan Strait. The current in

the Taiwan Strait primarily originated from the northern South China Sea shelf break or even further south, from the eastern boundary of Vietnam.

The main feature of Kuroshio intrusion in December was similar to that in June, but with some noticeable differences. In December, the region of NEC greatly expanded northward and the origination of the Kuroshio moved slightly northward. The surface current velocity distributions, obtained from the World Ocean Circulation Experiment/Tropical Oceans Global Atmosphere (WOCE/TOGA) drifting buoys (Hansen and Poulain, 1996), also revealed the feature of seasonal expansion/contraction of the NEC in the western Pacific. The westward NEC reached the northern tip of Luzon. The Kuroshio immediately curves to the northwest, as it leaves Luzon. It again separates into two branches in the Luzon Strait. One leaps across the Strait. The other branch intrudes into the South China Sea and gradually merges with the South China Sea cyclonic flow. This cyclonic flow extends nearly basin-wide. A strong low-SSH appears west of northern Luzon and southern Luzon Strait. The intruded Kuroshio flows primarily with the South China Sea cyclonic flow into the central and southern South China Sea. A small portion of the intruded Kuroshio curves clockwise, flowing along the southern opening of Taiwan Strait. It either enters the Taiwan Strait or flows out through the southern tip of Taiwan added to the Kuroshio. The current on the northern South China Sea shelf break is weaker

in December than in June. The Kuroshio becomes an important source for current in the Taiwan Strait in December. It is noteworthy that the meridional gradient of the SSH across the Luzon Strait is larger in December than in June.

4. Kuroshio Intrusion

a. Current around the Luzon Strait

Focusing on Kuroshio intrusion, Figure 11 shows the current velocity distributions at 50 m and SSH around the Luzon Strait. The figure contains 20 panels, 5 rows by 4 columns. Four columns, from top to bottom, represent the current velocity on 15th of March, June, September and December, while 5 rows, from left to right, represent years 1997, 1998, 1999, 2000, and 2001. The current velocity distributions in 1997 are used to illustrate the annual evolution. The greatest Kuroshio intrusion into the South China Sea occurred in March. The South China Sea cyclonic flow with strong low SSH center was found immediately west of the southern Luzon Strait. The intruded Kuroshio flowed with the South China Sea cyclonic flow. A small portion of the Kuroshio spilled out, entering the Taiwan Strait. In June, the Kuroshio consistently intruded into the South China Sea and merged with the cyclonic flow. However, when the South China Sea cyclonic flow was weak and shifted to the west, the strength of the Kuroshio in the Luzon Strait weakened,

and the current on the northern shelf break of the South China Sea intensified. The westward shift of the South China Sea cyclonic flow opened a space that allowed a portion of intruded Kuroshio to turn clockwise south of the Taiwan Strait. This clockwise flow either entered into the Taiwan Strait or poured back into the Kuroshio. However, the main source of Taiwan Strait current was from the northern South China Sea shelf break. In September, the South China Sea cyclonic flow and low SSH moved further west. West of the Luzon Strait, the flow became complicated. The Kuroshio in the Luzon Strait also weakened, but it still intruded into the South China Sea. A large portion of intruded Kuroshio retroflexed in a clockwise motion, south of the Taiwan Strait, and then partially entered the Strait. Some exited the South China Sea by flowing out through the northern Luzon Strait. In December, the South China Sea cyclonic flow re-intensified itself, and expanded throughout the basin. The speed of the Kuroshio in the Luzon Strait increased, and the amplitude of the current in the northern South China Sea shelf break decreased. An annual cycle was completed. Obviously, the location and strength of South China Sea cyclonic flow has large impact on the annual variation of Kuroshio intrusion and the flow west of Luzon Strait. Although the pattern of annual evolution was basically repeated in subsequent years, there were some differences. The most visible difference was that the South China Sea cyclonic flow (or low SSH center) was much stronger in 1997 than in

1998, except for December. The weak SSH center regained its strength gradually from 1999-2001. This interannual variation of South China Sea Cyclonic flow caused the variation of Kuroshio intrusion and flow west of Luzon Strait. For example, the low SSH center was greatest and closest to Taiwan in March of 1997. It caused the Kuroshio to intrude more northward, directly impinging on the southern opening of the Taiwan Strait. The small anti-cyclonic flow that was consistently seen south of Taiwan Strait disappeared.

b. Volume Transport across Luzon Strait

Using the model output and taking a slice along 120.75°E from 18.5 to 22°N, the depth-averaged U in the upper 300 m water column and SSH as a function of time and latitude, are shown in Fig. 12. The 3 straight lines indicate mooring locations. The distribution of U in the Luzon Strait could be separated into 3 parts. The U at the northern and southern parts was essentially eastward, flowing out of the South China Sea. It was generally quite stable and the annual and interannual variations were small. The U in the central Luzon Strait varied annually as well as interannually. The westward current velocity was high in winter and low in summer. The model result suggests that annual variations at L2 should be obvious, but at L1 and L3, they might be difficult to discern. However, the annual variations could be hidden by the interannual variations. The annual

variations, even in the model output, were unclear in 1997 because of the large interannual variations. This might explain why the observations at L2 in 1997 did not reveal annual variations.

Both annual and interannual SSH variation was small in the northern Luzon Strait, and large in the central southern Luzon Strait, with the lowest and highest SSH generally appearing in November-December and July-August, respectively. For the interannual, the SSH appears to have had its lowest value early in 1997, increasing for the subsequent two winters, and finally decreasing again for the next two winters. The lowest SSH had no significant differences between 2000 and 2001. The position of the lowest SSH moved interannually, but only slightly. The development/ contraction of South China Sea cyclonic flow is related to these variations.

Integrating the modeled U in the upper 300 m along 120.75°E from 18.5 to 22°N, Figure 13 shows the time series of zonal transport across the Luzon Strait. The negative and positive values represent the westward and eastward transport, respectively. The zonal transport across the Luzon Strait displayed a clear annual variation. The massive westward Kuroshio intrusion occurred from November through December, when the SSH at the central southern Luzon Strait also reached its lowest value. Its maximum amplitude was over -6 Sv. The westward intrusion generally stopped, and even reversed in summer.

Eastward transport in summer was not only related to the reduction of Kuroshio, but was also related to the increased flow in the northern South China Sea shelf break. This shelf flow eventually worked its way out of the South China Sea through the northern Luzon Strait. The annual variation of zonal transport in the upper 300 m across the Luzon Strait generally varied from 0.2 to −5.4 Sv. The zonal volume transport also displayed an interannual variation. In 1997, the major westward intrusion was extraordinarily large through late March. No reversed zonal transport was found in the summer. Westward transport developed unusually small amplitude in winter. Large eastward transport observed in the summer of 1998. Since then, the annual evolutions in subsequent years were similar, but the transport gradually increased westwardly. In 2001, the eastward transport was barely seen in summer, and the amount of annual westward transport was close to that of 1997. The amplitude of interannual variation of zonal transport could reach as large as 3 Sv. The El Niño occurred in 1997 (Boulanger and Menkes 1999; McPhaden 1999; McPhaden and Yu 1999; Kutsuwada et al. 2002) and was predicted to occur in 2002 (CPC/NCEP 2002). Apparently, the interannual variation of zonal transport across the Luzon Strait may have a cycle with El Niño.

To explore the mechanism causing the variation of zonal transport across the Luzon Strait, the zonal Ekman transport across the Luzon Strait was calculated first using the

ECMWF wind stress. Figure 14 shows the principle component (northeast-southwest) of ECMWF wind stress at the center of the Luzon Strait and zonal Ekman transport across the Luzon Strait. The wind stress varied annually, as well as interannually. The northeast monsoon, prevalent from September through April, displayed larger amplitude than the southwest monsoon, which was dominant from May through August. The monsoon was weaker starting in the late El Niño Year (1997) and remained weak for about one year. These variations have been described in detail by several oceanographers, including, Chao and Shaw (1996), Liang et al. (2000), etc. The zonal Ekman transport, calculated directly from the wind stress, also varied annually as well as interannually. It had good correlation with the total zonal transport, but its amplitude was much smaller. The contribution of Ekman transport to the total zonal transport was generally less than 15%, which is close to the estimate of Qu (2000). Obviously, some other mechanism is important for causing the zonal transport variation across the Luzon Strait.

Figure 15 shows the SSH west of the southern tip of Taiwan (marked as A), SSH west of the northern tip of Luzon (marked as B) and SSH differences between A and B. The SSH at A had little variation; while at B it displayed clear annual and interannual variation. Consequently, the difference of SSH between A and B also showed annual and interannual variation. The variation of SSH differences correlates (correlation coefficient is 0.9) well

with the modeled zonal transport across the Luzon Strait. The SSH difference varied from 0 to 26 cm. It could generate the zonal geostrophic transport having the same order of the modeled zonal transport across the Luzon Strait. Apparently, the meridional pressure gradient across the Luzon Strait was the primary factor causing the intrusion of Kuroshio. Qu (2000) and Metzger and Hurlburt (1996) had similar findings. However, the present finding indicates that the SSH difference was mainly due to low SSH north of Luzon. A conclusion, similar to the previous one, could be reached. The location and strength of South China Sea cyclonic flow (or low SSH center) has great impact on the Kuroshio intrusion across the Luzon Strait.

5. Discussion and summary:

Figure 16 shows the meridional volume transports south (along 18.5°N from 122°E to 125°E) and north (along 22.5°N from 121°E to 124°E) of the Luzon Strait, respectively. The former is treated as the transport of the upstream Kuroshio before it entered the Luzon Strait. The latter is regarded as the transport of Kuroshio after it left the Luzon Strait. Both time series displayed large interannual and intraseasonal variation, but small annual variation. They were quite different characteristics than time series of zonal transport across the Luzon strait. The coherence between the meridional and zonal transport was

low (not shown). The transport of upstream Kuroshio was greatest early in 1997. Theoretically, the swifter Kuroshio causes less zonal intrusion because of the larger inertia effect (Sheremet, 2001). Conversely, the zonal intrusion was greatest early in 1997. These results indicate that the variation of Kuroshio may have little impact on the zonal Kuroshio intrusion across the Luzon strait. It is noted that the meridional transport increased after it crossed the Luzon Strait. The eastward transport across the Luzon Strait in summer and the westward flow east of Kuroshio are the resources for such increase.

The low SSH west of Luzon was primarily related to the wind stress curl, which was largest around November and smallest (turning to negative) around August. The positive wind stress curl caused the water divergence, depressed SSH and cooled upper ocean heat content. Liang et al. (2000) found that the correlation between the wind stress curl and upper 300 m ocean heat content in the South China Sea is highest (correlation coefficient is over 0.8) west of Luzon. However, the wind stress curl and upper 300 m ocean heat content was almost uncorrelated south of the Taiwan Strait. This could illustrate that the SSH had little seasonal variation south of Taiwan Strait while the wind stress curl did display seasonal variation. The pressure gradient (or even the Kuroshio intrusion) across the Luzon Strait is primarily caused by the low SSH center (South China Sea cyclonic flow) west of Luzon.

In summary, the current velocities, recorded by the three ADCPs in the Luzon Strait, indicate that the Kuroshio consistently intruded into the South China Sea through the central Luzon Strait. The observed current velocity had large intraseasonal, but small annual variation. The local wind is not the only factor causing these fluctuations. The observation validated the results of MICOM forced by the wind data provided by the ECMWF. The model confirmed that the Kuroshio intruded consistently into the South China Sea through the central Luzon Strait. The intrusion varied annually as well as interannually. The large interannual variation, which occurred in 1997-1998, made the annual variation indistinct and almost indiscernible in the observed current velocity. The Kuroshio intruded deeply into the South China Sea when the South China Sea cyclonic flow became a basin-wide feature, which primarily occurred during the northeast monsoon period. In the southwest monsoon period, the cyclonic flow was primarily confined to the northern South China Sea. The intruded Kuroshio was also confined to the northern South China Sea.

The zonal transport across the Luzon Strait varied annually, as well as interannually. It was primarily westward. Eastward transport was only observed in summer of certain years. When eastward transport occurred, the Kuroshio still intruded into the South China Sea but was weak. The current on the northern South China Sea shelf break flowing out of

the South China Sea through the northern Luzon Strait exceeds the Kuroshio intrusion. The annual and interannual variations of zonal transport correlated with the meridional pressure gradient across the Luzon Strait. The pressure gradient varied primarily with the SSH west of northern Luzon. The wind stress curl is responsible for that SSH variation. The interannual variation of Kuroshio intrusion might have a cycle with El Niño.

Acknowledgements

This study was supported by the National Science Council, Taiwan, ROC, under grant NSC 89-2611-M-002-023-OP2, NSC 89-2611-M-002-031-OP2, and NSC 90-2611-M-012-001-OP2. The authors would like to acknowledge the RSMAS/MPO, University of Miami, for opening the source code of MICOM. The data processing and graphic plots have greatly benefited from the use of FERRET and GMT developed by NOAA's Pacific Marine Environmental laboratory and SOEST, University of Hawaii, respectively. The bathymetry and hydrographic data were offered by the Ocean Data Bank, National Center for Ocean Research, Taiwan, ROC. The assistance of the captain and crews of the R/V Ocean Researcher I are greatly appreciated. We also want to thank Mr. Wen-Hwa Ho for the mooring preparation.

References

Bleck, R., and L. T. Smith, 1990: A wind-driven isopycnic coordinate model of the North and Equatorial Atlantic Ocean. 1: Model development and supporting experiments. *J. Geophys. Res.*, **95**, 3273-3285.

——, C. Rooth, D. Hu, and L. T. Smith, 1992: Salinity-driven thermocline transients in a wind and thermohaline-forced isopycnic coordinate model of the North Atlantic. *J. Phys. Oceanogr.*, **22**, 1486-1505.

——, and E. Chassignet, 1994: Simulating the oceanic circulation with isopycnic-coordinate models. In: Majundar, S.K. (Ed.), The Oceans: Physical-Chemical Dynamics and Human Impact, 17-39.

Boulanger, J.-P., and C. Menkes, 1999: Long equatorial wave reflection in the Pacific Ocean from TOPEX/Poseidon data during the 1992-1998 period. *Climate Dyn.*, **15**, 205-225.

Chao, S.-Y., P.-T. Shaw, and S. Y. Wu, 1996: El Niño Modulation of the South China Sea Circulation. *Prog. Oceanogr.*, **38**, 51-93.

Chassignet, E. P., L. T. Smith, R. Bleck, and F. O. Bryan, 1996: A model comparison: Numerical simulations of the North Atlantic oceanic circulation in depth and isopycnic coordinates. *J. Phys. Oceanogr.*, **26**, 1849-1867.

Chu, P. C., and R. Li, 2000: South China Sea Isopycnal-Surface Circulation. *J. Phys. Oceanogr.*, **30**, 2419-2438.

Chuang, W.-S. and W.-D. Liang, 1994: Seasonal variability of intrusion of the Kuroshio water across the continental shelf northeast of Taiwan. *J. Oceanogr.*, **50**, 531-542

CPC/NCEP, 2002: El Niño/Southern Oscillation (ENSO) diagnostic discussion. NOAA, Climate Prediction Center/NCEP, MD, 1 pp

da Silva, A. M., C. C. Young, and S. Levitus, 1994: *Atlas of surface marine data 1994*. Vol. 1: *Algorithms and Procedures*. NOAA Atlas NESDIS 8, U.S. Department of Commerce, NOAA, NESDIS, 83 pp.

ECMWF, 1995: User Guide to ECMWF products. Meteorological Bulletin M3.2, 71 pp

Farris, A. and M. Wimbush, 1996: Wind-induced Kuroshio intrusion into the South China Sea. *J. Oceanogr.*, **52**, 771-784.

Hansen, D.V. and P.M. Poulain, 1996: Quality Control and Interpolation of WOCE/TOGA drifter data, *J. Atmos. Oceanic Technol.*, **13**, 900-909.

Kraus, E. B., and J. S. Turner, 1967: A one-dimensional model of the seasonal thermocline: II. The general theory and its consequence. *Tellus*, **19**, 98-106.

Kutsuwada, K. and M. J. McPhaden, 2002: Intraseasonal Variations in the upper equatorial Pacific Ocean prior to and during the 1997-98 El Niño. *J. Phys. Oceanogr.*, **32**,

1133-1149.

Levitus, S., 1982: *Climatological atlas of the World Ocean.* NOAA Professional Paper No. 13, U.S. Government Printing Office, Washington, DC, 173 pp.

——, and T. P. Boyer, 1994: *World Ocean Atlas 1994.* Vol. 4: *Temperature*, NOAA Atlas NESDIS, 117 pp.

——, R. Burgett, and T. P. Boyer, 1994, *World Ocean Atlas 1994.* Vol. 3: *Salinity*, NOAA Atlas NESDIS, 99 pp.

Liang, W.-D., J. C. Jan, and T. Y. Tang, 2000: Climatological wind and upper ocean heat content in the South China Sea. *Acta Oceanogr. Taiwanica* , **38**, 91-114.

——, T. Y. Tang, Y. J. Yang, M. T. Ko, and W.-S. Chuang, 2002: Upper ocean current around Taiwan. *Deep-Sea Res. Part II.* (accepted)

McPhaden, M. J., 1999: Genesis and evolution of the 1997-98 El Niño. *Science.*, **283**, 950-954.

——, and X. Yu, 1999: Equatorial waves and the 1997-98 El Niño. *Geophys. Res. Lett.*, **16**, 2961-1964.

Metzger, E. J., and H. E. Hurlbert, 1996: Coupled dynamics of the South China Sea, the Sulu Sea, and the Pacific Ocean. *J. Geophys. Res.*, **101**, 12 331-12 352.

Nitani, H., 1972: Beginning of the Kuroshio. In: *Kuroshio, its physical aspects*, H. Stommel and K. Yoshida, editors, University of Tokyo Press, Tokyo, 129-163.

NOAA, 1988: ETOPO5 digital relief of the Surface of the Earth. Data Announcement 88-MGG-02, NOAA, National Geophysical Data Center, Boulder, CO, 1 p.

Qiu, B., and R. Lukas, 1996: Seasonal and interannual variability of the North Equatorial Current, the Mindanao Current, and the Kuroshio along the Pacific western boundary. *J. Geophys. Res.*, **101**, 12 315-12 330.

Qu, T., 2000: Upper-layer circulation in the South China Sea. *J. Phys. Oceanogr.*, **30**, 1450-1460.

Shaw, P.-T., 1991: The seasonal variation of the intrusion of the Philippine Sea Water into the South China Sea. *J. Geophys. Res.*, **96**, 821-827.

——, and S.-Y. Chao, 1994: Surface circulation in the South China Sea. *Deep Sea Res.*, **41**, 1663-1683.

——, ——, K.-K. Liu, S.-C. Pai, and C.-T. Liu, 1996: Winter Upwelling off Luzon in the Northeastern South China Sea. *J. Geophys. Res.*, **101**, 16 435-16 448.

Sheremet, V. A., 2001: Hysteresis of a western boundary current leaping across a gap. *J. Phys. Oceanogr.*, **31**, 1247-1259.

Stommel, H., and A. B. Arons, 1960: On the abyssal circulation of the world ocean - I. Stationary planetary flow patterns on a sphere. *Deep-Sea Res.*, **6**, 140-154.

Trenberth, K. E., J. G. Olson, and W. G. Large, 1989: A global ocean wind stress

climatology based on ECMWF analyses, *NCAR Tech. NOTE NCAR/TN-338+STR*, Natl. Cent. For Atmos. Res., Boulder, Colo., 93 pp.

Wang, J., and C. S. Chern, 1987: The warm-core eddy in the northern South China Sea, I. Preliminary observations on the warm-core eddy. *Acta Oceanogr. Taiwanica* , **18**, 92-103. (in Chinese with English abstract)

Wyrtki, K., 1961: Physical oceanography of the southeast Asian Waters, NAGA Rep. 2, Scripps Institution of Oceanography, La Jolla, CA , 195 pp.

Table Lists

TABLE 1. Mooring locations, instrument and water depths, and durations at L1, L2, and L3, respectively.

Station	Location	Water depth	Instrument depth	Duration
L1	120° 56.0'E 20° 48.5'N	1288 m	282 m	1997/08/05-1997/09/12
L1	120° 56.4'E 20° 47.7'N	1313 m	290 m	1998/04/21-1998/06/11
L1	120° 56.4'E 20° 47.8'N	1319 m	328 m	1998/06/15-1999/04/07
L2	120° 54.5'E 20° 19.9'N	2057 m	193 m	1996/12/28-1997/08/05
L2	120° 54.3'E 20° 20.5'N	2011 m	199 m	1997/08/06-1997/09/12
L2	120° 54.9'E 20 19.7'N	2100 m	250 m	1998/06/15-1998/10/03
L3	120° 56.4'E 19° 48.7'N	1645 m	197 m	1996/12/28-1997/09/13

Figure Captions

Fig. 1. Locations of ADCP moorings (solid circle) and wind record station (asterisk) used in this study. The bathymetry is color shaded. It is overlaid on the composite Sb-ADCP current velocity vectors at 30 m from Liang et al. (2002). The reference vector is 100 cm s^{-1}. Regions A and B show the area of average used in Fig. 15.

Fig. 2. Time series of current velocity observed at L1. (a) U (dashed line), V (thick solid line) components and stick diagram (thin solid vector) of the depth-averaged (from 30 to 220 m) current velocity are shown. Vertical sections of (b) U and (c) V components of current velocity are shown in the middle and bottom panels, respectively. Contour interval is 50 cm s^{-1}. The time series was low-pass filtered to remove the fluctuations, for frequencies higher than 0.0139 cph.

Fig. 3. Same as Fig. 2 except at L2. The range of depth average is from 20 m to 120 m in 1997 and from 140 m to 240m in 1998.

Fig. 4. Same as Fig. 2 except at L3. The range of depth average is from 20 m to 160 m.

Fig. 5. T-S diagram at L1, L2, L3, the South China Sea, and the upstream Kuroshio: Dashed line: L1, dash-dotted line: L2, dotted line: L3, thin line: South China Sea, and thick line: Kuroshio. The inset shows the locations.

Fig. 6. Northeast-southwest component wind velocity (thick line) at Lanyu Island is shown. The depth-averaged current velocity (same as Fig. 3a) at L2 is also shown. A 5-day convolution average was applied to both wind and current velocity.

Fig. 7. Domain of MICOM model used in this study. The land is shaded as black. The minimum depth of ocean is 50 m. Open ocean boundary includes about 4° sponge area.

Fig. 8. Comparisons between the monthly average velocity vectors of the observation (thick vector) and model result (thin vector) at (a) L1, (b) L2, and (c) L3 are shown.

Fig. 9. Comparisons between the depth-averaged current velocity of the observation and model result at (a) L1, (b) L2, and (c) L3 are shown. The thin and dotted lines are the U and V component of observed depth-averaged current velocity, respectively. The thick and dashed lines are the U and V component of model result, respectively. The ranges of depth average are the same as Fig. 2a, 3a, and 4a, except that a 5-day convolution average was applied to both observation and model results.

Fig. 10. Current velocity (vector stick) at 50 m and sea surface height (color filled area)

on 15th of (a) June and (b) December from the 10th spin up model results are shown.

Fig. 11. Same as Fig. 10 except for the results of the model started from the 10th spin up model results and continually forced by the 1997-2001 monthly mean momentum flux. Current velocities at depth 50m and SSHs in 1997-2001 are shown in (a)-(e), respectively. From top to bottom, it is shown for the 15th of March, June, September, and December.

Fig. 12. (a) Depth-averaged U in the upper 300 m water column, (b) SSH of model results along 120.75°E from 18.5°N to 22°N are shown. A 5-day convolution average was applied to both. Shaded areas show the positive value. Contour intervals are 10 cm s^{-1} and 5 cm in (a) and (b), respectively. The 3 straight lines indicate mooring locations.

Fig. 13. Zonal volume transport along 127.5°E of model results in the upper 300 m water column between 18.5°N and 22°N is shown. A 5-day convolution average was applied. Negative and positive values represent the westward and eastward transport, respectively.

Fig. 14. Time series of (a) northeast-southwest component of ECMWF wind stress at L2 and (b) zonal Ekman volume transport along 120.75°E between 18.5°N and

22°N. A 30-day convolution average was applied to all.

Fig. 15. Time series of (a) SSH of model results at A , (b) SSH of model results at B, (c) the SSH difference between A and B. A 5-day convolution average was applied to all. The locations of A and B are show in Fig. 1.

Fig. 16. Meridional volume transports (a) along 18.5°N from 122°E to 125°E and (b) along 22.5°N from 15°N to 18°N of model results are shown. A 5-day convolution average was applied to both.

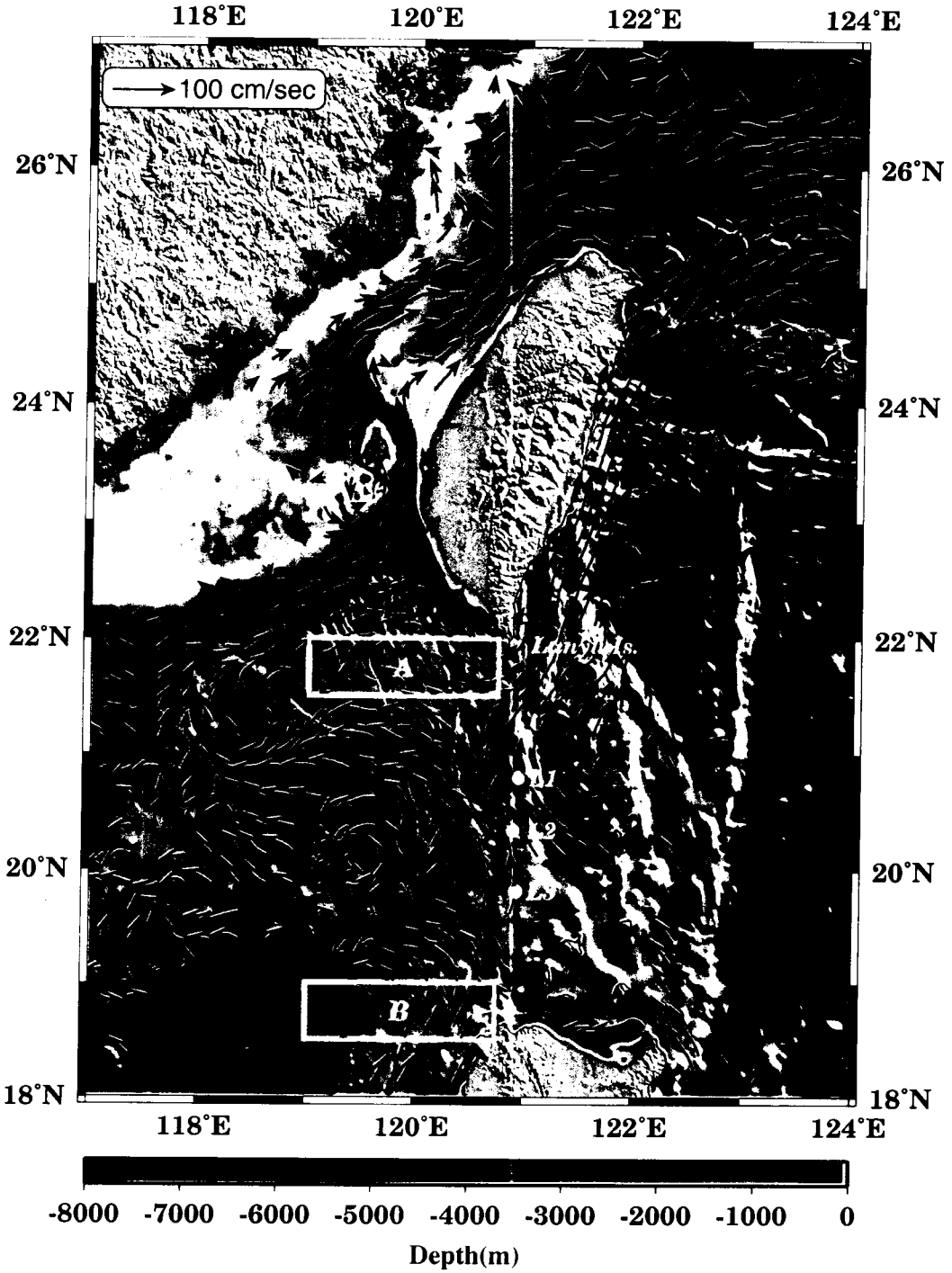
118°E
120°E
122°E
124°E
100 cm/sec
26°N
24°N
22°N
20°N
18°N
A
B
Lanyu Is.
-8000 -7000 -6000 -5000 -4000 -3000 -2000 -1000 0
Depth(m)

Fig. 1

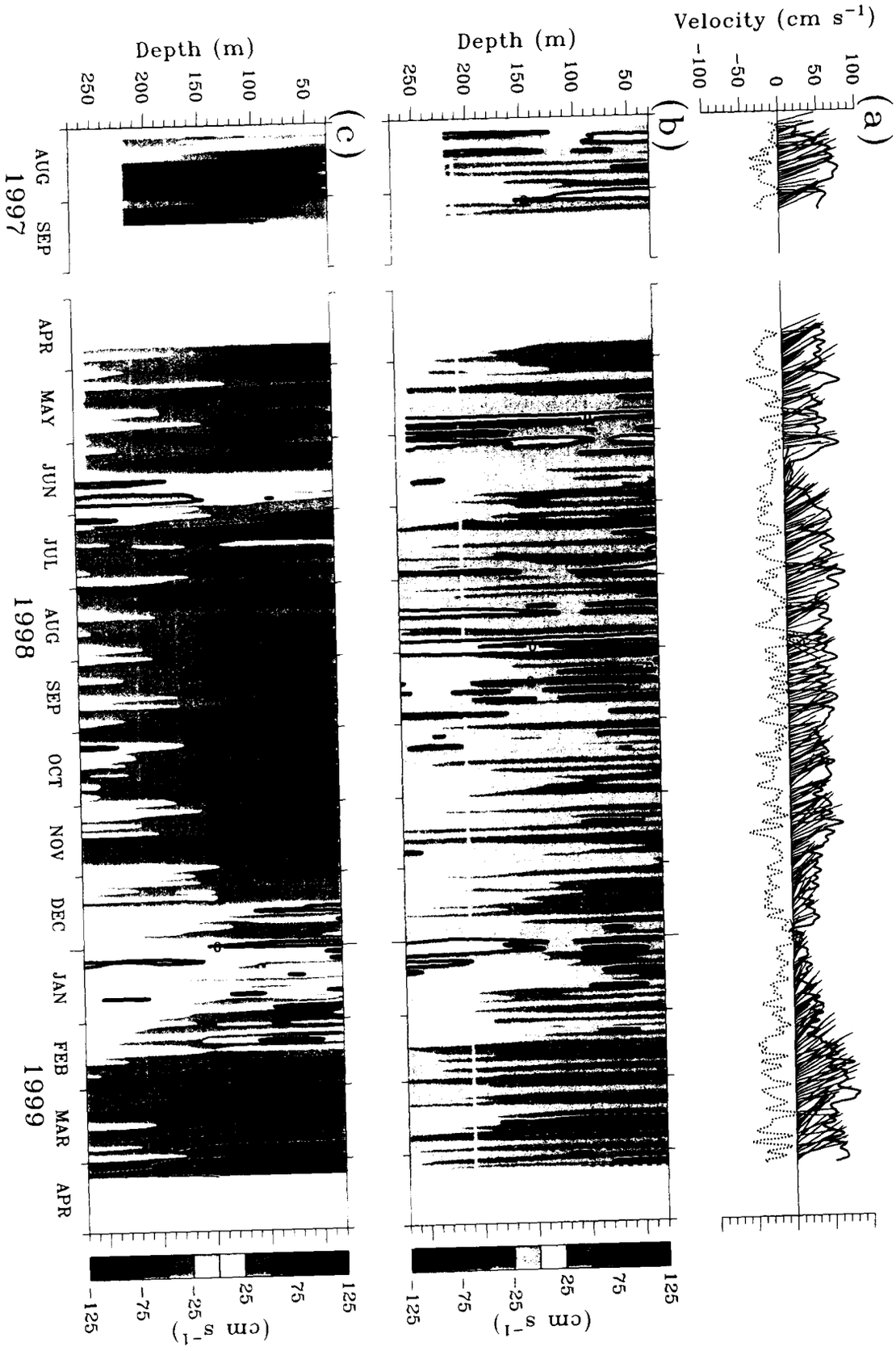
Velocity (cm s^{-1})
−100
−50
0
50
100
(a)
Depth (m)
250
200
150
100
50
(b)
(c)
AUG
SEP
1997
APR
MAY
JUN
JUL
AUG
SEP
OCT
NOV
DEC
JAN
FEB
MAR
APR
1998
1999
−125
−75
−25
25
75
125
(cm s^{-1})

Fig. 2

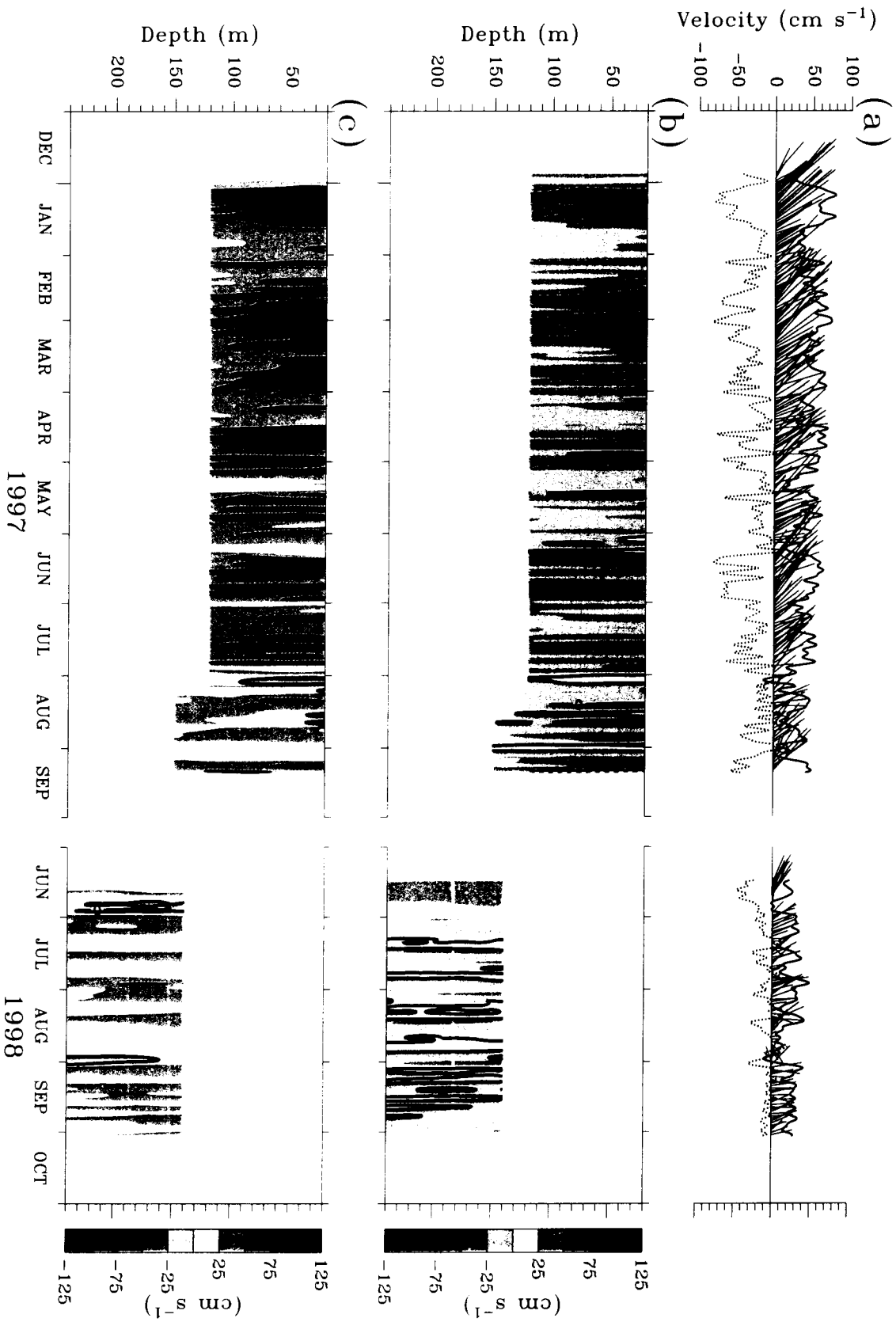
Velocity (cm s^{-1})
-100
-50
0
50
100
(a)
Depth (m)
200
150
100
50
(b)
(c)
DEC
JAN
FEB
MAR
APR
MAY
JUN
JUL
AUG
SEP
1997
JUN
JUL
AUG
SEP
OCT
1998
-125
-75
-25
25
75
125
(cm s^{-1})

Fig. 3

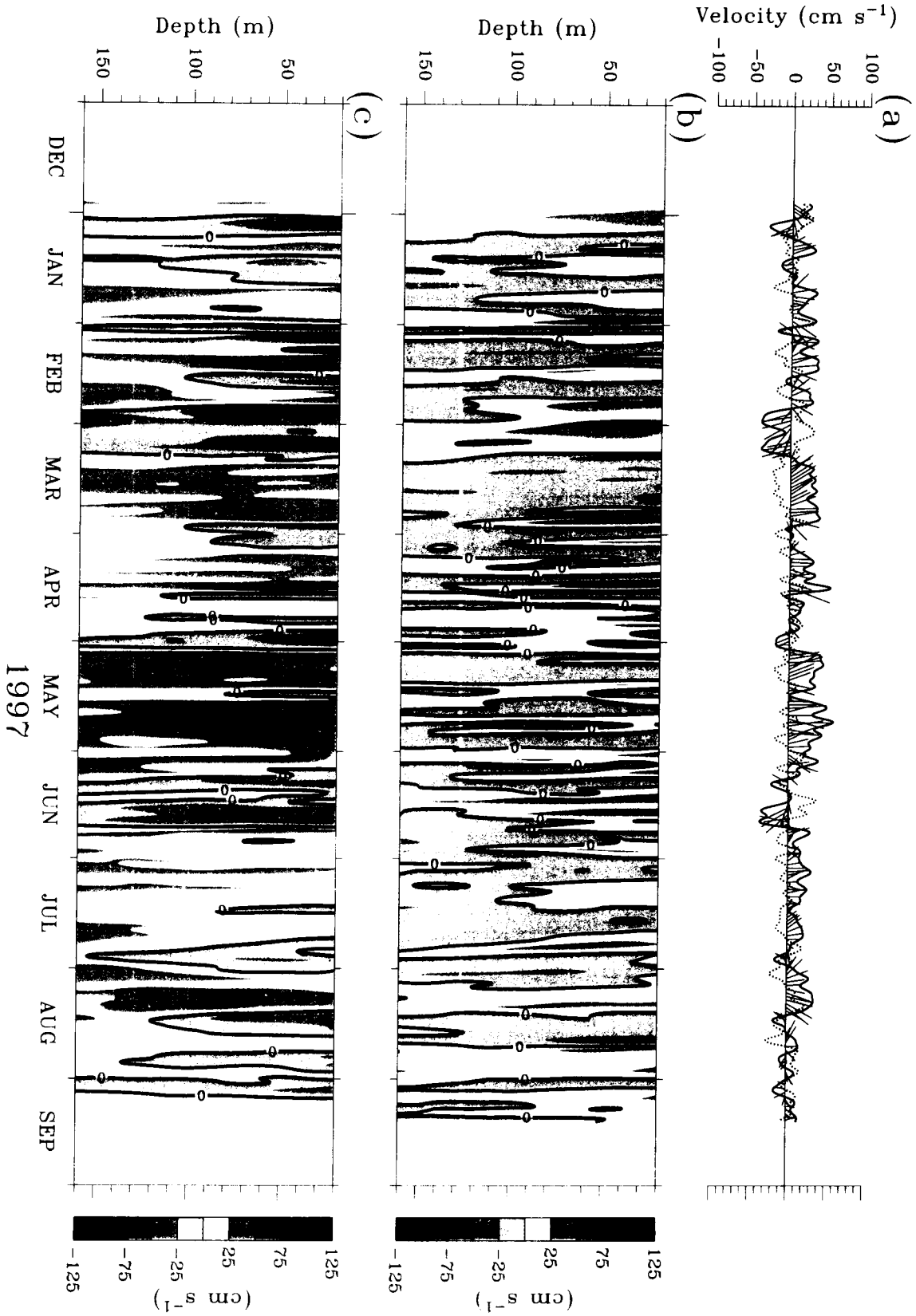
Velocity (cm s^{-1})
−100
−50
0
50
100
(a)
Depth (m)
150
100
50
(b)
(c)
DEC
JAN
FEB
MAR
APR
MAY
JUN
JUL
AUG
SEP
1997
−125
−75
−25
25
75
125
(cm s^{-1})

Fig. 4

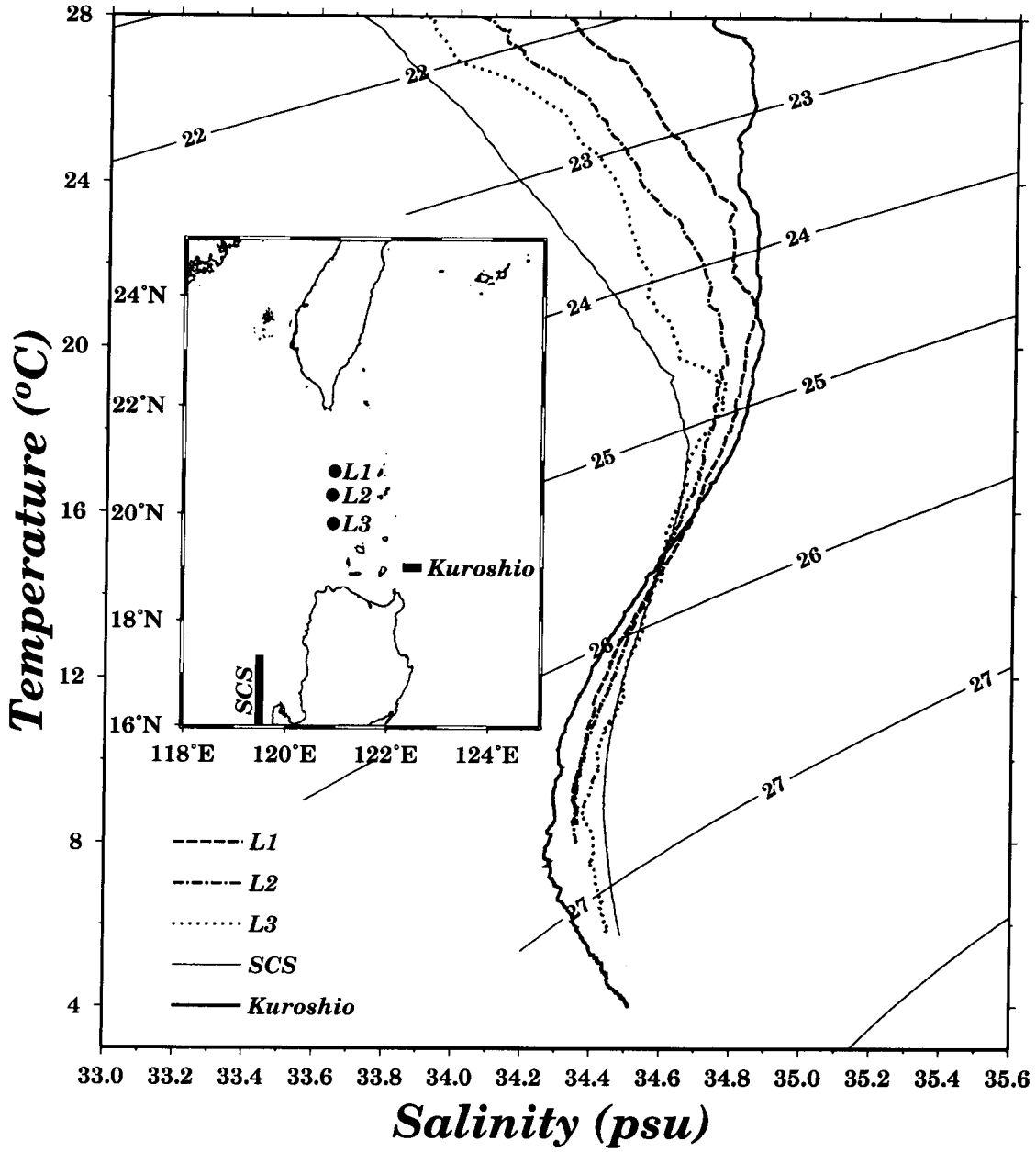
Temperature (°C)
Salinity (psu)
28
24
20
16
12
8
4
33.0
33.2
33.4
33.6
33.8
34.0
34.2
34.4
34.6
34.8
35.0
35.2
35.4
35.6
22
23
24
25
26
27
24°N
22°N
20°N
18°N
16°N
118°E
120°E
122°E
124°E
L1
L2
L3
Kuroshio
SCS
L1
L2
L3
SCS
Kuroshio

Fig. 5

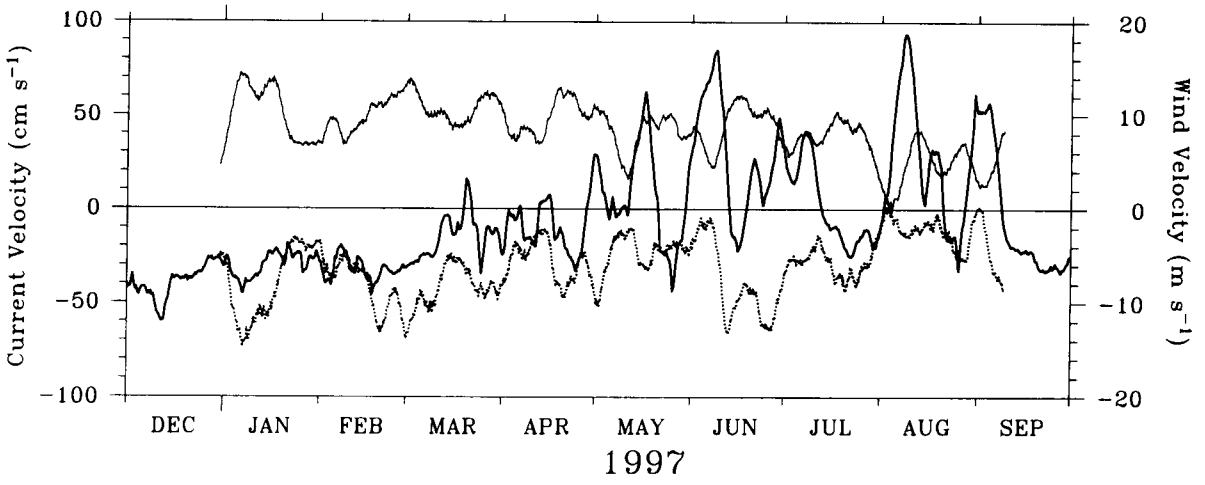
100
50
0
−50
−100
Current Velocity (cm s−1)
20
10
0
−10
−20
Wind Velocity (m s−1)
DEC
JAN
FEB
MAR
APR
MAY
JUN
JUL
AUG
SEP
1997

Fig. 6

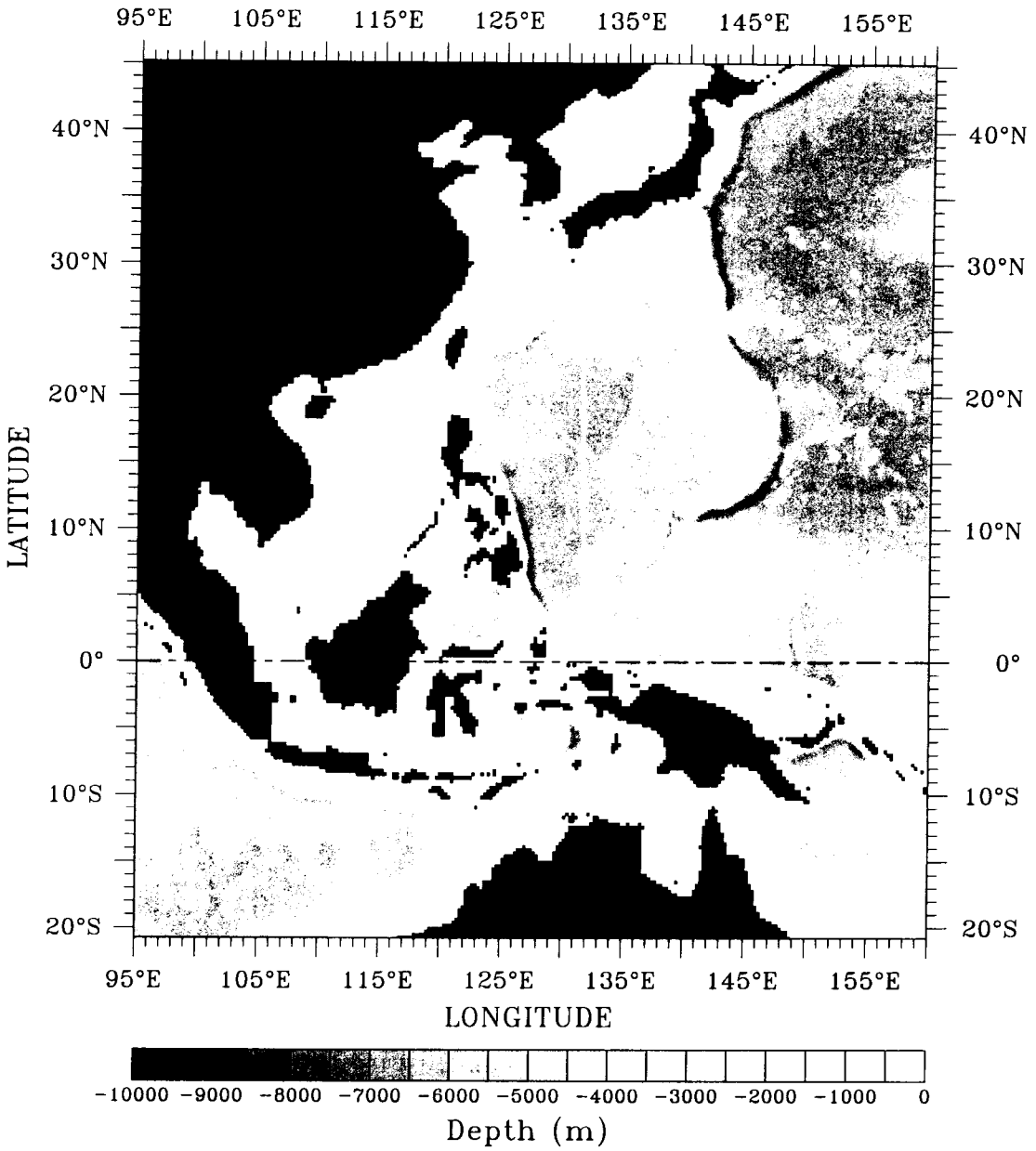
95°E
105°E
115°E
125°E
135°E
145°E
155°E
40°N
30°N
20°N
10°N
0°
10°S
20°S
LATITUDE
LONGITUDE
-10000 -9000 -8000 -7000 -6000 -5000 -4000 -3000 -2000 -1000 0
Depth (m)

Fig. 7

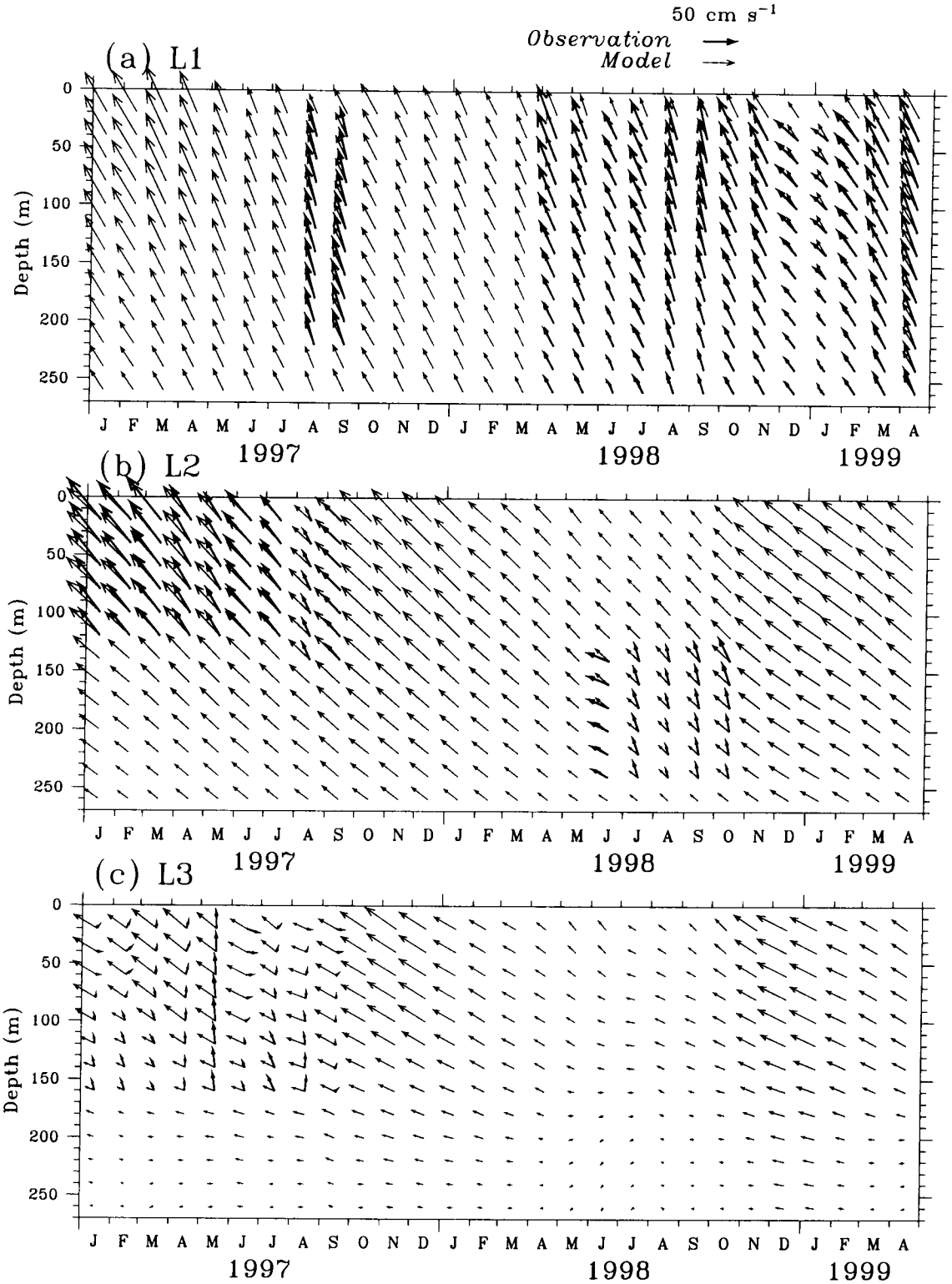
50 cm s^{-1}
Observation
Model
(a) L1
(b) L2
(c) L3
Depth (m)
0
50
100
150
200
250
J F M A M J J A S O N D J F M A M J J A S O N D J F M A
1997
1998
1999

Fig. 8

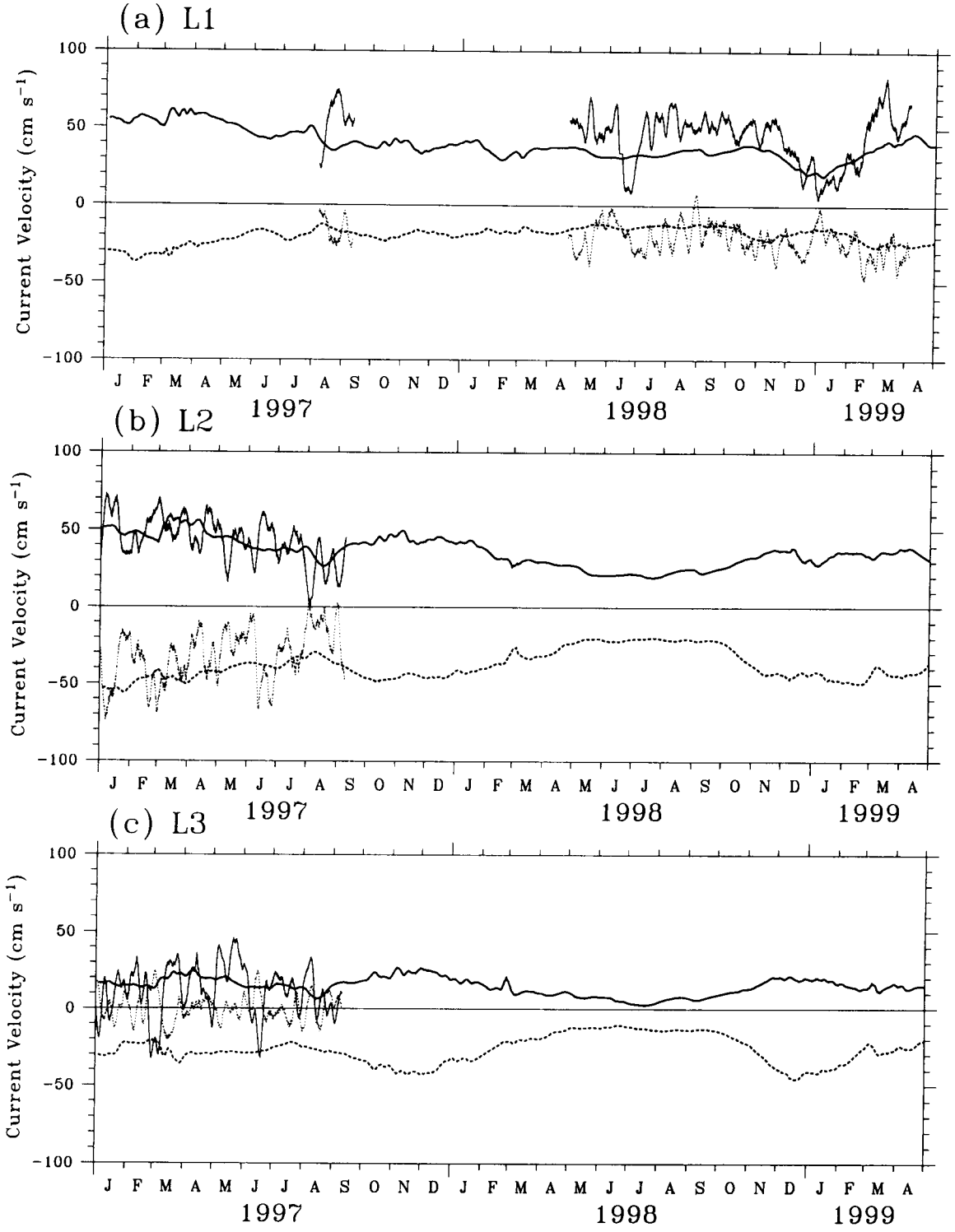
(a) L1
(b) L2
(c) L3
Current Velocity (cm s^{-1})
100
50
0
−50
−100
J F M A M J J A S O N D J F M A M J J A S O N D J F M A
1997
1998
1999

Fig. 9

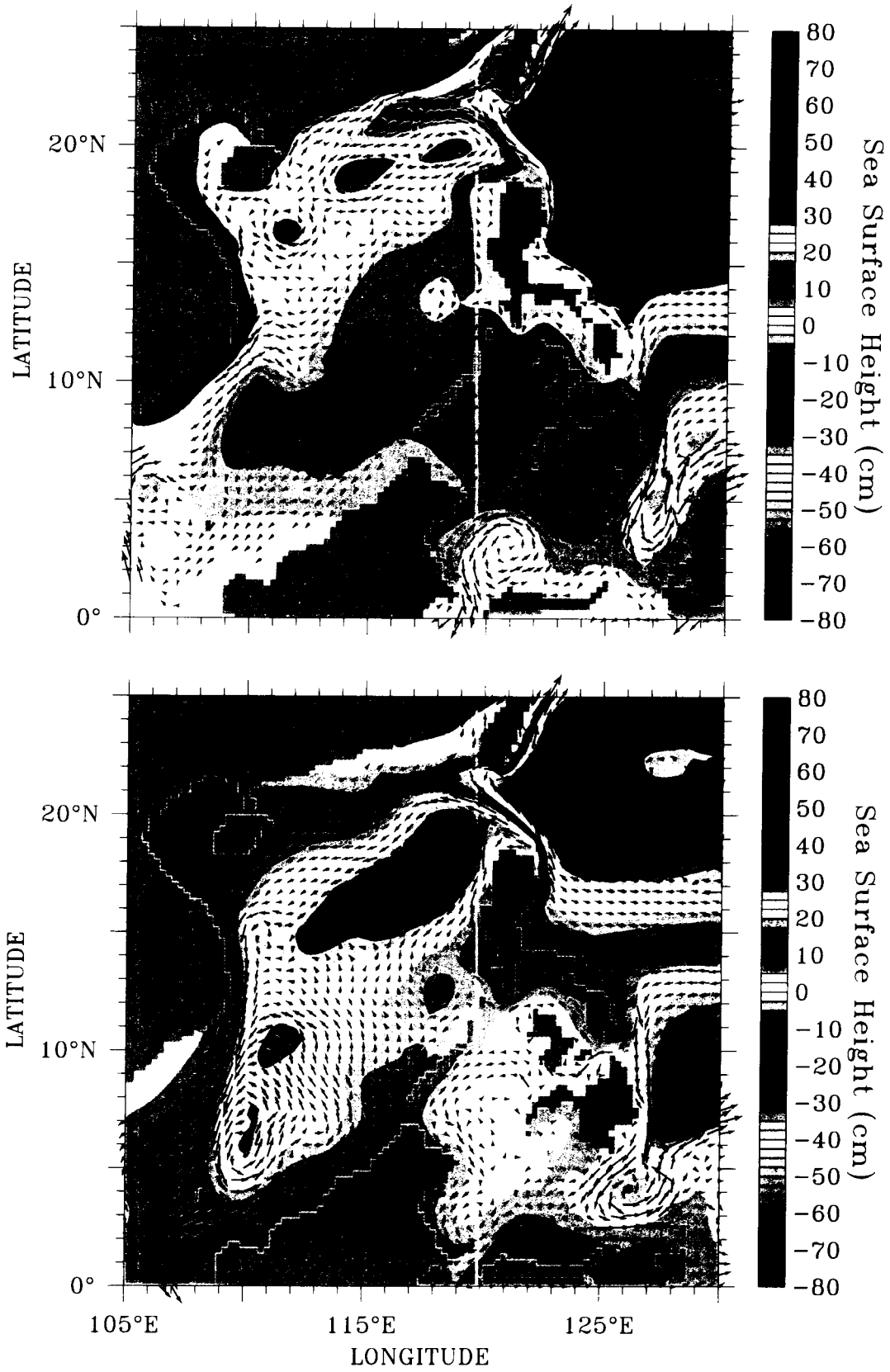
20°N
10°N
0°
LATITUDE
80
70
60
50
40
30
20
10
0
−10
−20
−30
−40
−50
−60
−70
−80
Sea Surface Height (cm)
105°E
115°E
125°E
LONGITUDE

Fig. 10

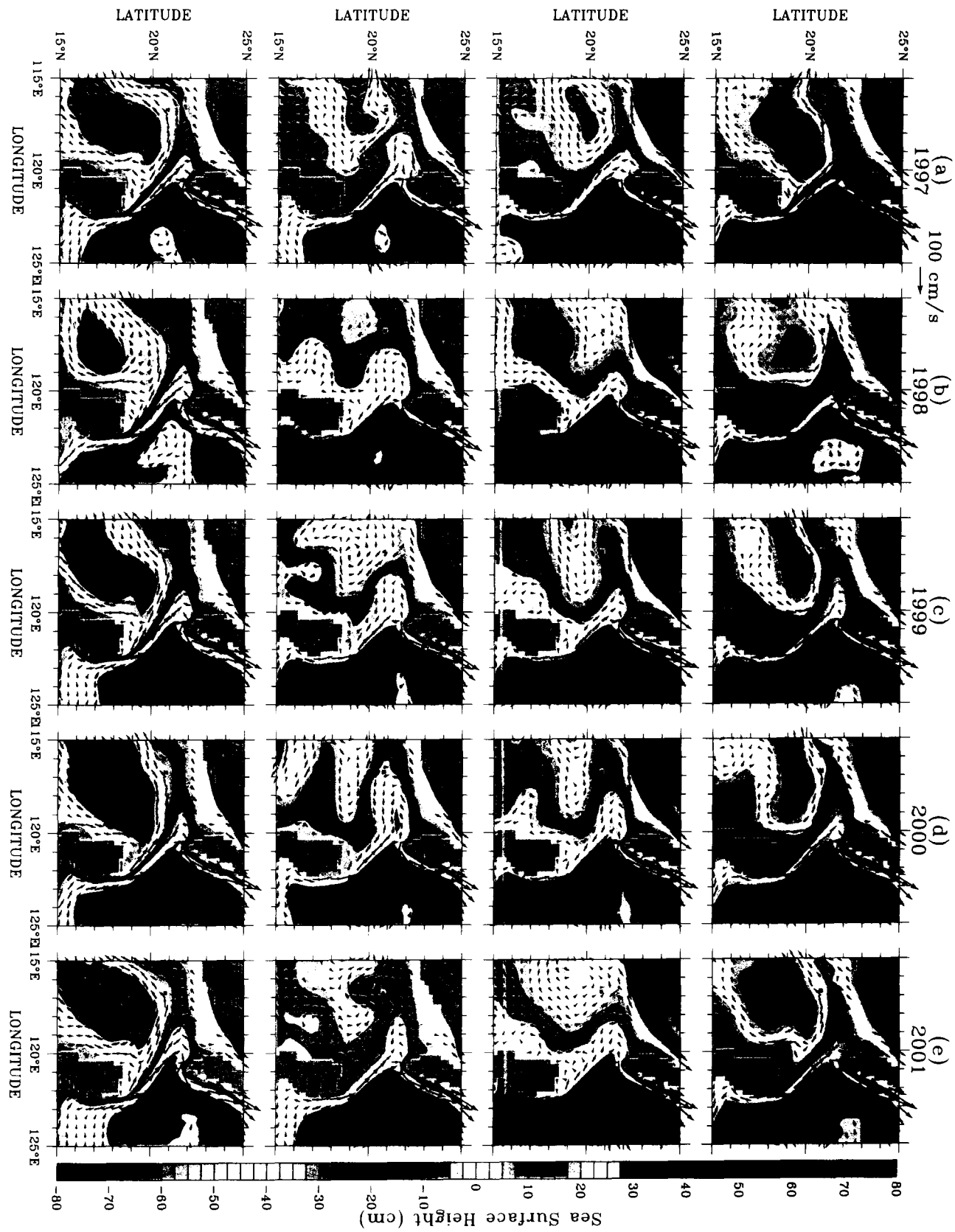
(a) 1997
(b) 1998
(c) 1999
(d) 2000
(e) 2001
100 cm/s
LATITUDE
LONGITUDE
15°N
20°N
25°N
115°E
120°E
125°E
Sea Surface Height (cm)
-80
-70
-60
-50
-40
-30
-20
-10
0
10
20
30
40
50
60
70
80

Fig. 11

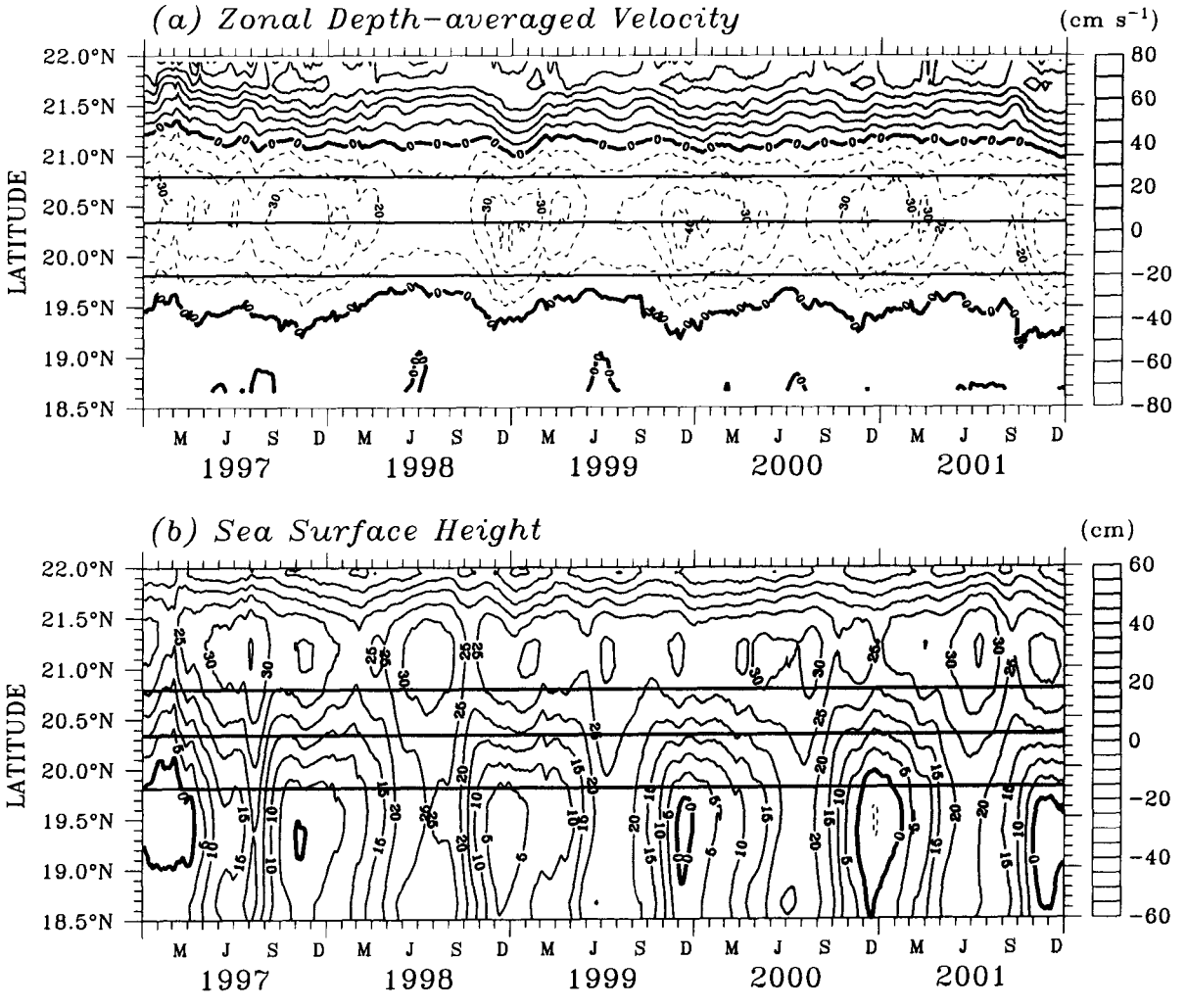
(a) Zonal Depth-averaged Velocity
(cm s-1)
LATITUDE
22.0°N
21.5°N
21.0°N
20.5°N
20.0°N
19.5°N
19.0°N
18.5°N
80
60
40
20
0
-20
-40
-60
-80
M J S D M J S D M J S D M J S D M J S D
1997 1998 1999 2000 2001
(b) Sea Surface Height
(cm)
60
40
20
0
-20
-40
-60

Fig. 12

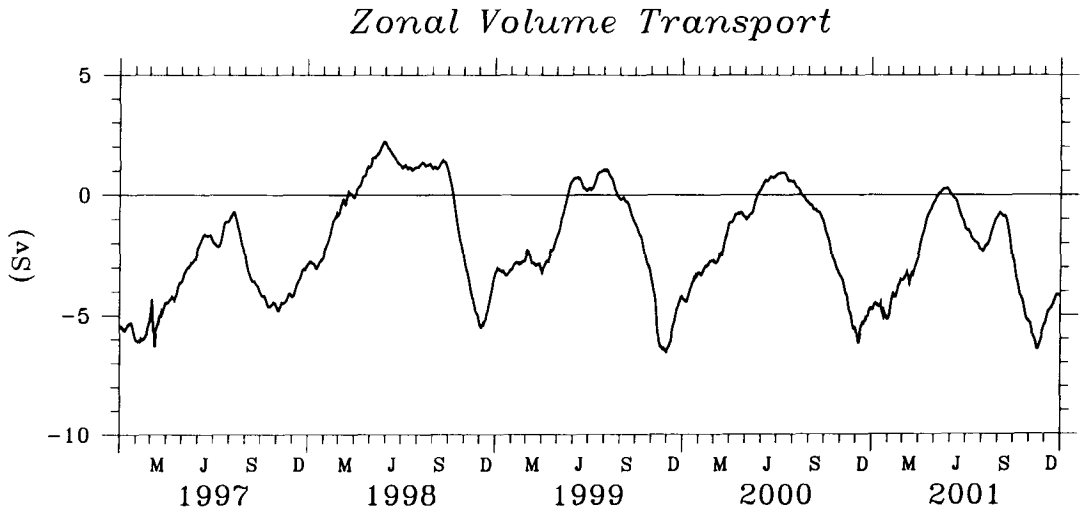
Zonal Volume Transport
5
0
−5
−10
(aS)
M J S D M J S D M J S D M J S D M J S D
1997
1998
1999
2000
2001

Fig. 13

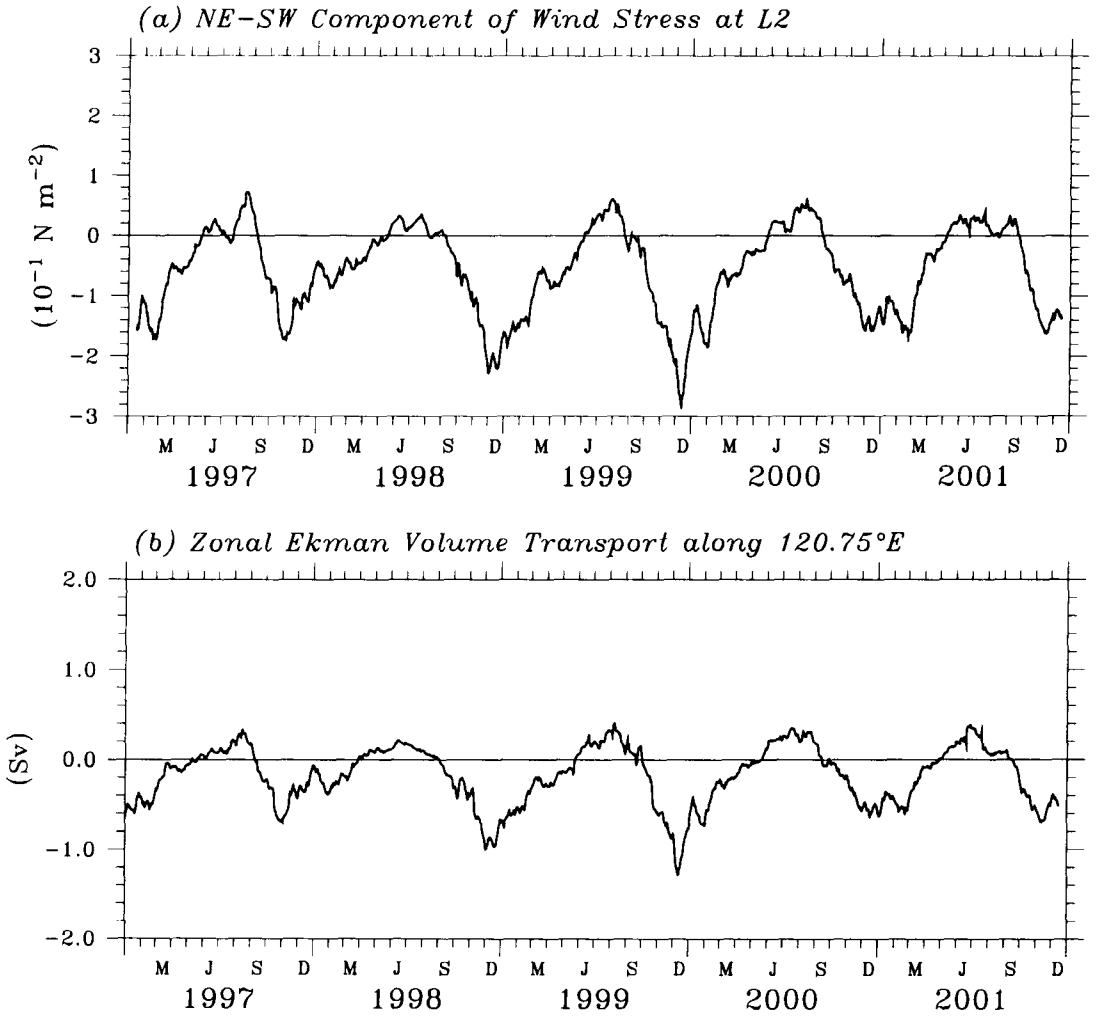
(a) NE–SW Component of Wind Stress at L2
3
2
1
0
−1
−2
−3
(10⁻¹ N m⁻²)
M J S D M J S D M J S D M J S D M J S D
1997 1998 1999 2000 2001
(b) Zonal Ekman Volume Transport along 120.75°E
2.0
1.0
0.0
−1.0
−2.0
(Sv)
M J S D M J S D M J S D M J S D M J S D
1997 1998 1999 2000 2001

Fig. 14

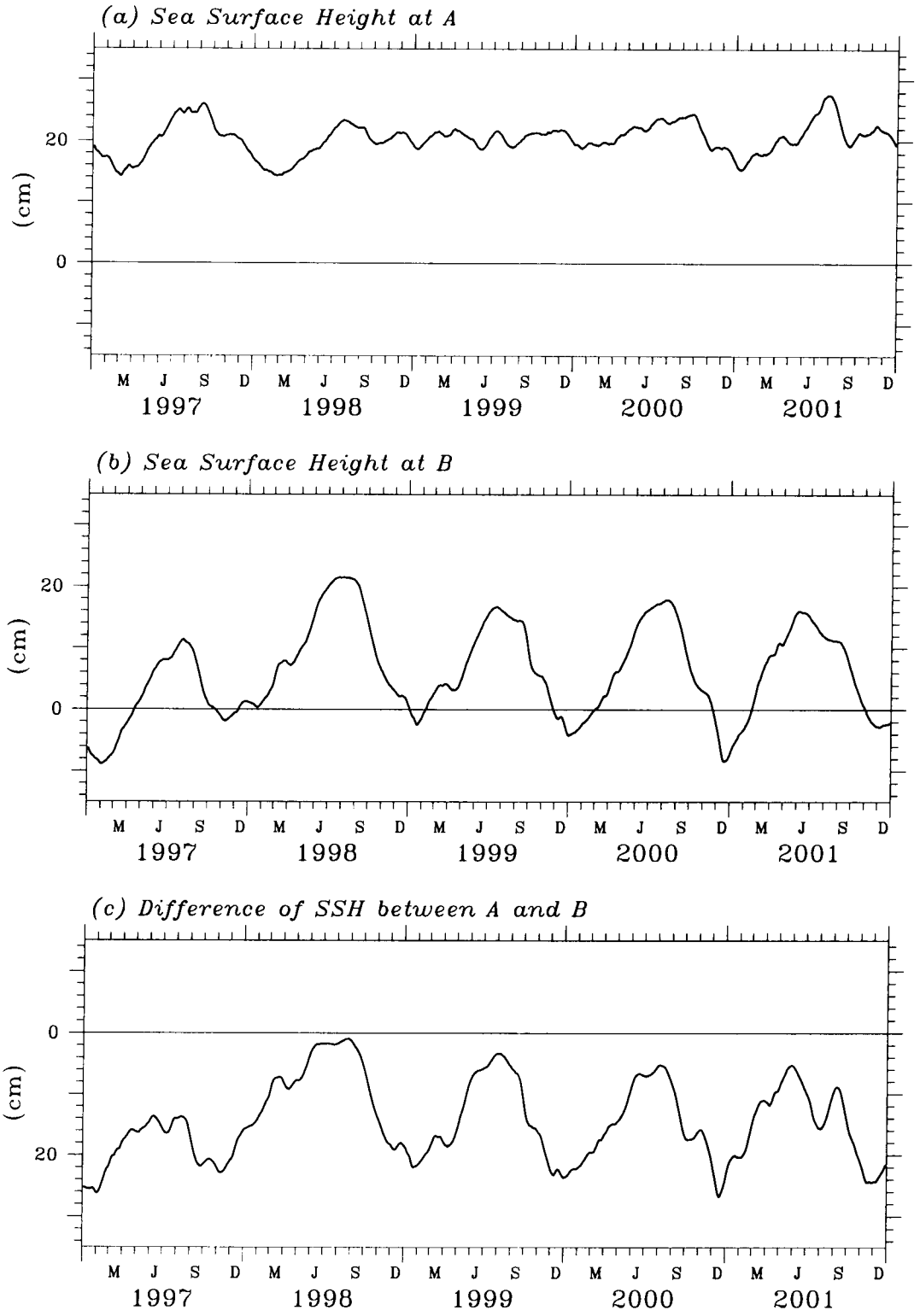
(a) Sea Surface Height at A
20
0
(cm)
M J S D M J S D M J S D M J S D M J S D
1997 1998 1999 2000 2001
(b) Sea Surface Height at B
20
0
(cm)
M J S D M J S D M J S D M J S D M J S D
1997 1998 1999 2000 2001
(c) Difference of SSH between A and B
0
20
(cm)
M J S D M J S D M J S D M J S D M J S D
1997 1998 1999 2000 2001

Fig. 15

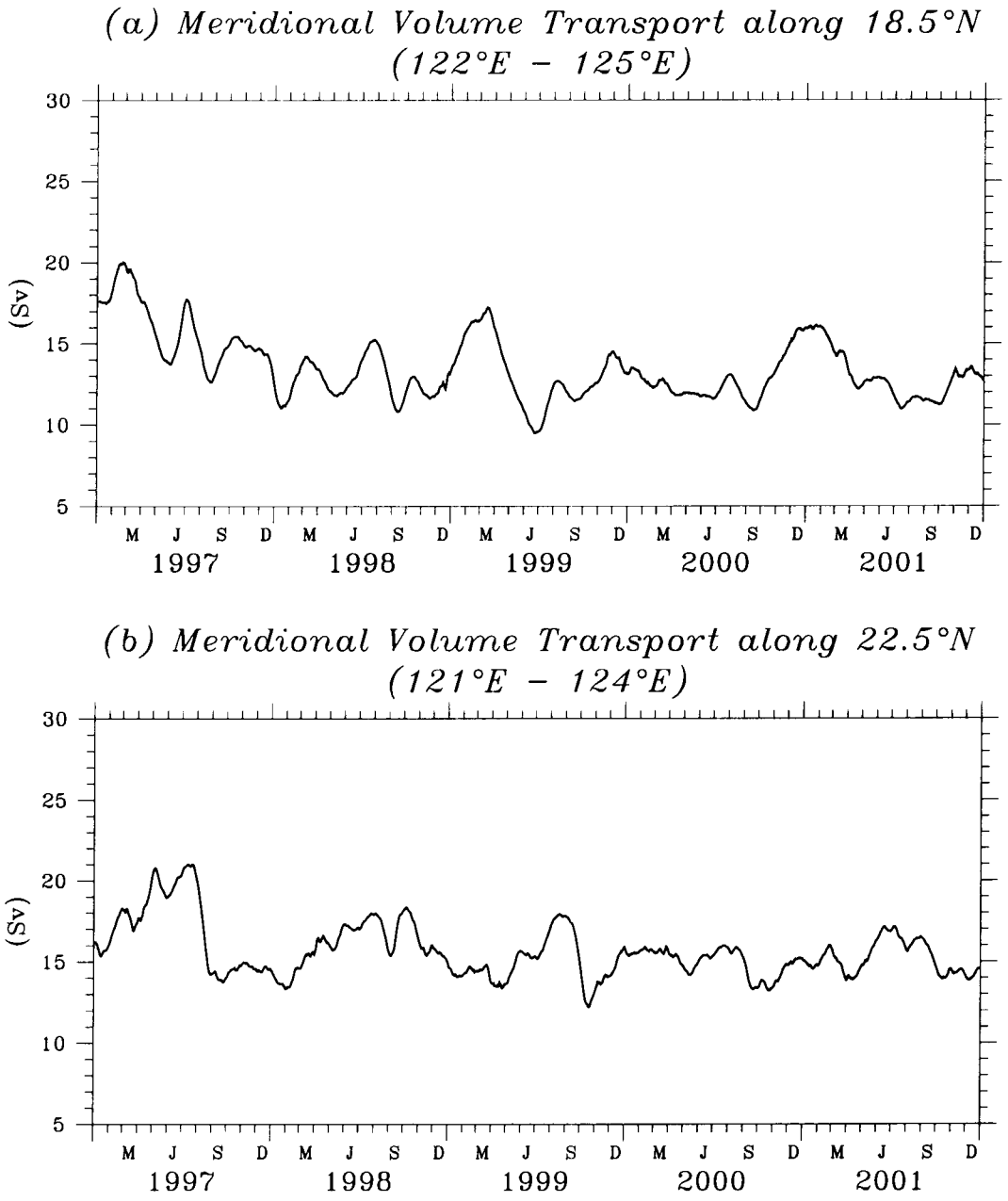
(a) Meridional Volume Transport along 18.5°N
(122°E - 125°E)
30
25
20
15
10
5
(Sv)
M J S D M J S D M J S D M J S D M J S D
1997 1998 1999 2000 2001
(b) Meridional Volume Transport along 22.5°N
(121°E - 124°E)
30
25
20
15
10
5
(Sv)
M J S D M J S D M J S D M J S D M J S D
1997 1998 1999 2000 2001

Fig. 16

Appendix II

Upper Ocean Currents around Taiwan

W.-D. Liang[a], T. Y. Tang[a,*], Y. J. Yang[b], M. T. Ko[a], and W.-S. Chuang[a]

[a]*Institute of Oceanography, National Taiwan University, Taipei, Taiwan, Republic of China*

[b]*Department of Marine Science, Chinese Naval Academy, Kaohsiung, Taiwan, Republic of China*

[*]*Corresponding Author: E-mail: tyt@ccms.ntu.edu.tw*

Deep-Sea Research, Part II

June 2002

Abstract

Current velocity, measured by Shipboard Acoustic Doppler Current Profiler (Sb-ADCP) during 1991-2000, was used to study the upper ocean (< 300 m) current around Taiwan. The collected data were debugged, calibrated, grid, and averaged to compose a three-dimensional current velocity distribution. The validity of the composite current velocity was supported by twelve sets of moored current velocity time series. Qualitative agreement was obtained. The moored time series also indicated that the seasonal variation of current around Taiwan was generally weak except for the shallow water regimes.

The composite and moored current velocity revealed a branch of the Kuroshio that intruded steadily and persistently into the South China Sea. Part of the intruded Kuroshio flowed out of the South China Sea through the northern Luzon Strait and re-united with the main stream Kuroshio. The Kuroshio had two velocity maximum cores southeast of Taiwan, but gradually combined into one as the Kuroshio flowed north. The Kuroshio was deflected by the I-Lan Ridge east of Taiwan and the zonal-running shelf break northeast of Taiwan. At the shelf break, the Kuroshio split, with one branch intruding onto the shelf.

West of the Luzon Strait, the Kuroshio intruded into the South China Sea. Some water flowed northward into the Taiwan Strait and re-joined the Kuroshio. Currents in the Taiwan Strait flowed primarily in a northward direction, except for the southward current near the coast of Mainland

China. North of the Taiwan Strait, a branch of the northward flow followed the northern coast of Taiwan to join the Kuroshio.

The composite current velocity varied consistently from season to season. There was generally poor correlation between currents and local winds, especially in the deep-water regime. Remote forces were important in the currents around Taiwan.

Keywords: Kuroshio; Upper Ocean Currents; Taiwan Strait; Luzon Strait; South China Sea

1. Introduction

Taiwan is an island located in the tropic to sub-tropic western Pacific. Its geographic location and bathymetry are shown in Fig. 1. East of Taiwan, where the shelf is narrow and the water is deep, lie Green Island, Yonaguni Island and the islands of Lan-Yu. The I-Lan Ridge connects Yonaguni Island to Taiwan. Northeast of Taiwan, the shelf break extends northeastward, and turns abruptly toward the zonal direction around 26°N. The North Mien-Hwa Canyon, which stretches across the shelf break around the turning point, connects the shelf of the East China Sea with the deep ocean basin. The shelf north of Taiwan is broad. The Taiwan Strait between Taiwan and Mainland China measures 200 km in width, 400 km in length, and 60 m in average depth. Only at the southeastern portion of the Taiwan Strait, is the water deeper than 200m. The funnel shaped Peng-Hu Channel is located between Taiwan and the Peng-Hu Archipelagos. West of Peng-Hu Channel is the shallow Taiwan Bank, which connects the northern shelf of the South China Sea. The Luzon Strait between Taiwan and Luzon is a passage between the western Pacific Ocean and the South China Sea. Its width is around 400 km and its maximum depth is 2000 m. On both sides of the Luzon Strait, the water is deep.

The predominant wind system around Taiwan is the monsoon. The northeasterly monsoon prevails November through March, and the southwesterly monsoons prevail from May through September. April and October are transition months. (Chuang and Liang, 1994). The monsoon

system is the primary force causing current variation around Taiwan (e.g. Wyrtki, 1961). Nitani (1972) described surface currents around Taiwan in summer and winter (see Fig. 2). The Kuroshio flows to the north along the coast of Taiwan and the shelf break of the East China Sea. In winter, the Kuroshio intrudes into the South China Sea in the Luzon Strait. In summer, water from the South China Sea enters the western edge of the Kuroshio. East of Taiwan, the width of the Kuroshio is around 100 km with a maximum speed of around 100 cm s^{-1}. The Kuroshio's pathway parallels the shoreline of Taiwan and demonstrated no obvious seasonal variation. South of Peng-Hu Archipelagos, current in the Taiwan Strait is flows predominantly northeastward regardless of the seasons. North of the Peng-Hu Archipelagos, the current flows northeastward in summer and southwestward in winter. The seasonal variation is significant only in the Luzon Strait and in the northern Taiwan Strait.

Many oceanographers believe that the Kuroshio intrudes into the South China Sea through the Luzon Strait in winter and stops in summer. This was first described by Wyrtki (1961), and has been re-confirmed by a number of studies (e. g. Shaw, 1989). There are however, a few studies, e.g. Qu et al. (2000) and Li and Wu (1989), which indicate that the intrusion of the Kuroshio also occurs in summer. The potential intrusion of the Kuroshio through the Luzon Strait is controversial. Prior studies were largely based upon hydrographic measurements. This study will

provide direct current velocity measurements and clarify the issue of Kuroshio intrusion.

Based upon hydrographic measurements and geostrophy, the width, maximum speed, and transport of the Kuroshio east of Taiwan have been estimated in a number of earlier studies. The findings were similar, but contained some notable differences. For example, the transports estimated by Nitani (1972), Chu (1976), and Liu (1983) varied from 19 to 47 Sv. The estimated depth of the Kuroshio varied from a few hundred to a thousand meters. Sun (1987) indicated that the main axis of the Kuroshio varied seasonally, especially north of the I-Lan Ridge, moving close to the coast in winter and away from the coast in summer. Chu (1976) found that the Kuroshio had no clear annual signal but did have a large interannual variation. Recently, moored current velocity measurements along the I-Lan Ridge and altimetry obtained from the TOPEX/POSEDIENT satellite indicated that westward propagating eddies from the Pacific Ocean had a significant impact on the Kuroshio (Yang et al., 1999; Zhang et al., 2001). The transport of Kuroshio reveals significant intra-seasonal variation, with a time scale of 100 days, but with annual variation that is vague.

Analysis of the moored current velocity, temperature, and salinity time series northeast of Taiwan, Tang et al. (2000) suggested that the axis of the Kuroshio migrates not only seasonally, but also intra-seasonally. Such migration has a great impact on the flow pattern north of Taiwan, where the Kuroshio intrudes onto the shelf and interacts with the Taiwan Strait outflow. A

southwestward countercurrent, flowing opposite of the Kuroshio, was observed along the shelf edge northeast of Taiwan (Chuang and Wu, 1991; Tang and Yang, 1993; Chuang et al., 1993). As the Kuroshio moves close to shore, it intrudes directly onto the shelf along northeastern Taiwan. The northwestward current prevails in the upper ocean (< 150 m) and the countercurrent is submerged. When the Kuroshio moves away from the shore, the Kuroshio intrudes onto the shelf primarily through the North Mien-Hwa Canyon. A cyclonic eddy forms between the North Mien-Hwa Canyon and Taiwan (Tang et al., 1999). The countercurrent surfaces to complete the annual cycle. Using the Shipboard Acoustic Doppler Current Profiler (Sb-ADCP), Tang et al. (2000) pointed out that the current on the shelf north of Taiwan is primarily northward flowing, regardless of season. The impact of monsoon on the current is minimal.

Chu (1961) claimed that the current in Taiwan Strait is influenced by a number of factors, including the intrusion of the Kuroshio, the South China Sea current, monsoon, and the China coastal current. Wang and Chern (1988) found that the current in the Taiwan Strait was swift and northward under the southwesterly monsoon in summer, while the Mainland China coastal current flowed southward in the northern Taiwan Strait under the northeasterly monsoon. The northward warm and salty Kuroshio water met the cold, fresh China coastal water around the central Taiwan Strait and a thermohaline front formed, largely prohibiting the Kuroshio from flowing farther north (Wang and Chern, 1989). Chuang (1986) found that the current in the Peng-Hu Channel was

northward almost year around. The monsoon does not reverse the current direction except under persistent strong northeasterly monsoon.

This study explores the distribution of three-dimensional upper (< 300 m) ocean current velocity around Taiwan. The current velocity data collected during 1991-2000 from the R/Vs Ocean Researcher I, II, and III by the Sb-ADCP were analyzed. Twelve sets of moored current velocity data were used to verify the composite current velocity and to infer the temporal variation of the current. This paper will proceed as follows. Section 2 describes the data and the composite current velocity distribution around Taiwan. Section 3 discusses the qualitative comparison between the composite current velocity and the moored current velocity measurements. Section 4 investigates the 3-dimensional upper (< 300 m) ocean current velocity around Taiwan in vertical-meridianal or vertical-zonal sections of current velocity. A discussion and summary are provided in Section 5.

2. Data and Composite Current Velocity

The Sb-ADCP measurements used in this study have been provided by the Ocean Data Bank/National Center for Ocean Research (ODB/NCOR) of National Science Council (NSC), Republic of China (ROC). Three Taiwanese research vessels, Ocean Researcher I, II, and III collected the Sb-ADCP measurements from 1991 to 2000. In general, the Sb-ADCP was set to

measure the current velocity every second and then to record the ensemble average every 1-2 minutes. The depth bin was 8-16 m and the depth of range of measurement was from 16 to 320 m. The Global Positioning System (GPS) recorded the ship location. The ship velocity was estimated based on the position time series. To obtain the composite current velocity, the data was processed as follows. The current velocity was first debugged, calibrated, and aligned using the method described by Tang and Ma (1995). To reduce the random error of estimated ship velocity, which was calculated from the ship positions recorded by the GPS, a 30-minute running average was applied. The current velocity was also averaged every 30-minutes. Hereafter, each averaged current velocity is treated as a single data point. The mean ship track during that 30-minutes was used as the location of averaged current velocity. The root mean square (rms) error associated with the calibrated and averaged current velocities was less than ± 3.5 cm s^{-1}. Finally, the velocities were linearly interpolated vertically with 10 m intervals and averaged horizontally within the grid of size of $0.25° \times 0.25°$. No further interpolation or smoothing was applied.

Since the Sb-ADCP measurements were not evenly distributed, the number of data points in each grid varied. The averaged current velocity in each grid is more representative when there is more data. Conversely, the more data required within each grid, the more fragmented the obtained composite current velocity distribution becomes. A choice has to be made between the minimum requirement of data and integration of composite current velocity. The semidiurnal tidal current is

the primary high-frequency fluctuation to bias the composite current velocity in each grid. The semidiurnal tidal velocity has an amplitude of 50 cm s^{-1}. Similar to the Sb-ADCP data, the 30-mintue averaged tidal velocity, $\bar{u}$, was calculated. To randomly choose N pieces of $\bar{u}$, its average, $\bar{u}_N$, would be the noise causing the difference between the composite current velocity and true mean current velocity. Theoretically, $\bar{u}_N$ should decrease as N increases. Finally, to repeat the experiment 100 times, the rms of $\bar{u}_N$ is calculated. Possible error caused by the semidiurnal tidal current in the composite current velocity is estimated. Fig. 3 shows the distribution of numbers of the data, the plot of rms value of $\bar{u}_N$ versus the N, and the available number of grids versus N. The numbers of the data in the grids were distributed unevenly. In general, the grid further away from the Taiwan shoreline had less data. The grids had maximum data in the regions of research vessel harbors, at the northern tip and southwestern tip of Taiwan. The rms value deceases rapidly with N increase initially, but gradually flattens out. The available number of grids also decreases with N increase. To remain the relatively integrated distribution of composite current velocity, N=6 was chosen as the minimum requirement. The estimated bias caused by the semidiurnal tidal current would be 14 cm s^{-1}, around 1/4 of tidal amplitude. Therefore, we limit our description and discussion on the composite current velocity distribution to qualitative comments.

Fig. 4 shows the composite velocity vectors at 30 and 100 m around Taiwan. In general, the

currents at these tow-depths showed no significant difference. North of Luzon, the Kuroshio flowed to the northwest, and turned clockwise, forming a clockwise path in the Luzon Strait. The main path of the Kuroshio returned to the east of Taiwan, but some Kuroshio water intruded into the northern South China Sea. West of Luzon, current flowed northeastward and turned counterclockwise to the west as it encountered the Kuroshio. The intruding Kuroshio water and the South China Sea water moved west (seen more clearly at 100 m). The westward current seems to split into two branches. The southern branch was diverse and vague, perhaps due to insufficient data. Results from Numerical models (e.g. Shaw and Chao 1994; Metzger and Hurlburt, 2001; etc) indicate that this is part of the South China Sea circulation, which flows along the edge of the shelf into the central basin of South China Sea. The northern branch is better shown in Fig 4. It turned clockwise and toward the Kuroshio along the southern tip of Taiwan or else flowed into the Taiwan Strait through the Peng-Hu Channel, producing a clockwise circulation pattern south of the Taiwan Strait.

The current in the Kuroshio is swift along the east coast of Taiwan. Its maximum speed and width were around 100 cm s^{-1} and 100 km, respectively. Over the I-Lan Ridge, the Kuroshio turned northeastward and left the coast of Taiwan. Only a weak flow was deflected eastward by the I-Lan Ridge, indicating that the I-Lan Ridge did not block the Kuroshio. The Kuroshio flowed northeastwardly along the shelf break after it left Taiwan. Around 26°N, the zonal shelf break

blocked the Kuroshio, and the Kuroshio turned eastward. Some water entered the shelf. On the shelf north of Taiwan, current was weak in the region around 25.3°N-25.8°N, 121.7°E-122.2°E. Outflow of the Taiwan Strait was observed along the northern coast of Taiwan. North of this region, the current velocity was disorderly and confused. This clutter distribution might be caused by the insufficient data and the large bias induced by the tidal currents on the shelf. Tang el al. (2000) claimed that the region of weak current was visional. Because of the seasonal migration of the Kuroshio, the upper (< 150 m) ocean currents reversed during the seasons of northeasterly and southwesterly monsoon. Consequently, a weak composite current velocity occurred.

The currents converged at the funnel-shaped Peng-Hu Channel and flowed northward in the Taiwan Strait. As the northward current passed over the northern opening of the Peng-Hu Channel, a ridge separated it into two branches. One branch was deflected westward, following the topography. The other branch flowed over the ridge to the north. Currents with double peaks in the Taiwan Strait were observed north of the ridge, but became vague farther north. Some outflow from the Taiwan Strait followed the northern coast of Taiwan into the Kuroshio. The majority of the Taiwan Strait outflow moved to the north, interacting partially with the intruding Kuroshio.

The composite current velocities at 30 m under southwesterly and northeasterly monsoons are shown in Fig. 5. During southwesterly monsoon, the flow pattern was similar to the previous velocities distribution. The lack of data in the northeasterly monsoon season was primarily the

result of rough sea conditions prohibiting research vessel activities. Current velocity distributions in the two seasons were similar except a few notable differences. The Kuroshio entered the Luzon Strait primarily during the southwesterly monsoon. Only a small amount of water entered the South China Sea. The Kuroshio intrusion in the Luzon Strait had a larger incident angle during the season of northeasterly monsoon than during the season of southwesterly monsoon. Northeast of Taiwan, a small cyclonic flow seen on the edge of the shelf (centered around 25.5°N, 122.5°E) was observed during the season of southwesterly monsoon. The cyclonic flow disappeared and the Kuroshio moved close to the shelf when the northeasterly monsoon prevailed. In the Taiwan Strait, the current velocity was weaker during the northeasterly monsoon than during the southwesterly monsoon, but the flow was always northeastward. No southward current velocity was observed.

3. Comparison of Moored and Shipboard Current Velocity Measurements

Twelve sets of moored current velocity time series, measured by the self-contained Acoustic Doppler Current Profiler (ADCP), are used to affirm the validity of composite current velocity. The seasonal and intra-seasonal variations of current velocity are noted.

Fig. 6 shows four sets of daily current velocity stick time series at M1, M2, M3, and M4, locations which are shown in Fig. 1. M1 to M3 are in the central portion of Luzon Strait and the M4 is around 230 km west of M2. The current velocity was most often at 100 m. The 2nd

segment at M2 was at 140 m because of a missed count of the mooring rope length. The duration of the measurement at each site was longer than 5 months. In general, the current velocities at varied depths correlated well in the upper 200 m water column, but their amplitude decreased with the depth. The current velocity at M1 and M2 were essentially northwestward, but M1 was more northward than M2. The transition of monsoons from southwest to northeast usually occurred in October (Chuang and Liang, 1994), and had little impact on the current velocity. The current at M1 and M2 indicated that the Kuroshio flowed into the South China Sea steadily and persistently. Differing from the current at M1 and M2, the current velocity at M3 was weak and varied frequently from northeastward to northwestward. The current alternated in and out of the South China Sea. The southern boundary of Kuroshio intrusion could be around M3. The current velocity at M4 also was weak and varied, but it only changed direction from northwest to southwest. A westward component current velocity was consistently observed. The Kuroshio might intrude further to the west.

The variability and mean of current velocities obtained from the moored and shipboard ADCP at each location were compared (Fig. 7). One diagram contains the 30-minute average Sb-ADCP current velocity in the grid where the mooring occurred. The other diagram contains the hourly moored current velocity. The best agreement was obtained at M1, where the current primarily flowed northwest or north-northwest. The mean moored current velocity vector and

composite current velocity are nearly identical. At M2, the moored current velocity primarily flowed northwest while the Sb-ADCP current velocity was more diverse. However, both current velocity directions varied in the same range, from north to west (second quadrant). The mean and composite current velocity vectors had similar direction, but the former one had larger amplitude. Similarly, the two types of measurement at M3 had some similar characteristics but also had notable differences. Both of them showed they were weaker and had more fluctuations than the current at M1 and M2. Considering the difference in the two sampling methods, it is reasonable to conclude that the two types of measurement agreed qualitatively.

Fig. 8 shows the three daily current velocity stick time series. One is located at the I-Lan Ridge and had the shortest record (less than two months). The other two are located at the shelf break northeast of Taiwan. The velocities were at 30 m. At M5, the current was quite stable and flowed to the north-northeast. A similar observation with much longer time series also showed that the current velocity was generally stable, except when the westward-propagated eddy collided with the Kuroshio. The collision occurred about every 100 days (Yang et al., 1999; Zhang et al., 2001). At M6, the current was first southwestward, and then changed to become northwestward by mid-October. The migration of Kuroshio caused the variation of current velocity. Tang and Yang (1993) and Chuang et al. (1993) described the moored current velocities at M6 in detail. At M7, the current velocity was mainly northeastward, but generally became more eastward in

October-April. Tang et al. (2000) claimed the Kuroshio impinged onto the East China Sea shelf around M7. The migration of the Kuroshio also caused the variation of current at M7. However, such variation was not large. In the above three moored current velocities, the large seasonal variation was only seen at M6.

The comparison between the moored and shipboard ADCP current velocity is shown in Fig. 9. In spite of the record being shorter than 2 months, the moored current velocity at M5 agreed well with the shipboard ADCP current velocity in both variability and mean. At M6, the two types of measurement showed a relatively large disparity; though they also had some similarities. Their variability was roughly in the same range. The mean and composite current velocity vectors had small amplitude and similar direction. The moored and shipboard ADCP current velocity at M7 agreed well in both variability and mean. Generally speaking, the agreement between the two types of measurement was good when the current velocity variation was small, as occurred at M5. When the current velocity had large fluctuations, as it did at M6, a disparity between the two types of measurement occurred. But overall, the shipboard ADCP current velocity properly represents the current velocity - at least, qualitatively.

Fig. 10 shows the five sets, M8, M9, M10, M11, and M12, daily moored current velocity time series in Taiwan Strait. The velocities were at 30 m. The first four time series were obtained from a mooring array deployed across the Taiwan Strait. The current was observed in the duration of

mid-fall to early winter when the northeasterly monsoon prevailed. M12 was located at the southern opening of the Peng-Hu Channel. The current was observed from June--when the southeasterly monsoon prevailed--to November, when the northeasterly monsoon was dominant. In general, the current velocities at M8, M9, M10, and M11 fluctuated considerably in the several day time scale. The coherence between the local wind, which was northeasterly, and current velocity was calculated and generally poor (not shown). At M11, the current flowed even against wind for most of the observed period. However, the impact of local wind on the current velocity was still seen by peak-to-peak comparison. The current velocity at M12 primarily flowed with wind moving toward the southwest. The coherences between the current velocities at various stations were also poor. The above result implies that the local wind was not the only dominant external force in the Taiwan Strait. Remote force, such as the intruded Kuroshio, could play an important role. At M12, the current velocity persistently flowed into the Peng-Hu Channel, whether the local wind was southwesterly or northeasterly. The northeasterly monsoon, which intensified after October, only caused fluctuation in the current velocity. Again, the local wind poorly correlated with the current velocity. The former inference was reconfirmed: Both remote and local forces were important in the Taiwan Strait.

The comparison between the moored and Sb-ADCP current velocities in the Taiwan Strait is shown in Fig. 11. Strong agreement between the two types of measurement was found at M11 and

M12. At M8, M9, and M10, a large disparity was observed. The disparity could arise from a number of factors. For example, the data were sparse, especially in the western Taiwan Strait. The Sb-ADCP data were lacking when the northeasterly monsoon was large. There was no moored current velocity during the southwesterly monsoon season. The large semidiurnal tidal current velocity could also be a source of error for the composite current velocity.

The composite current velocity might inadequately represent the current where there was a large current velocity variation. However, this type of current is limited around Taiwan. The above comparison between moored and Sb-ADCP current velocity indicates that the composite current velocity obtained from the Sb-ADCP measurements represents the current around Taiwan qualitatively, but not quantitatively.

4. Vertical Sections of Current Velocity

Fig. 12 shows the vertical sections of zonal (U) and meridional (V) components of current velocity along the Luzon Strait and along 21°N. The blank region indicates where the data was insufficient. The latitude-vertical section of U along the Luzon Strait showed that the eastward/westward current velocity alternately occurred from northern Luzon to southern Taiwan. The westward current occupied a larger area and had larger amplitude than the eastward current. The largest westward current occurred in the central-northern Luzon Strait, while the largest

eastward current appeared at the southern tip of Taiwan. The northward current dominated in the *V* section. Its maximum speed was over 50 cm s^{-1}. The southward current was only observed at the tips of northern Luzon and southern Taiwan. The westward current, indicating that the water intruded into the South China Sea from Pacific Ocean, generally accompanied the large northward current. The intruded current should primarily be the Kuroshio. The South China Sea outflow at southern Luzon Strait could retroflex back to the South China Sea though the central Luzon Strait, but its amount was small. The zonal volume transport, calculated by simply integrating the *U* along the section, was around -3 Sv. westwardly. Smaller, but also negative, value was obtained by using the Sb-ADCP measurement collected only in the season of southwest monsoon. Apparently, the Kuroshio intruded into the South China Sea even in the southwest monsoon season. Although the transport of Kuroshio intrusion was only estimated qualitatively, the moored current velocity supported such inference because the Kuroshio intrusion occurred persistently. The earlier belief that no Kuroshio intrusion occurred in the Luzon Strait in summer might need to be reconsidered.

Along 21°N, the longitude-vertical section of *U* was primarily westward of the Luzon Strait signifying that the intruded Kuroshio flowed continuously westward. The maximum westward speed was around 30 cm s^{-1}. East of the Luzon Strait, the *U* was fragmented, with eastward/westward current reciprocally shown. The northward current dominated in the *V* section.

A weak southward current was observed west of 119°E. East of this southward current, the northward current extended from 119°E to 121.75°E. The region was wide - around 300 km. The maximum northward current, around 60 cm s^{-1}, was in the Luzon Strait. East of this northward current, the V was negative/positive reciprocally. The Kuroshio became vague around the Luzon Strait, possibly because the western boundary current is deficient in its western continental boundary. Local topography might also play a role. A few islands, which fall near the 122°E parallel with the Luzon Strait, might cause the spatial current fluctuation east of Luzon Strait.

East of Taiwan, four longitude-vertical current velocity sections along 22°N, 23°N, 24°N, and 25°N are shown in Fig. 13. The Kuroshio dominated all four sections. On the southernmost section (along 22°N), the U was weak. It was primarily positive (eastward) between Taiwan and Lan-Yu near 121.5°E. East of Lan-Yu, the U gradually turned to negative (westward). A weak eastward component velocity was seen again east of 124°N. The V was chiefly positive (northward) and had two maximum velocity cores located on two sides of Lan-Yu, respectively. The western core with maximum speed over 90 cm s^{-1} was near the surface. The eastern core with maximum speed around 70 cm s^{-1} was at subsurface (70 m). The eastward current generally accompanied the western core while the westward current accompanied the eastern core. This implies that the two cores eventually combined together as the Kuroshio flowed further north. The feature of double maximum velocity cores could be caused by the local topography or the fact that

the split Kuroshio in the Luzon Strait had not fully re-united. The southwestward countercurrent was observed close to Taiwan at subsurface as well as east of Kuroshio.

The velocity section along 23°N was similar to it along 22°N. The Kuroshio had double velocity cores. The western core had greater speed and was at surface, while the eastern core had smaller speed and was at subsurface. Again, the cores seemed to merge further north. The subsurface countercurrent close to Taiwan was barely observed. West of the Kuroshio, the countercurrent was weaker than that at the section of 22°N.

The two velocity cores merged into a single velocity core at the section of 24°N, south of I-Lan Ridge. The U and V were mostly positive, but the V had much greater amplitude. The negative U and V were only seen at subsurface close to Taiwan. The Kuroshio was mainly northward; its eastward component was small. I-Lan Ridge is quite close to the section of 24°N, but its impact on the Kuroshio was not observed here.

The velocity at section of 25°N, north of I-Lan Ridge, showed that the U and V were still primarily positive but the amplitude of U increased and the amplitude of V decreased. This result indicates that the Kuroshio was deflected as it flowed over the I-Lan Ridge. The countercurrent was observed close to Taiwan. Its southward component velocity extended to the surface indicating the Kuroshio departed from Taiwan coast. Such separation could be due to the deflection of Kuroshio. Using the similar data, Tang et al. (2000) found that the Kuroshio

migrated seasonally, but the migration was small.

Fig. 14 shows the width, main axis, and upper ocean (< 300 m) northward volume transport of Kuroshio. The 10 cm s^{-1} isotach of northward velocity was used as an indicator for the boundaries of the Kuroshio. The maximum northward speed defined the main axis of the Kuroshio. The linear integration was applied to estimate the northward volume transport. From south to north, the main axis of the Kuroshio was close to the coast of Taiwan south of I-Lan Ridge. It departed from the coast as it flowed over the I-Lan Ridge. The maximum speed along the main axis of the Kuroshio showed little variation. It was over 100 cm s^{-1}. The width of the Kuroshio was around 170 km, but narrowed to 120 km on I-Lan Ridge. The northward volume transport of Kuroshio demonstrated no significant and systematic change south of I-Lan Ridge. It reduced as the Kuroshio approached and flowed over the I-Lan Ridge. The reduction of the northward transport of Kuroshio was essentially caused by deflection of Kuroshio. A part of northward transport turned to eastward transport. The values of northward volume transport are listed as a reference only since the composite current velocity might be inappropriate to make a quantitative estimate. However, the present estimated volume transport in the I-Lan Ridge agreed well with the transport estimated by Johns et al. (2001), whose estimate was obtained from an array of moored current velocity time series.

In summary, the Kuroshio flowed primarily northward along the eastern coast of Taiwan.

East of southern Taiwan, the Kuroshio split, but gradually re-united. As the Kuroshio flowed over the I-Lan Ridge, it was deflected eastwardly. The velocity became more eastward. The Kuroshio departed from the Taiwan coast. A subsurface countercurrent close to the island was consistently observed. It surfaced north of I-Lan Ridge.

Since the previous studies indicated that the current along the shelf break northeast of Taiwan had noticeable seasonal variations, Fig. 15 shows the U and V sections along 25.5°N in the seasons of southwesterly and northeasterly monsoon. The seasonal variation was observed. Regardless of the seasons, a negative U occurred around shelf break. It clearly separated the main stream of Kuroshio and the current on the shelf. Corresponding to this negative U, the V was positive and negative in the upper and lower water column, respectively. However, this distribution of V varied seasonally. The negative V occurred in the deep water in the northeasterly monsoon season, but it extended upwardly to near surface in the southwesterly monsoon season. This result agrees with the earlier finding (Tang et al., 2000) that the subsurface southwestward countercurrent at the shelf break northeast of Taiwan was submerged when the northeasterly monsoon intensified. East of the countercurrents, both U and V were positive. The northeastward Kuroshio was presented and showed much more complicated spatial velocity distribution than it did east of Taiwan. The locations of maximum velocity cores of U and V were different, implying that the Kuroshio was branching. The influence of the zonal-running shelf break north of this section on the Kuroshio

was noted. A part of the Kuroshio in the upper ocean flowed northward or even northwestward intruding onto the shelf. The shelf blocked the subsurface Kuroshio, which flowed northeastward or even eastward. The Kuroshio also varied significantly with monsoons. In the southwesterly monsoon season, the Kuroshio was weak and its maximum speed core was at subsurface. In the northeasterly monsoon, the weak Kuroshio intensified and the subsurface core nearly disappeared. However, the feature of the Kuroshio having greater speed in winter than summer could be meaningless if we give consideration to the seasonal migration. When the Kuroshio moved away from the shore in the southwesterly monsoon season, it may be that only a portion of the Kuroshio was observed. Such migration also caused more Kuroshio intrusion northwestwardly onto the shelf in the northeasterly monsoon season.

On the shelf north of Taiwan, the current was generally complicated. The complicated flow distribution could be related to the intrusion of Kuroshio, Taiwan Strait outflow, and their interaction. However, the large semidiurnal tidal current velocity on the shelf could result in a large error in the computed composite current velocity. Such an error could further increase the complication of current velocity distribution. Therefore, there is no detailed description of the spatial current velocity distribution on the shelf. Nevertheless, the current on the shelf seems to prefer flowing northeastward regardless of season. The local wind could not be the only dominant force on the shelf north of Taiwan.

Fig. 16 shows four velocity vertical sections along 22°N, 23°N, 24°N, and 25°N in the Taiwan Strait. On the southern opening of Taiwan Strait (section along 22°N), the V was positive and negative in the western and eastern portions, respectively, while the positive U dominated nearly the entire section. This type of velocity distribution supports the former finding, a clockwise circulation south of Taiwan Strait. In the Peng-Hu Channel, the current velocity was mainly northward in the deep channel where the U was weak. West of the deep channel, the U was positive and had relatively simple distribution. The V varied from positive to negative and then to positive again. A couple of maximum speed cores were near bottom. The Peng-Hu Archipelagos north of this section could be responsible for this complicated flow distribution. However, the net northward transport was positive, indicating that the water flowed into the Taiwan Strait. Along the section of 24°N, the U was negative at the shallow end of the funnel-shaped Peng-Hu Channel, which curved northwestward. It was positive at two sides of the end. The V was primarily positive, except in the region close to Mainland China. The region's large V and negative U nearly coincided, indicating that the Peng-Hu Channel conducted the water flow into the Taiwan Strait. Near the northern opening of the Taiwan Strait (section of 25°N), both U and V were principally positive. Their negative values were seen in the region close to Mainland China. Two regions demonstrated relatively large velocity. One was close to the Taiwan coast. The other one was near the bottom east of Wu-Chiu Island. West of Wu-Chiu Island, a weak southwestward current was

observed.

5. Discussion and Summary

Generally speaking, the Kuroshio around Taiwan demonstrated moderate temporal variation, but complicated spatial distribution, especially around the Luzon Strait and northeast of Taiwan. The spatial complication was caused primarily by local topography. Ignoring variation caused by westward propagating eddies, the observed current velocity at I-Lan Ridge (Johns et al., 2001) did not vary with time significantly. The Kuroshio had small temporal fluctuations also confirmed by the moored current velocity in Luzon Strait. This result implies that the Kuroshio around Taiwan might be stable in time. In contrast to the velocity, the Kuroshio migrated intra-seasonally and seasonally. The seasonal migration was especially obvious north of I-Lan Ridge. Such seasonal migration caused large temporal variations in the moored current velocity at shelf break northeast of Taiwan.

Because of insufficient data, cross-section of seasonal current distributions was not presented. Rough seas frequently prohibited the activities of research vessels in winter. The Sb-ADCP data were less in the northeasterly than the southwesterly monsoon seasons. Inevitably, the composite current velocity was biased favoring the current velocity distribution in the southwesterly

monsoon season. Nevertheless, the moored current velocity showed that the current around Taiwan had little seasonal variation, especially in the deep-water region. In the shallow regions, such as Taiwan Strait, the composite current velocity vectors showed that similar tendencies as the mean moored current velocity vectors obtained during mainly the northeasterly monsoon. Therefore, the bias could not change the distribution of composite current velocity significantly.

The qualitative, but not quantitative, validity of composite current velocity was supported by twelve sets of moored current velocity. The results showed that the Kuroshio intruded into the South China Sea through the northern-central Luzon Strait regardless of season, but its incident angle could vary with season. The Kuroshio with double velocity cores was seen east of southern Taiwan, but the two cores gradually combined into one before the I-Lan Ridge, which deflected the Kuroshio. The Kuroshio branched as it collided with the zonal-running shelf break northeast of Taiwan. The main stream of the Kuroshio flowed along the shelf break to the east and a part of the Kuroshio intruded into the shelf. A submerged countercurrent between the Kuroshio and the shelf break was consistently observed. The seasonal migration of the Kuroshio influenced the countercurrent and the current northeast of Taiwan.

The intruding Kuroshio water in the South China Sea interacted with the South China Sea current. A clockwise flow pattern was seen southwest of Taiwan. Most of the water in this

clockwise current returned to the Kuroshio at the tip of southern Taiwan. The rest of the water flowed into the Taiwan Strait through the Peng-Hu Channel and is an important resource for current in the Taiwan Strait. The current in the Taiwan Strait primarily flowed to the north. A countercurrent was faintly visible along the coast of Mainland China. The Taiwan Strait outflow interacted with the intruding Kuroshio north of Taiwan. Only a small portion of outflow entered the Kuroshio along the northern coast of Taiwan. The rest of outflow continued north.

Acknowledgements

The research was supported by NSC of ROC under grants NSC 89-2611-M-002-031-OP2 for T. Y. Tang, NSC 90-2611-M-012-001-OP2 for Y. J. Yang, and NSC 89-2611-M-002-023-OP2 for W.-S. Chuang. We would like to express our heartfelt thanks to the ODB/NCOR for the historical Sb-ADCP and bathymetry data. The assistance of the captains and crews of the R/Vs ORI, II, and III are also greatly appreciated. The plotting software of curved velocity vectors was kindly provided by Dr. D. S. Ko at Naval Research Laboratory, Stennis Space Center (NRLSSC).

References

Chu, T.-Y., 1961. On ocean currents in East China Sea and the Variability of Taiwan. Meteorological Bulletin 4, 7-17. (in Chinese with English abstract)

Chu, T.-Y., 1976. Study of the Kuroshio current between the Taiwan and Ishigakijima. Acta Oceanographic Taiwanica 13, 140-153.

Chuang, W.-S., 1986. A note on the driving mechanisms of current in the Taiwan Strait. Journal of Oceanography Society Japan 42, 355-361.

Chuang, W.-S., Wu, C.-K., 1991. Slope-current fluctuation northeast of Taiwan, winter 1990. Journal of Oceanography Society Japan 47, 185-193.

Chuang, W.-S., Li, H.-W., Tang, T. Y., Wu, C.-K., 1993. Observation of the countercurrent on the inshore side of the Kuroshio northeast of Taiwan. Journal of Oceanography 49, 581-592.

Chuang, W.-S., Liang, W.-D., 1994. Seasonal variability of intrusion of the Kuroshio water across the continental shelf northeast of Taiwan. Journal of Oceanography 50, 531-542.

Johns, W. E., Lee, T. N., Zhang, D., Zantopp, R., Liu, C.-T., Yang, Y., 2001. The Kuroshio east of Taiwan: Moored transport observations from the WOCE PCM-1 array. Journal of Physical Oceanography 31, 1031-1053.

Li, L., Wu, B., 1989. A Kuroshio loop in South China Sea? On circulation of the northeaster South China Sea. Journal of Oceanography in Taiwan Strait 8, 89-95.

Liu, C.-T., 1983. As the Kuroshio turns: (I) Characteristics of the current. Acta Oceanographic Taiwanica 14, 88-95.

Metzger, E. J., Hurlburt, H. E., 2001. The nondeterministic nature of Kuroshio penetration and eddy shedding in the South China Sea. Journal of Physical Oceanography 31, 1712-1732.

Nitani, H., 1972. Beginning of the Kuroshio. In: Kuroshio, its physical aspects, H. Stommel and K. Yoshida, editors, University of Tokyo Press, Tokyo, pp. 129-163.

Qu, T., Mitsudera, H., Yamagata, T., 2000. Instruction of the North Pacific waters into the South China Sea. Journal Geophysical Research 105, 6415-6424.

Shaw, P.-T., 1989. The instruction of water masses into the sea southwest of Taiwan. Journal Geophysical Research 94, 18,213-18,226.

Shaw, P.-T., Chao, S.-Y., 1994. Surface circulation in the South China Sea. Deep-Sea Research 41, 1663-1683.

Sun, X., 1987. Analysis of the surface path of the Kuroshio in the East China Sea. In: Essays of the Investigation of Kuroshio, X. Sun, editor, Ocean Press, Beijing, pp. 1-14 (in Chinese with

English Abstract).

Tang, T. Y., Yang, Y. J., 1993. Low frequency current variability on the shelf break northeast of Taiwan. Journal of Oceanography 49, 193-210.

Tang, T. Y., Ma, J. C., 1995. A note on the accuracy of shipboard ADCP on Ocean Researcher I. Acta Oceanographic Taiwanica 34, 71-81.

Tang, T. Y., Hsueh, Y., Yang, Y. J., Ma, J. C., 1999. Continental slope flow northeast of Taiwan. Journal of Physical Oceanography 29, 1353-1362.

Tang, T. Y., Tai, J. H., Yang, Y. J., 2000. The flow pattern north of Taiwan and migration of the Kuroshio. Continental Shelf Research 20, 349-371.

Wang, J., Chern, C.-S., 1988. On the Kuroshio branch in the Taiwan Strait during wintertime. Progress in Oceanography 21, 469-491.

Wang, J., Chern, C.-S., 1989. On cold water instructions in the eastern Taiwan Strait during the cold season. Acta Oceanographic Taiwanica 21, 469-491.

Wyrtki, K., 1961. Physical oceanography of the southeast Asia waters. Scripps Institute of Oceanography NAGA Report 2, 195pp.

Yang, Y., Liu, C.-T., Hu, J.-H., Koga, M., 1999. Taiwan Current (Kuroshio) and impinging eddies.

Journal of Oceanography 55, 609-617.

Zhang, D., Lee, T. N., Johns, W. E., Liu, C.-T., Zantopp, R., 2001. The Kuroshio east of Taiwan: Modes of variability and relationship to interior ocean mesoscale eddies. Journal of Physical Oceanography 31, 1054-1074.

Figure Captions

Fig. 1. Bathymetric chart showing areas around Taiwan and mooring locations.

Fig. 2. Current charts in knots: (a) summer, and (b) winter (after Nitani, 1972).

Fig. 3. The left panel denotes the distribution of numbers of data. The right-upper and right-lower panels represent the root mean square (rms) value of the $\overline{u}_N$, and the available percentage of grid versus the N, respectively.

Fig. 4. Composite of the Sb-ADCP current velocity vectors around Taiwan. The left and right panels represent the 30 and 100 m depths, respectively.

Fig. 5. Composite of the Sb-ADCP current velocity vectors at 30 m depths around Taiwan. The left and right panels represent the seasons of southwesterly monsoon and northeasterly monsoon, respectively.

Fig. 6. The stick diagrams of the 36-hour low-pass filtered current velocity. The upper to lower panels represent the time series data of M1 in 1997, 1998, and 1999, M2 in 1997 and 1998, M3 in 1997, and M4 in 2000. The current velocity data was primarily at 100 m depths except the M2 in 1998, which was at 140 m depths.

Fig. 7. The rose diagrams and mean current velocities obtained from shipboard and moored

ADCP measurement at M1, M2, M3, and M4. The left, central, and right panels represent the rose diagrams of the shipboard and moored ADCP data, and the mean velocities, respectively. The range of rose is 0-30% with 7.5% interval.

Fig. 8. The stick diagrams of the 36-hour low-pass filtered current velocity. The upper to lower panels represent the time series data of M5 in 1992, M6 in 1991, and M7 in 1992, 1993, and 1994. The current velocity data was at a depth of 30 m.

Fig. 9. Same as Fig. 7 except at M5, M6, and M7. The range of rose is 0-60% with 15% interval.

Fig. 10. The stick diagrams of the 36-hour low-pass filtered current velocity. The upper to lower panels represent the time series data of M8, M9, M10, and M11 in 1999, and M12 in 1996. The current velocity data was at a depth of 30 m.

Fig. 11. Same as Fig. 9 except at M8, M9, M10, M11, and M12.

Fig. 12. Vertical sections of composite Sb-ADCP current velocity of zonal (U) and meridional (V) components along the 120.75°E and 21°N are show in left and right panels, respectively. The depth range is from the surface to about 300 m. The continental shelf is darkened. The values are contoured at intervals of 10 cm s^{-1}. The zero contour appears in heavy line. Portions of positive values are shaded.

Fig. 13. Vertical sections of composite Sb-ADCP current velocity of zonal (U) and meridional (V) components along the 22°N, 23°N, 24°N, 25°N east of Taiwan are show in left and right panels, respectively. The depth range is from the surface to about 300 m. The continental shelf is darkened. The values are contoured at intervals of 10 cm s^{-1}. The zero contour appears in heavy line. Portions of positive values are shaded.

Fig. 14. The upper ocean (< 300 m) northward volume transport of Kuroshio and composite Sb-ADCP current velocity vectors at 30 m depths east of Taiwan. Bold and dashed lines indicate the width and main axis of Kuroshio.

Fig. 15. Vertical sections of composite Sb-ADCP current velocity of zonal (U) and meridional (V) components along the 25.5°N in seasons of southwesterly monsoon and northeasterly monsoon are show in left and right panels, respectively. The depth range is from the surface to about 300 m. The continental shelf is darkened. The values are contoured at intervals of 10 cm s^{-1}. The zero contour appears in heavy line. Portions of positive values are shaded.

Fig. 16. Same as Fig. 13 except in Taiwan Strait.

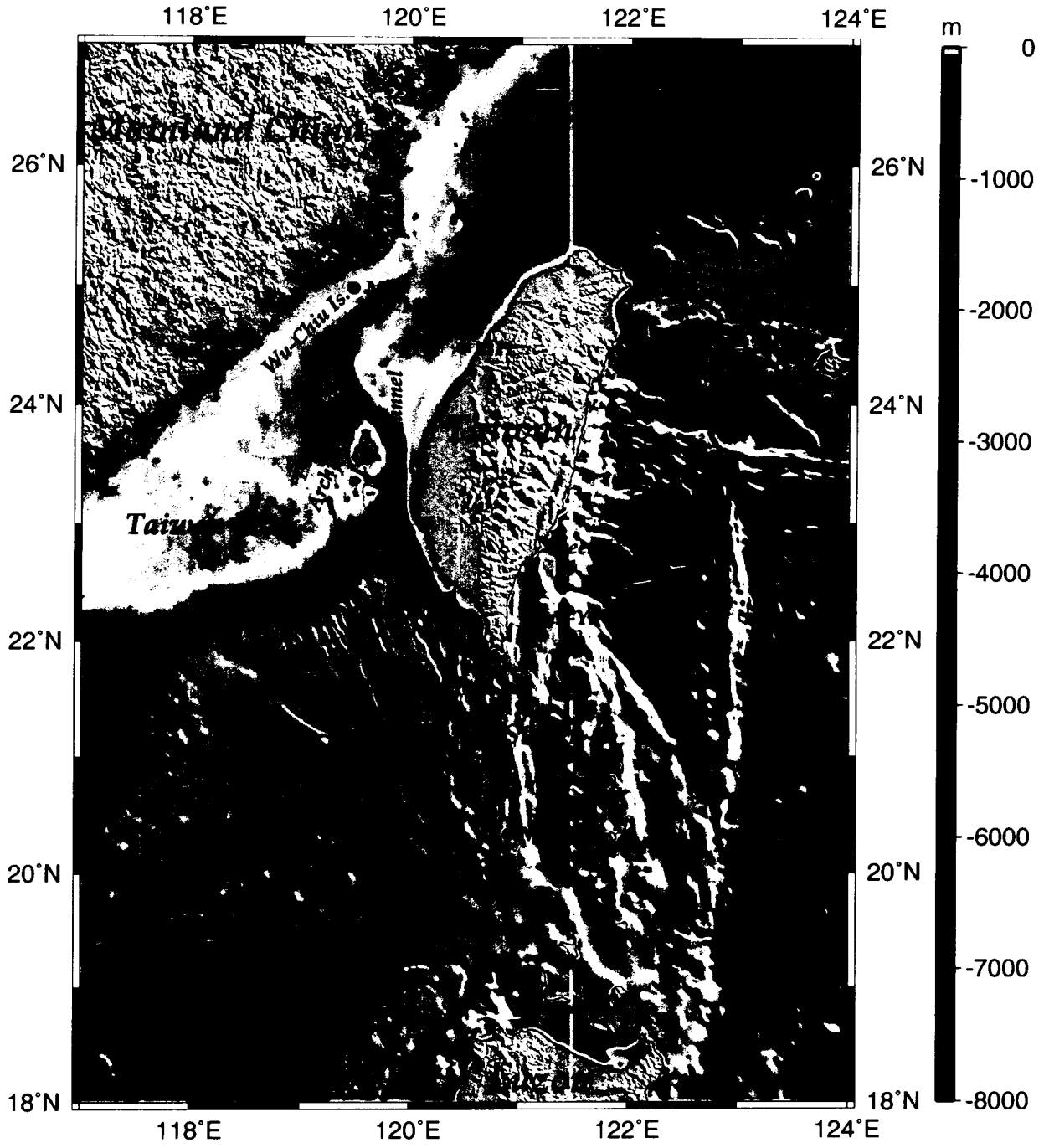
118°E
120°E
122°E
124°E
26°N
24°N
22°N
20°N
18°N
m
0
-1000
-2000
-3000
-4000
-5000
-6000
-7000
-8000
Wu-Chiu Is.
Taiwan

Fig. 1

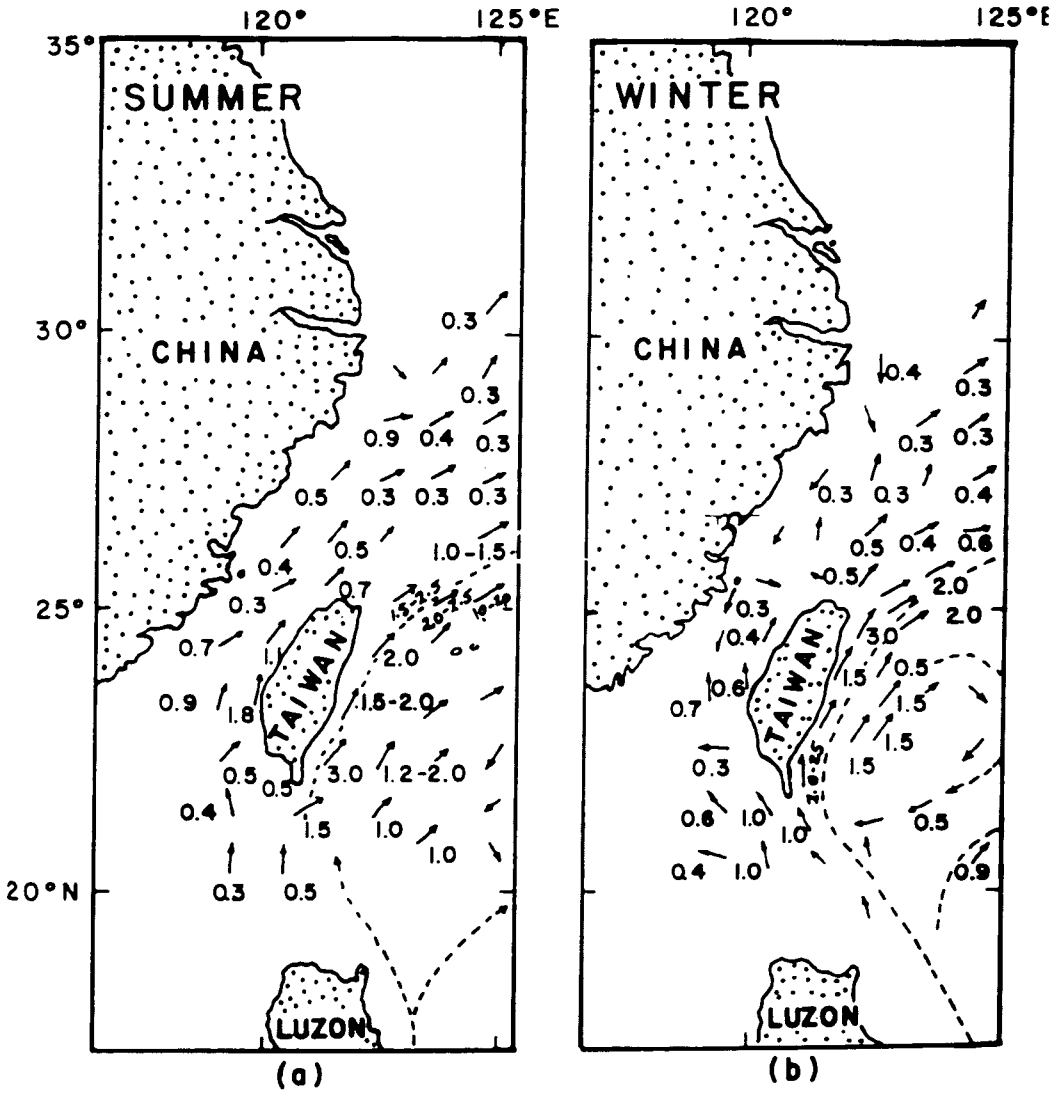
120°
125°E
35°
30°
25°
20°N
SUMMER
CHINA
TAIWAN
LUZON
(a)
WINTER
CHINA
TAIWAN
LUZON
(b)

Fig. 2

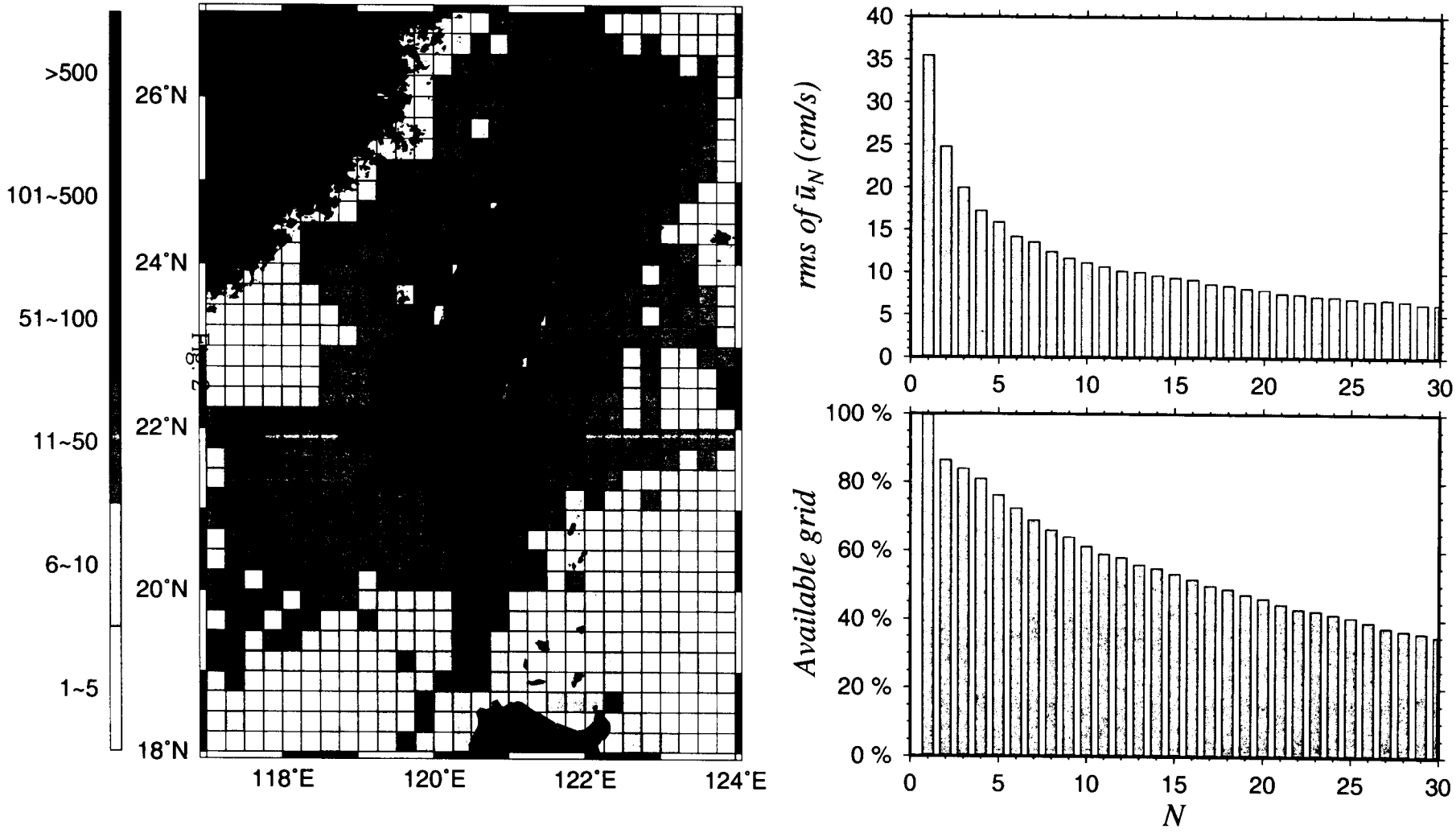
>500
101~500
51~100
11~50
6~10
1~5
26°N
24°N
22°N
20°N
18°N
118°E
120°E
122°E
124°E
Fig. 2
rms of $\bar{u}_N$ (cm/s)
40
35
30
25
20
15
10
5
0
0
5
10
15
20
25
30
Available grid
100 %
80 %
60 %
40 %
20 %
0 %
0
5
10
15
20
25
30
N

Fig. 3

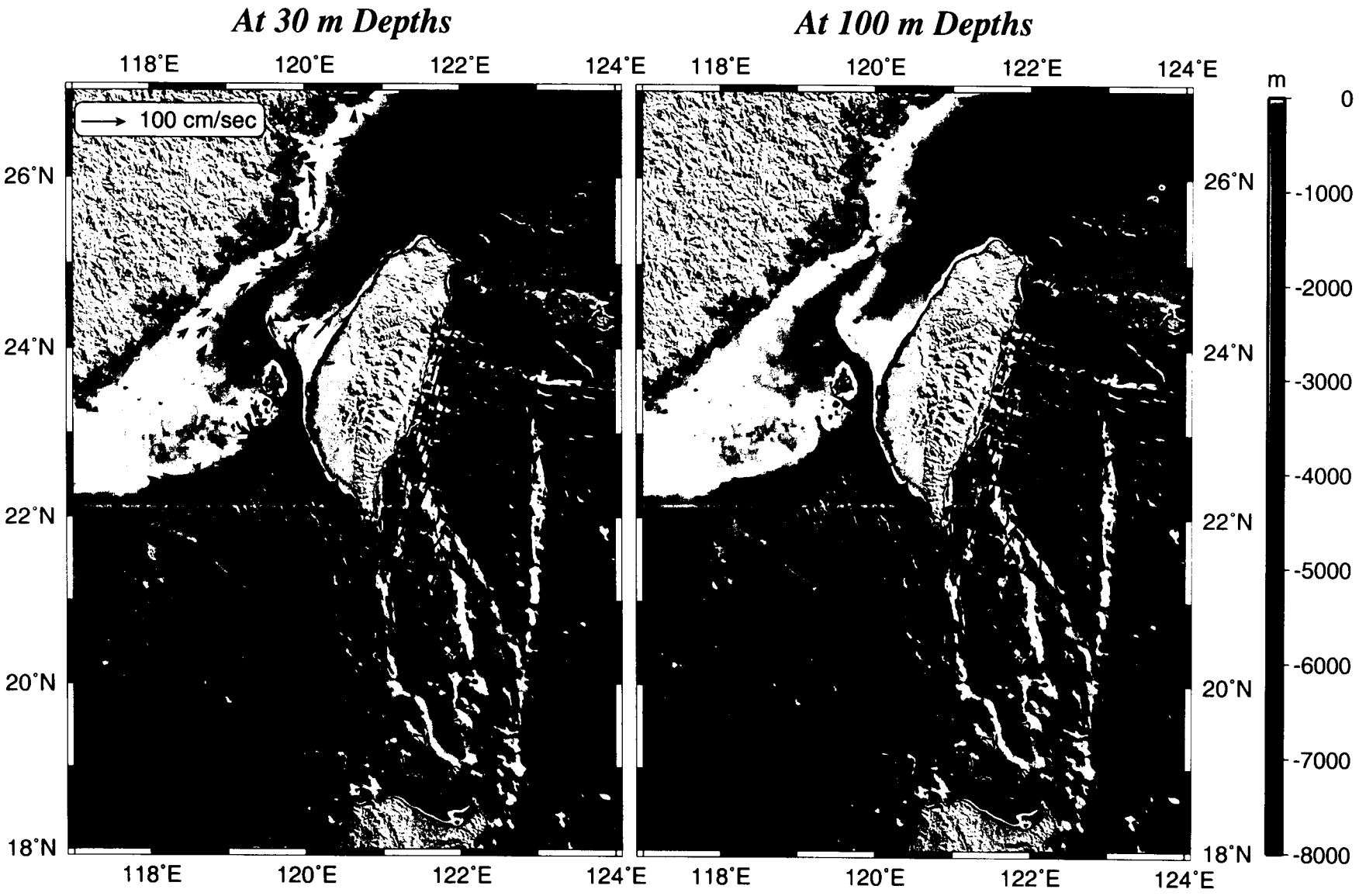
At 30 m Depths
At 100 m Depths
118°E
120°E
122°E
124°E
26°N
24°N
22°N
20°N
18°N
100 cm/sec
m
0
-1000
-2000
-3000
-4000
-5000
-6000
-7000
-8000

Fig. 4

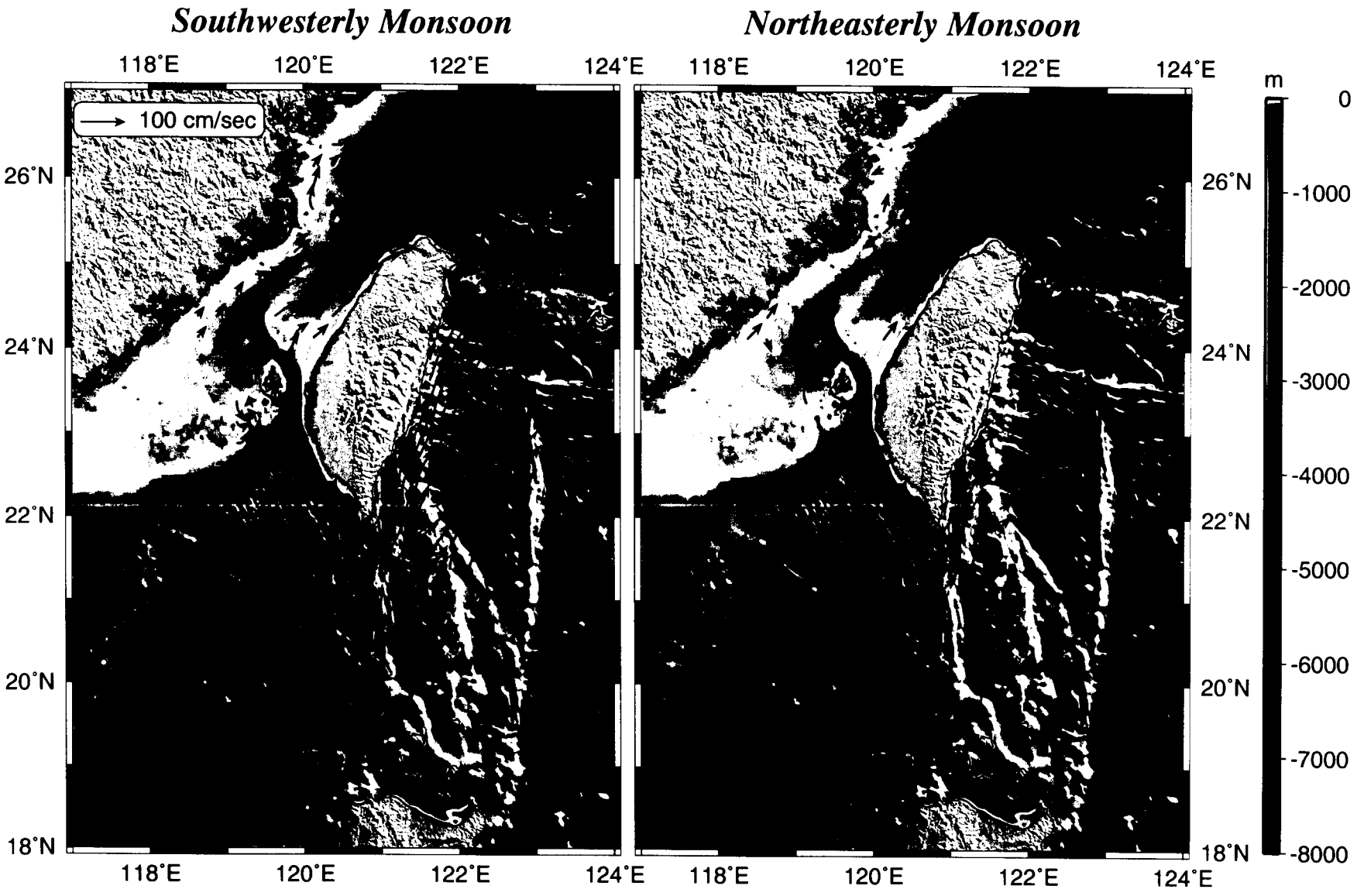
Southwesterly Monsoon
Northeasterly Monsoon
118°E
120°E
122°E
124°E
100 cm/sec
26°N
24°N
22°N
20°N
18°N
m
0
-1000
-2000
-3000
-4000
-5000
-6000
-7000
-8000

Fig. 5

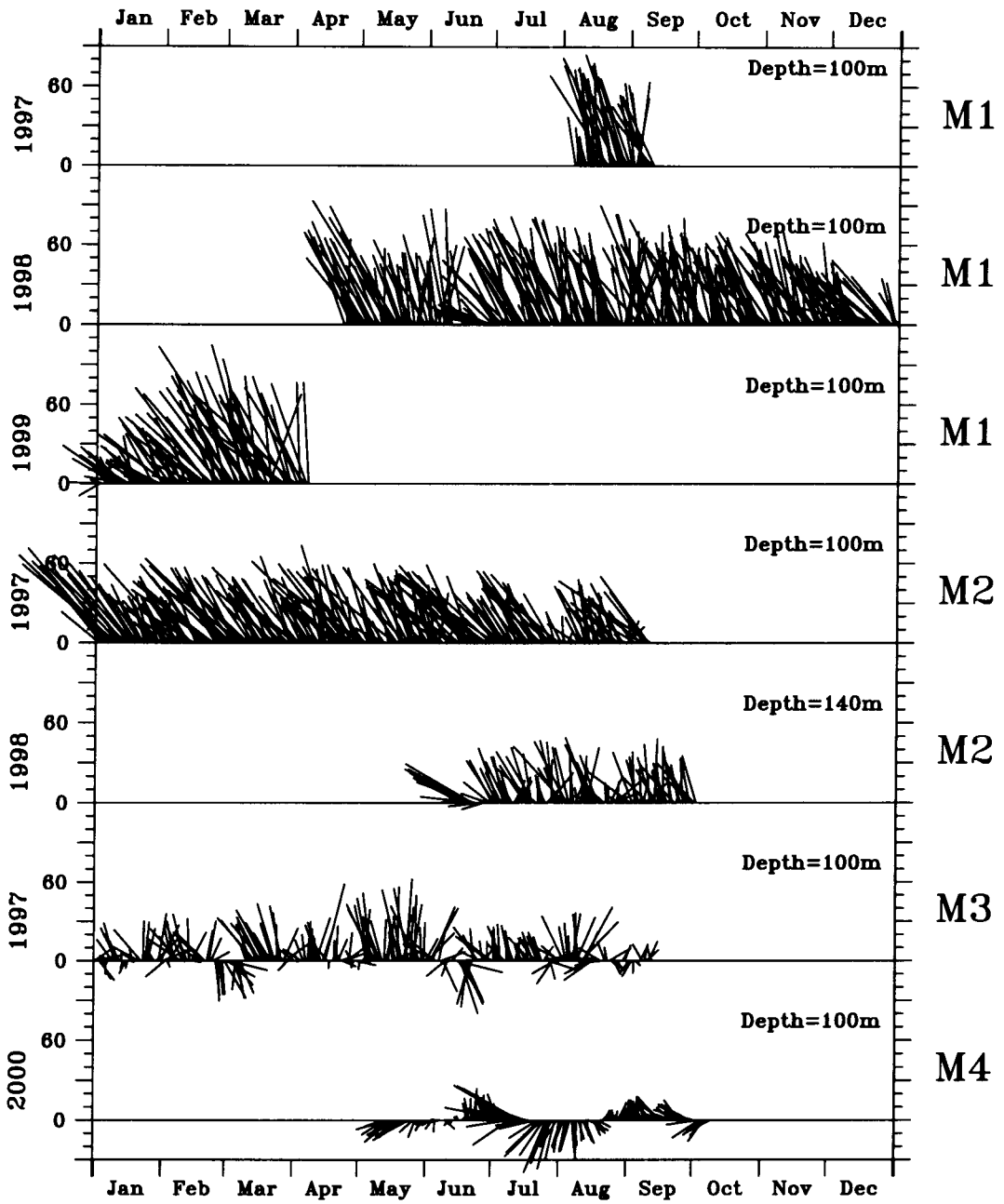
Jan
Feb
Mar
Apr
May
Jun
Jul
Aug
Sep
Oct
Nov
Dec
1997
1998
1999
2000
60
0
Depth=100m
Depth=140m
M1
M2
M3
M4

Fig. 6

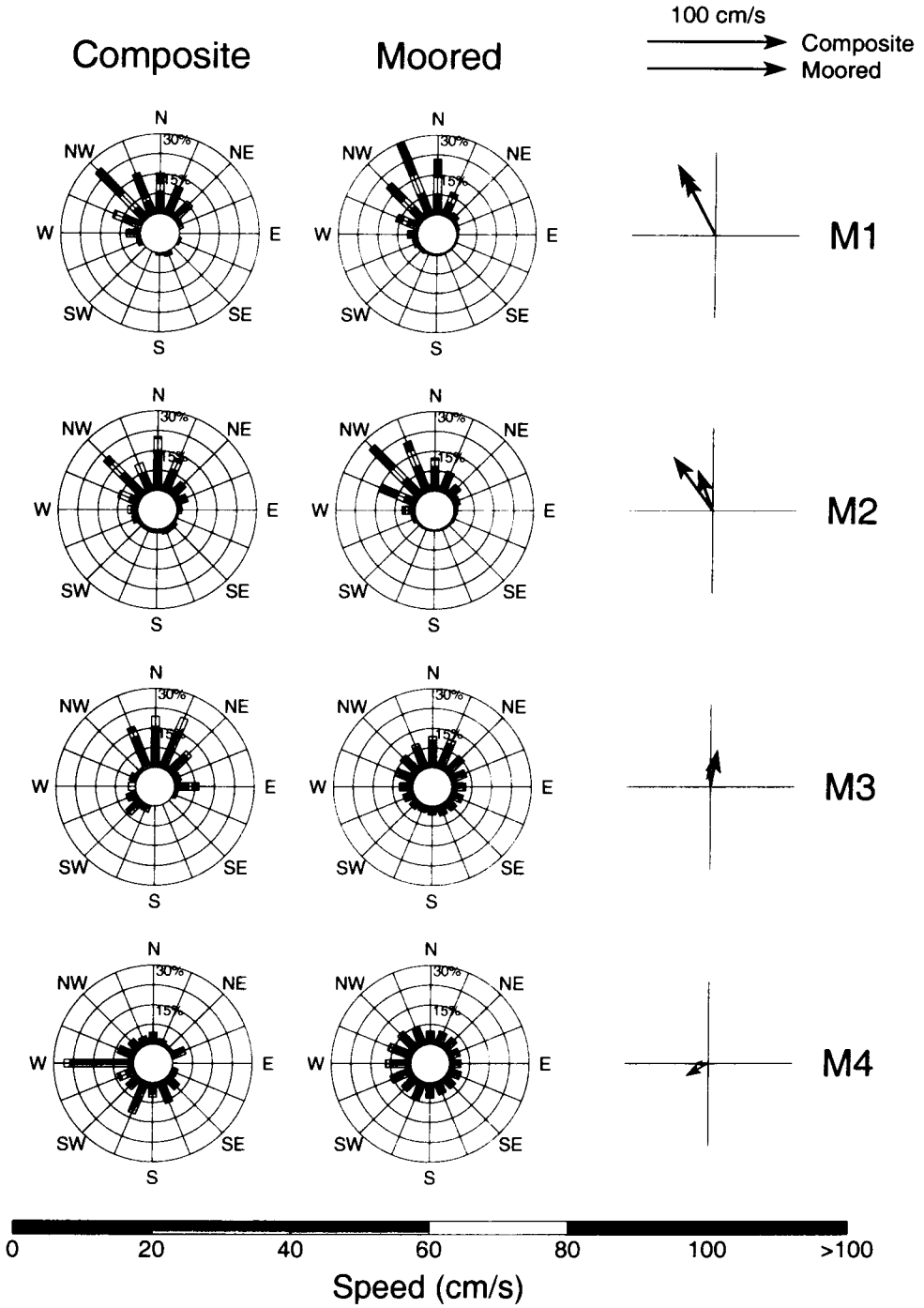
Composite
Moored
100 cm/s
Composite
Moored
N
NE
E
SE
S
SW
W
NW
30%
15%
M1
M2
M3
M4
0
20
40
60
80
100
>100
Speed (cm/s)

Fig. 7

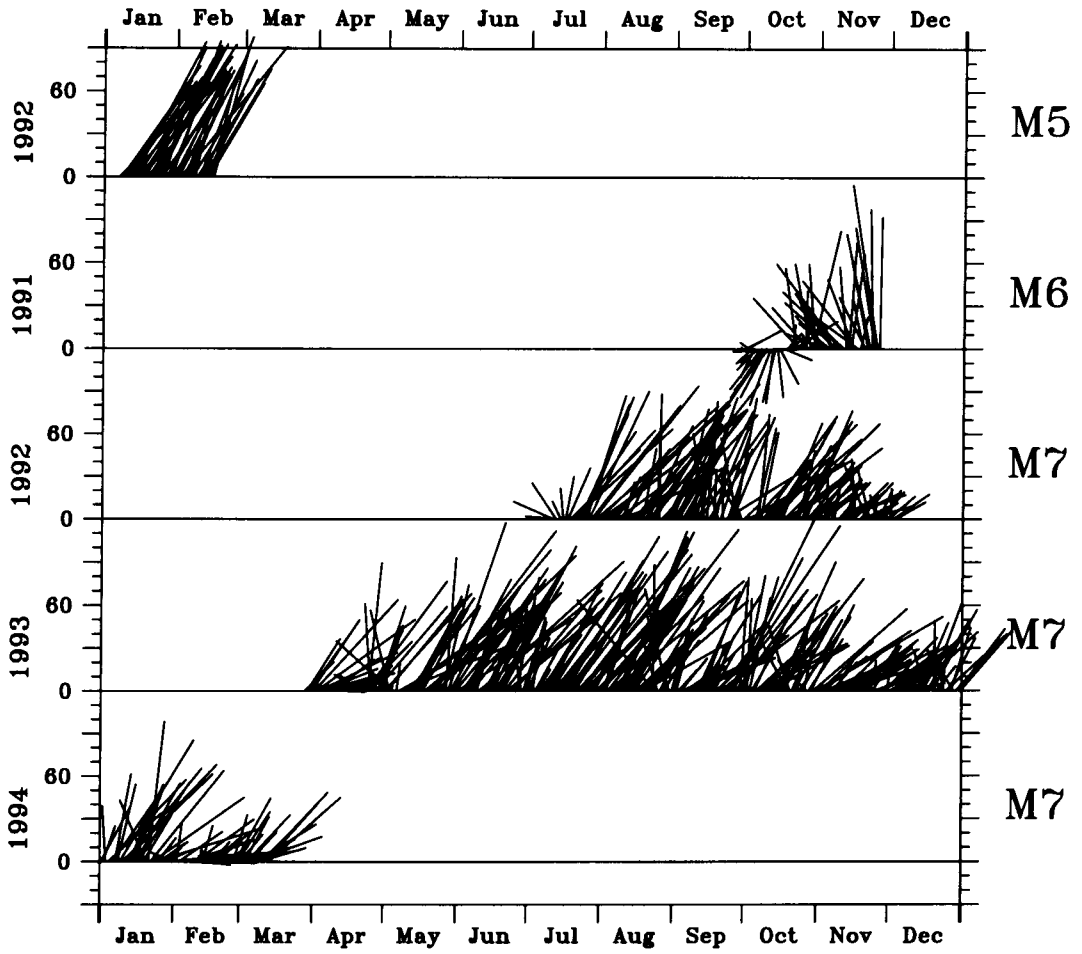
Jan
Feb
Mar
Apr
May
Jun
Jul
Aug
Sep
Oct
Nov
Dec
1992
1991
1992
1993
1994
60
0
M5
M6
M7
M7
M7

Fig. 8

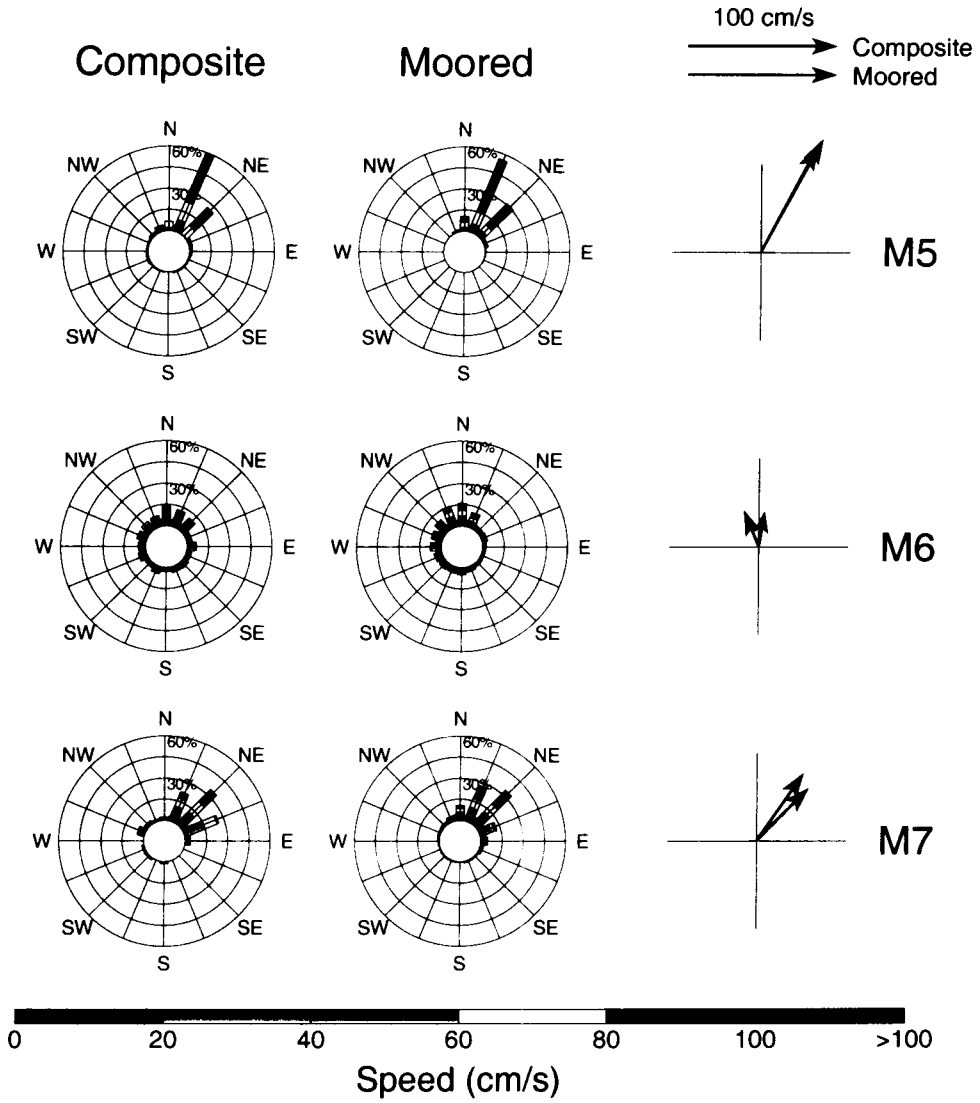
Composite
Moored
100 cm/s
Composite
Moored
N
NE
E
SE
S
SW
W
NW
60%
30%
M5
M6
M7
0
20
40
60
80
100
>100
Speed (cm/s)

Fig. 9

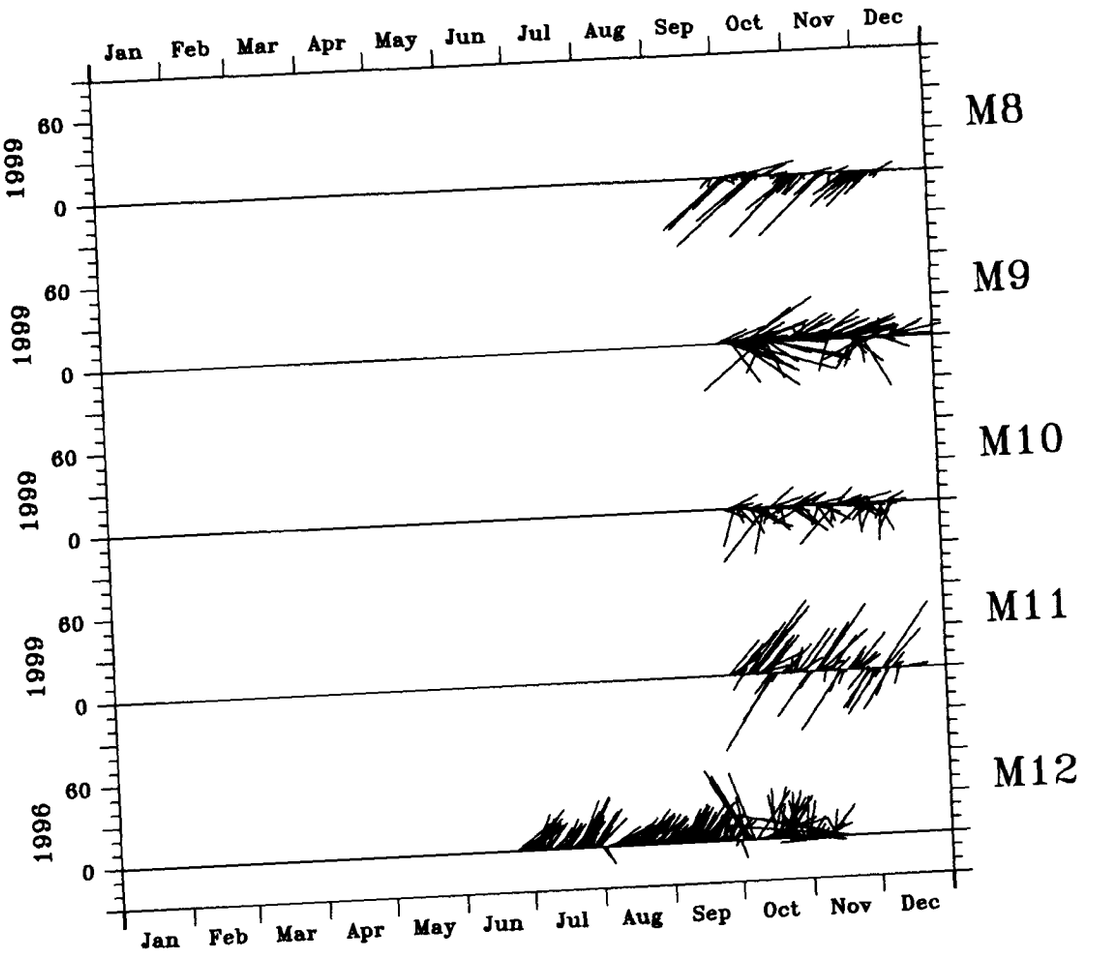
Jan
Feb
Mar
Apr
May
Jun
Jul
Aug
Sep
Oct
Nov
Dec
M8
M9
M10
M11
M12
1999
1996
60
0

Fig. 10

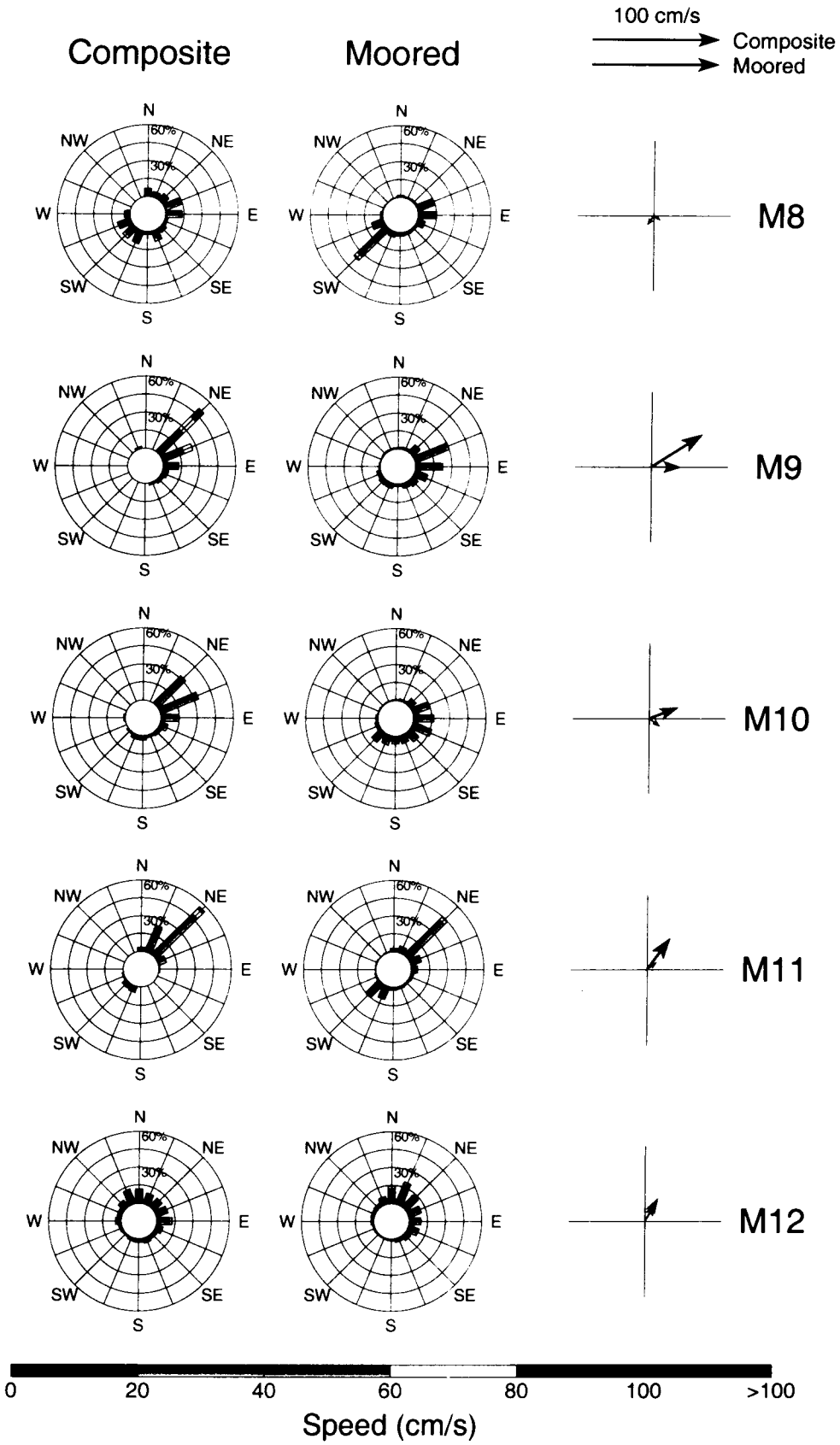
Composite
Moored
100 cm/s
Composite
Moored
N
NE
E
SE
S
SW
W
NW
60%
30%
M8
M9
M10
M11
M12
0
20
40
60
80
100
>100
Speed (cm/s)

Fig. 11

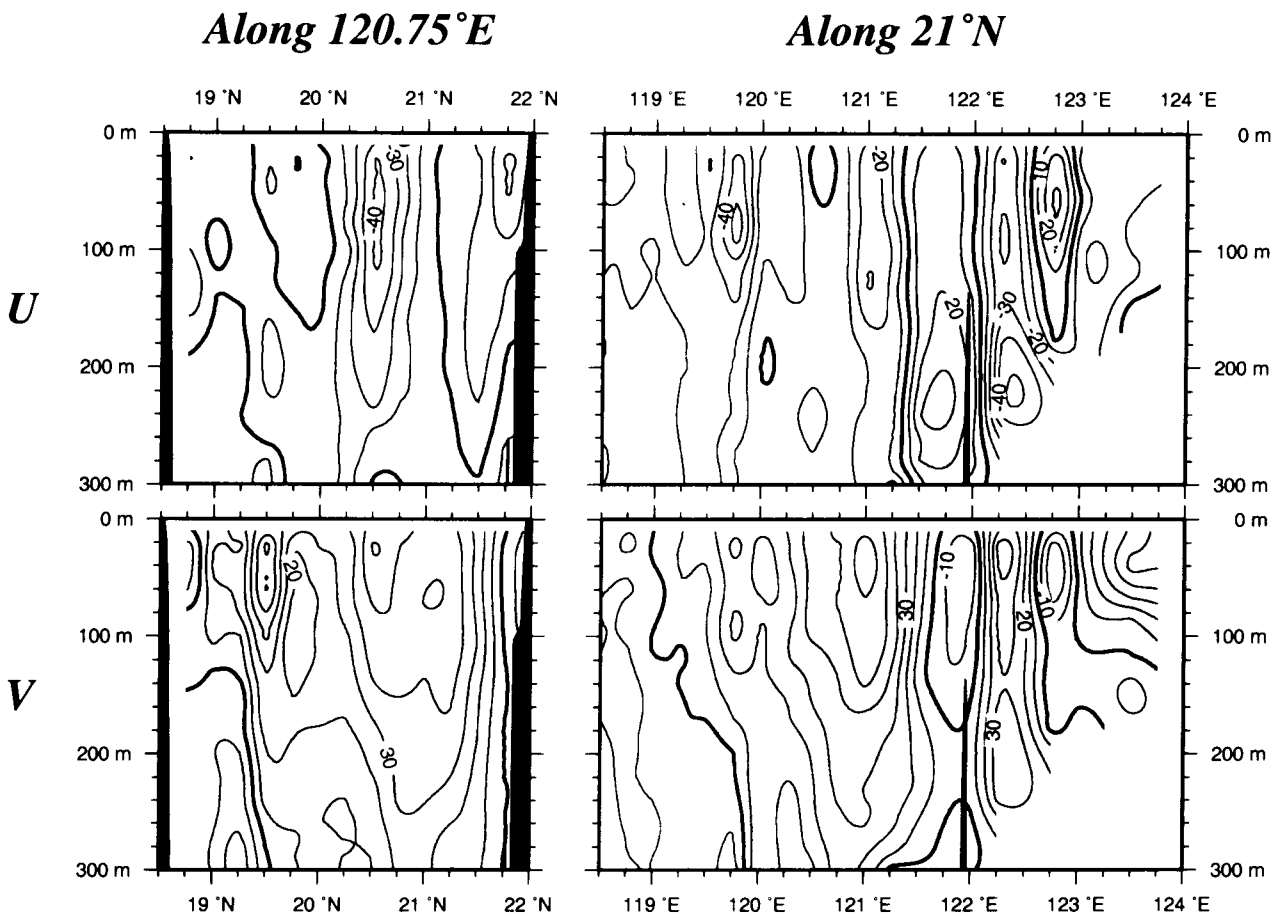
Along 120.75°E
Along 21°N
U
V
19 °N
20 °N
21 °N
22 °N
119 °E
120 °E
121 °E
122 °E
123 °E
124 °E
0 m
100 m
200 m
300 m

Fig. 12

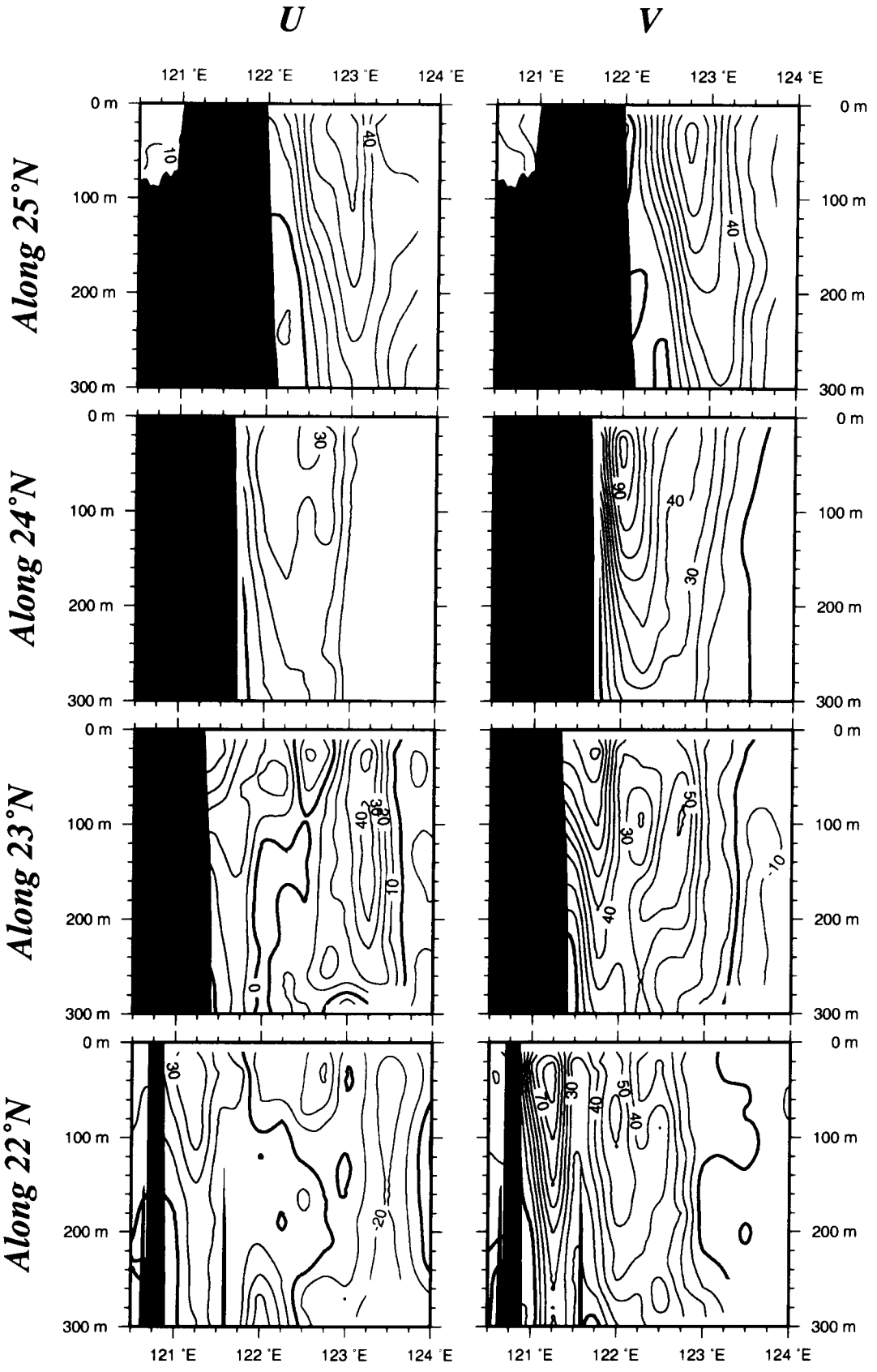
U
V
Along 25°N
Along 24°N
Along 23°N
Along 22°N
121 °E
122 °E
123 °E
124 °E
0 m
100 m
200 m
300 m

Fig. 13

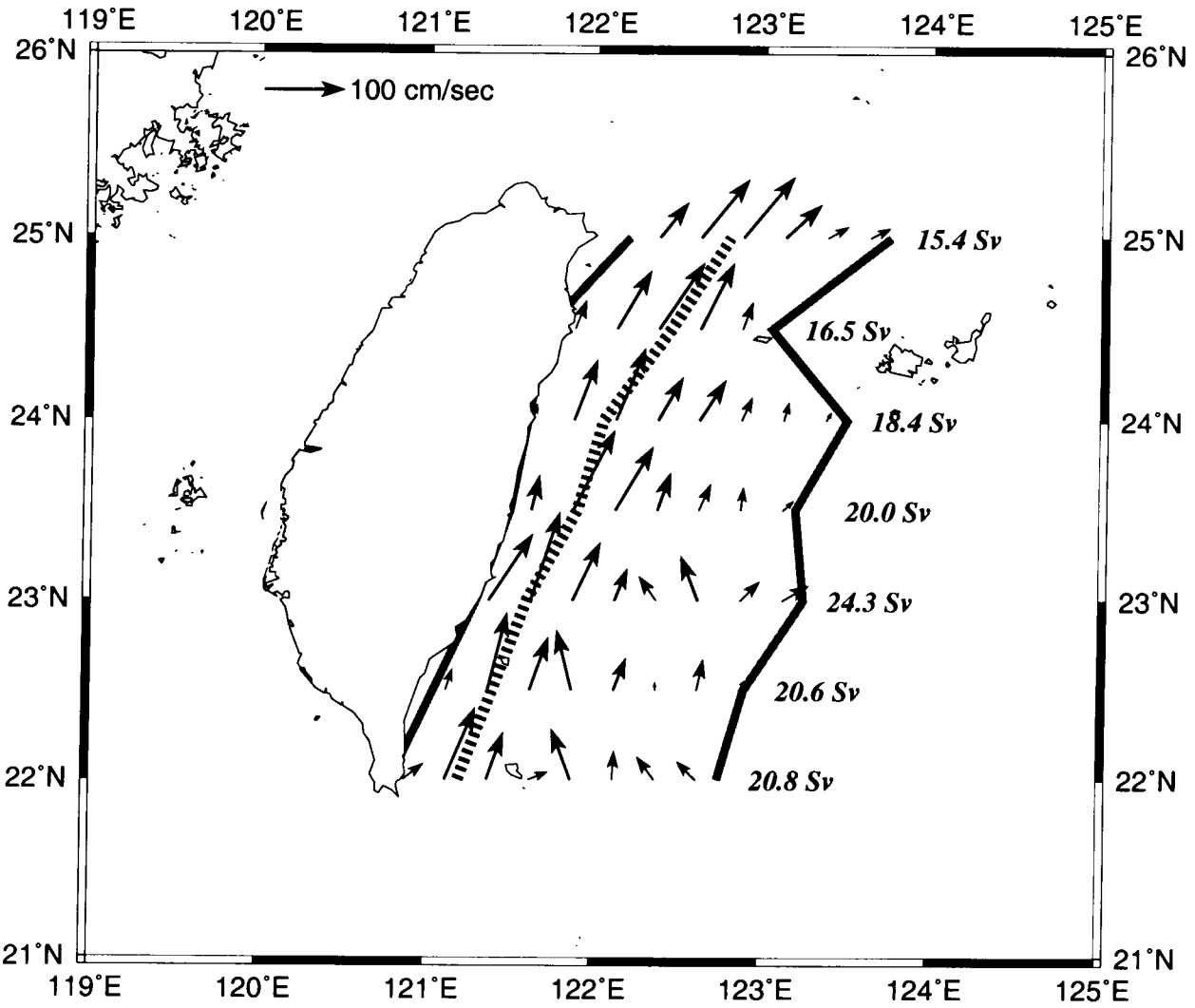
119°E
120°E
121°E
122°E
123°E
124°E
125°E
26°N
25°N
24°N
23°N
22°N
21°N
100 cm/sec
15.4 Sv
16.5 Sv
18.4 Sv
20.0 Sv
24.3 Sv
20.6 Sv
20.8 Sv

Fig. 14

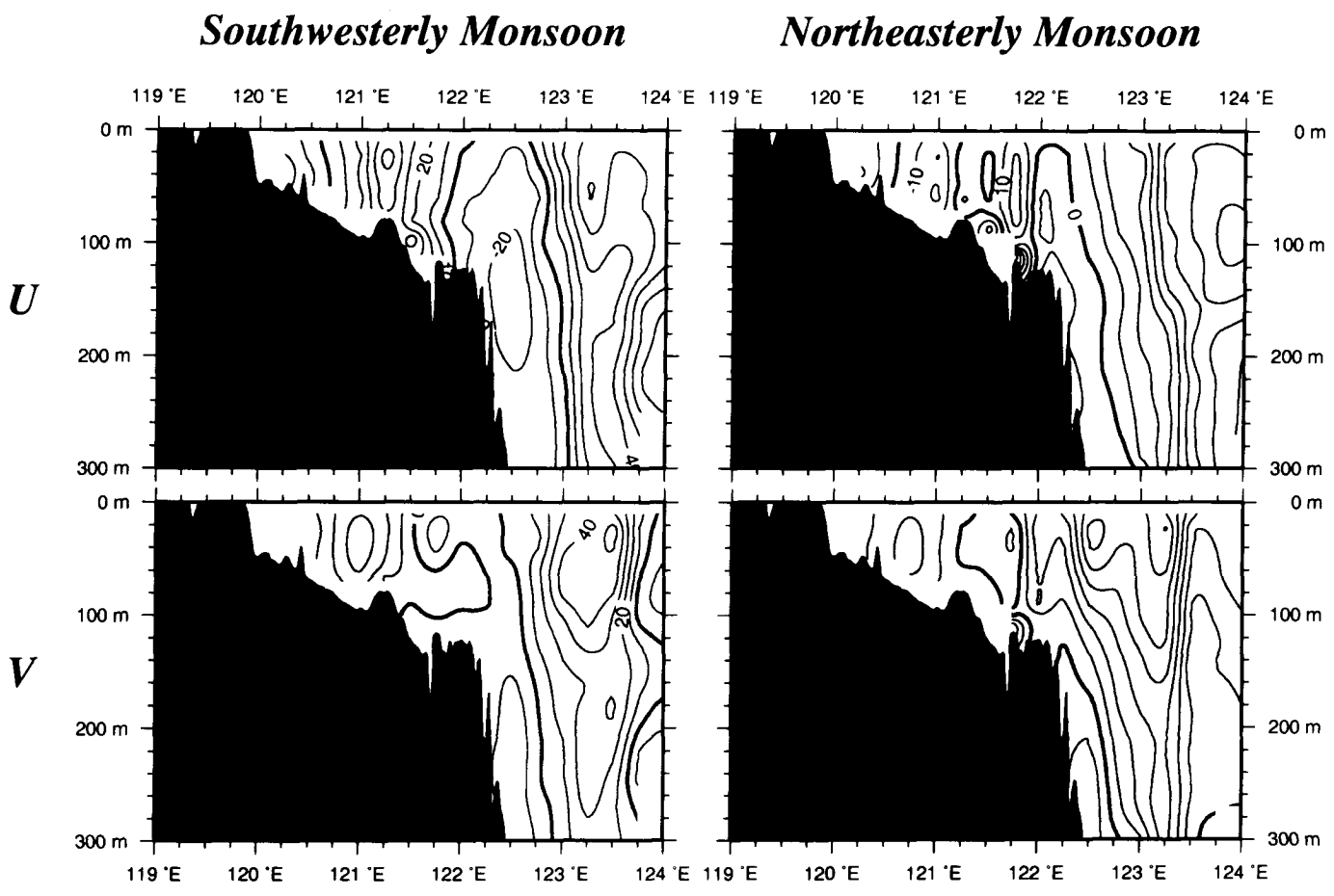
Southwesterly Monsoon
Northeasterly Monsoon
U
V
119 °E
120 °E
121 °E
122 °E
123 °E
124 °E
0 m
100 m
200 m
300 m

Fig. 15

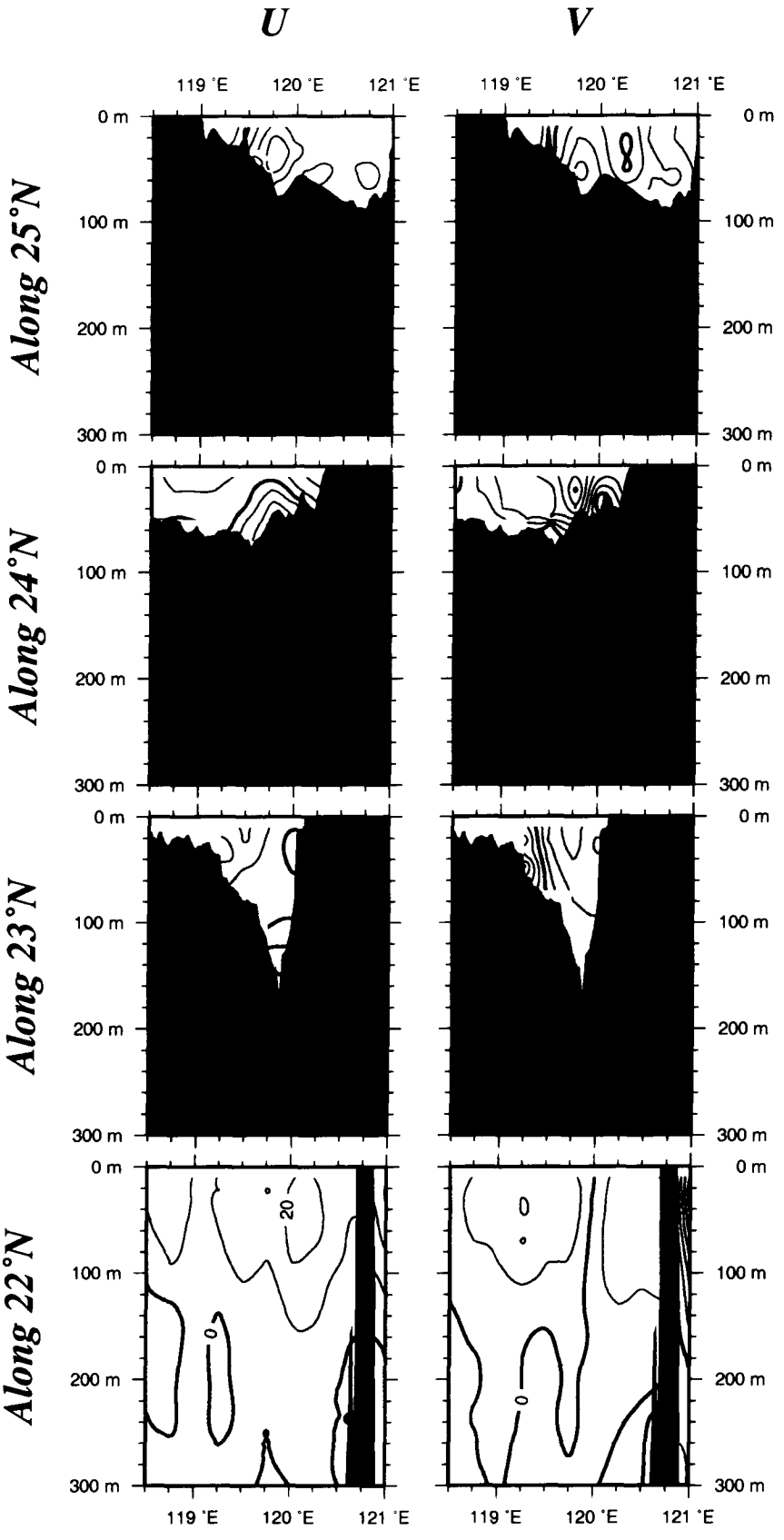
U
V
119 °E
120 °E
121 °E
0 m
100 m
200 m
300 m
Along 25°N
Along 24°N
Along 23°N
Along 22°N
20
0

Fig. 16